

The Pennsylvania State University

The Graduate School

The Huck Institutes of the Life Sciences

**STUDY OF A PACING NEUROBLASTOMA CELL LINE VIA A NOVEL
MACROELECTRODE TECHNIQUE**

A Thesis in

Integrative Biosciences

by

Ricardo Jose Silva

© 2005 Ricardo Jose Silva

Submitted in Partial Fulfillment
of the Requirements
for the Degree of

Doctor of Philosophy

August 2005

The thesis of Ricardo Jose Silva was reviewed and approved* by the following:

Roger P. Gaumond
Associate Professor of Bioengineering
Thesis Advisor
Chair of Committee

Gong Chen
Assistant Professor of Biology.

Byron C. Jones
Professor of Biobehavioral Health / Pharmacology

Harry R. Allcock
Professor of Chemistry, Evan Pugh Professor

Nandini Vasudevan
Assistant Professor of Biology

Jeffrey D. Zahn
Assistant Professor of Bioengineering

Richard J. Frisque
Professor of Molecular Virology
Co-director, Graduate Education of Integrative Biosciences Graduate
Program, Huck Institutes of the Life Sciences

*Signatures are on file in the Graduate School

ABSTRACT

A novel *in vitro* electrophysiological technique was developed, based on the use of a large summing population electrode (macroelectrode approach). The macroelectrode approach was utilized to study the evolution of the electrical response in the SK-N-BE(2c) human neuroblastoma cell line. Development of a large oscillatory electrical signal consistent with the establishment of a functional pacing network in culture was observed. Neural pacing is a phenomenon of fundamental importance in neurosciences. Pacing is an integrating factor in the developing brain, learning, memory and motor coordination. The nature and origin of this signal was studied by means of the macroelectrode approach as well as patch clamping, liquid chromatography, and immunofluorescence. By comparing the signal obtained with the macroelectrode approach to traditional methods the strength and weaknesses of the technique were explored. It was determined that pacing networks naturally develop in this cell line and are the result of synaptic communication mediated by dopamine as a neurotransmitter and dopamine D2 as a receptor. The macroelectrode technique was shown to provide unique information about the population behavior of cells growing in culture. The electrical properties of the SK-N-BE(2c) cell line as seen with the macroelectrode approach could serve as a cost effective solution for long term, real time study of pacing neural networks *in vitro* and the basis for the development of cell based biosensors and high throughput drug screening systems.

TABLE OF CONTENTS

LIST OF FIGURES	vi
LIST OF TABLES	xii
ACKNOWLEDGEMENTS	xiii
Chapter 1 Introduction	1
1. Chapter 2 Stochastic Model for Summed Neural Activity	5
2.1 Summation of Currents at the Electrode.....	9
2.2 RMS of the Electrode Signal	11
2.3 Simulation: Signal RMS versus Firing Rate.....	12
2.4 Action Potential Waveform Recovery.....	15
2.5 Chapter Summary	19
Chapter 3 Characterization of the SK-N-BE(2c) Neuroblastoma Cell Line.....	20
3.1 Introduction.....	20
3.2 Background.....	21
3.3 Patch Clamp Recordings.....	24
3.4 Analysis of Neurotransmitter Release	28
3.5 Imaging Studies	33
3.6 Additional Characterization.....	37
3.7 Chapter Summary	39
Chapter 4 Development of a Multiunit Cell Based System.....	41
4.1 Introduction.....	41
4.2 Cell Culture Chamber # 1	43
4.4 Cell Culture Chamber # 2	45
4.5 Novel Polyphosphazene Based Materials for Differential Cell Adhesion	50
4.5.1 Polymer Selection Criteria	52
4.5.2 MEEP Biocompatibility	52
4.5.3 Polymer Characterization	54
4.5.4 Differential Cell Adhesion	57
4.5.5 <i>Differential Cell Patterning</i>	60
4.5.6 <i>Impedance Analysis</i>	63
4.5.7 Cell Adhesion Mechanism	65
4.6 Chapter Summary	69
Chapter 5 Electrophysiology of Neuroblastoma Cell Clusters	72

5.1 Introduction.....	72
5.2 Continuous Time Signal Processing Strategy.....	74
5.3 Data Set Number 1.....	75
5.4 Data Set Number 2.....	83
5.5 Data Set Number 3.....	90
5.6 Chapter Discussion and Summary.....	96
 Chapter 6 Modulation of the Electrical Response	99
6.1 Introduction.....	99
6.2 Response of Cells to Stimulus	99
6.3 Driving Force behind the Multiunit Response.....	106
6.3.1 Dopamine Mediated Communication.....	109
6.4 Recovery of Action Potential Waveforms	119
6.5 Chapter Summary	125
 Chapter 7 Discussion and Conclusion	126
7.1 Products Envisioned:	129
Bibliography	131
Appendix A Program used for signal comparison with Matlab®	142
Appendix B Program for signal recovery via the Levinson Algorithm.....	146

LIST OF FIGURES

Figure 2-1: Neural cells on an electrode substrate. The electrode sums the neural activity of all cells. Currents produced by Action Potentials from cells contribute minute voltage fluctuations at the electrode surface.....	5
Figure 2-2: The AP waveshape of the extracellular voltage waveforms recorded in the vicinity of the polymodal nociceptor (modified from Pancrazio, 2003). Also shown is a hypothesized refractory "recovery" function R taking on values from 0 to 1 during the AP.....	6
Figure 2-3: Markov Chain stochastic model for a single neuron, firing randomly a constant mean rate. There is a recovered state (K) and K-1 refractory states associated with recovery of the neuron following an action potential.....	7
Figure 2-4: The model sums the action potentials from many randomly oriented, and randomly weighted neurons plus noise into a single composite signal.....	9
Figure 2-5: V_{rms} vs. Number of Neurons for Firing Rates of 5-25 Hz with Absolute Refractory Period	13
Figure 2-6: V_{rms} vs. Firing Rate for 5-25 Neurons with Absolute Refractory Period	14
Figure 2-7: $\log(V_{rms})$ vs. $\log(\text{Number of Neurons} * \text{Firing Rate})$ with Absolute Refractory Period	14
Figure 2-8: Original and recovered waveforms.....	17
Figure 2-9: : Original waveform with second spike and Recovered AP Waveforms with uniform weights.....	18
Figure 3-1: Typical SK-N-BE(2c) cell cluster after 10 days in culture.	22
Figure 3-2: (A) shows a 15 day after plating microphotograph of a surface adherent (S) cell being patched. (B) shows the voltage clamp protocol utilized to stimulate the cells; a sequential depolarizing potentials of -40, -30, -20, -10, 0, 10, 20 and 30 mV were applied from -70 mV and sustained for 1.5 s. (C) Membrane response for an electroactive S cell, note the large activation events. (D) Membrane response for a non electrogenic cell, note the absence of activation events.	26
Figure 3-3: Membrane response for an electroactive SK-N-BE(2c) S cell 12 days after plating, showing the activation and inactivation currents. Each trace	

<i>corresponds to sequential depolarizing potentials of -40, -30, -20, -10, 0, 10, 20 and 30 mV from -70 mV baseline.</i>	27
Figure 3-4: Dopamine Synthesis (Modified from Molson, 2000)	28
Figure 3-5: Dopamine Metabolic Pathways (Modified from Okereke, 2002)	29
Figure 3-6: HPLC-EC of the cell culture media and its response to a selective MAO-i inhibitors and Dopamine, as compared to the elution standards.	31
Figure 3-7: HPLC-EC comparing the response to MSG of the cells in culture, versus several standards. Notice that the matching peaks correspond to DOPAC, DA, HVA and n-Me-5HT	33
Figure 3-8: Digital microphotograph of cells after 35 days in culture, stained with Cell Tracker Green®. Notice the globular structures (bright “dots”) present in most of the neurite-like processes. Microphotographs were obtained using an Olympus BX-60 epi-fluorescent upright microscope.	34
Figure 3-9: 40 X Digital microphotograph of a group of cells after 6 days in culture, immunostained with anti-synaptophysin (green) and anti-dopamine receptor (red). The bottom right image shows the composite of the prior three panels overlaid. Yellow color in the bottom left panel implies colocalization of the fluorescent markers.	35
Figure 3-10: 60 X Digital microphotograph of cells after 20 days in culture, immunostained with anti-synaptophysin (green) and anti-dopamine receptor (red). The bottom right image shows the composite of the top two panels overlaid.	36
Figure 3-11: Bright field and fluorescent image of GFP transfected SKN-B-E(2)C cells. Transfection efficiency above 30% is commonly accomplished.	37
Figure 3-12: SK-N-BE(2c) cells, 7 days after plating, screened with live-dead assay: Fluorescein Diacetate (FDA), green fluorescence, serves as a marker of cell viability - Propidium Iodide (PI), red fluorescence, stains the nuclei of non-viable cells.	39
Figure 4-1: Idealized Biosensor Design	42
Figure 4-2: Cell culture chamber # 1, machined from Teflon®, incorporates ITO-coated glass, and Ag/AgCl ring electrode in an open chamber which can be covered during cell incubation, or when carrying out repeated measurements over time, but opened when access to the cell surface is required.	45

Figure 4-3: 3D rendering for the CCC #2 (Artwork by Donald Natale III.) This 3D model was utilized by the Penn State Engineering Machine Shop to manufacture the chamber out of Teflon®.....	47
Figure 4-4: Assembled CCC #2 showing the special DB9 to BNC adaptor in one side and fluidic connections to the input and output ports.....	48
Figure 4-5: Multi-microelectrode designs: Both panels represent independent masks for standard microscope slides, 2.5 x 7.5 cm. The top corresponds to a differential electrode arrangement; cells are grown in the central circular pads and recordings will be performed between the central electrode and the surrounding ring. The second corresponds to a stimulus/record setup, where cells can be grown between electrode pairs and one electrode can be used for stimulation and the second one for recording.....	49
Figure 4-6: Synthesis of poly(organophosphazenes) via macromolecular substitution. The procedure involves the nucleophilic substitution of the highly reactive intermediate, poly(dichlorophosphazene), by alkoxides and/or amines.....	51
Figure 4-7: Cytotoxicity experiments using commercially available cell lines: Hela (ATCC), L929 (ATCC) and MDCK (ATCC) cells in the presence of aqueous solutions of MEEP at various dilution factors.....	54
Figure 4-9: Confluence after 24 and 48 hours in culture, expressed in a percent basis for the tested materials. The whole cell culture substrate was coated with the specific cell culture material and the confluence measures were performed under a microscope with a 10x objective. N = 15 for each material tested.....	58
Figure 4-10: Differential Cell Adhesion after 3 days in culture: A) 2 (MEEP), B) 1 (TFE), C) 4 (PMCP), D) 3 (PMCPP), E) Photolithographically patterned circle of 2 onto 4, F) Microstamped pattern of 3 onto 1.....	61
Figure 4-11: TFE over TFE, 250 µm square stamps made out 50 µm square features	63
Figure 4-12: Magnitude plot for the specific impedance of TFE (1) and PMCPP (3) as compared to the test chamber.....	64
Figure 4-13: ToF-SIMS image of cells cultured over PMCP indicating: a) Total ions collected. b) m/z 184 phosphatidylcholine characteristic fragment c) m/z 1355 PMCP pentamer d) m/z 686 GlyHisTyrArgGlyAsp e) m/z 856 ProValAlaLeuPheArgGlyAsp	69

Figure 5-1: Bio-Electric-Potentials, recorded by means of the CCC #1, for 5 and 35 days after plating. Upper panels show individual field potential waveforms for days 5 and 35 after plating. Lower panel shows pacemaker-like slow potential spikes observed at day 35.	77
Figure 5-2: Time signals, and normalized ARy and Gy for 30 s recordings obtained using CCC#1; 5, 10, 20 and 35 days after plating. Blue and red tracings correspond to independent experiments performed at the same day. Recordings were performed under identical conditions using the same devices and settings.	79
Figure 5-3: Plot of Multiunit Spike amplitude versus Single Unit Spike Amplitude Ratio as a function of time (Silva, 2005).	81
Figure 5-4: Microphotograph of the Tungsten-Parylene 50 μm electrodes (TPE) in contact with a small cell cluster, 3 days after plating.	84
Figure 5-5: Microelectrode recording, from an SK-N-BE(2c) culture 3 day after plating over PMCP coated glass. Recordings were obtained using tungsten-parylene 50 μm electrodes (A-M Systems, Carlsborg, WA). As previously described (Section 5.1).	85
Figure 5-6: Power spectrum for the autocorrelations of signal and noise, as a measure of activity in the vicinity of the cells for a 3 day microelectrode recording. ARn corresponds to the electrode located 100 μm away from the cells ARap was obtained by subtracting ARn from ARy.	86
Figure 5-7: ARn for the TPE microelectrode at 150, 200 and 250 μm away from the cells.	87
Figure 5-8: Time signal and Normalized ARy and Gw for 3, 6, 9, 12 and 25 days after plating using the TPE microelectrode. Blue and red tracings correspond to independent experiments performed at the same day.	88
Figure 5-9: 20X microphotograph of the microelectrode in contact with the SK-N-BE(2c) cell substrate, 10 days after plating. There is a lensing effect in the area surrounding the electrode due to the displacement of fluid.	92
Figure 5-10: Confocal Microphotograph of a 10 DAP culture stained with Cell Tracker Green, (Cambrex Bio Science Walkersville, Inc.), showing vertical and horizontal cross sections.	92
Figure 5-11: Normalized ARy and Gw for 3 and 10 days after plating recordings. Green tracings correspond to the macroelectrode signal and magenta tracings correspond to microelectrode recordings. Recordings were	

<i>performed simultaneously under the same experimental conditions and using the same Ag-AgCl counter electrode.</i>	93
Figure 5-12: <i>Normalized ARy and Gw for 15 and 20 days after plating recordings. Green tracings correspond to the macroelectrode signal and magenta tracings correspond to microelectrode recordings. Recordings were performed simultaneously under the same experimental conditions and using the same Ag-AgCl counter electrode.</i>	94
Figure 6-1: <i>Macroelectrode signals from a 35 day cell culture using the CCC #1, showing the baseline activity as compared to 1 mM MSG stimulation, and the recovery from stimulation after washout of the MSG containing solution.</i>	101
Figure 6-2: <i>Signal, autocorrelation and power spectrum measures for the 35 DAP macroelectrode signals presented in Figure 6-1. The upper panels show the baseline activity from three consecutive 10 s segments as compared to 1 mM MSG stimulation, presented in the lower panels. The consecutive segments, in order, are red, green and magenta.</i>	102
Figure 6-3: <i>Signal, autocorrelation and power spectrum measures for a 6 DAP microelectrode recording. The upper panels show the baseline activity from three consecutive 10 s segments, as compared to 1 mM MSG stimulation, presented in the lower panels. The consecutive segments, in order, are red, green and magenta.</i>	103
Figure 6-4: <i>Average activity AR(0) for three consecutive 10 s segments in response to MSG for the 3 DAP macro electrode recording, from dataset number 3 (section 5.5). Base corresponds to baseline, recorded in the presence of MSG, prior to the addition of MSG; MSG, corresponds to the response to the three independent MSG concentrations, dissolved in DMEM and Recov, corresponds to the recovered signal after the chamber has been washed out with DMEM.</i>	105
Figure 6-5: <i>Behavior of cells 3 DAP in response to 50 μM carbexonolone. First row depicts baseline behavior, prior to the flow of carbexonolone. Second row shows the behavior as cells are being bathed with carbexonolone solution. Last row depicts the recovered behavior after the carbexonolone containing solution has been thoroughly washed out with DMEM.</i>	108
Figure 6-6: <i>Microphotography of cells growing on top of one of the differential electrode plates, 25 days after plating, superimposed to a cartoon of the differential electrode arrangement and the signal acquisition setup, to provide a relationship of the relative size of the electrodes as compared to the cells.</i>	110

Figure 6-7: Signal, autocorrelation and power spectrum measures for one of the differential electrode plates, 25 DAP. The upper panels show the baseline activity from three consecutive 10 s segments, as compared to 1 mM PH stimulation, presented in the lower panels. The consecutive segments, in order, are red, green and magenta	111
Figure 6-8: Average activity AR(0) for three consecutive 10 s segments and two electrodes located in the same cell culture substrate (N=6), in response to MSG and PH.....	112
Figure 6-10: Comparison between mean activation of cells responding to 50 and 500 μ M Sulpiride and SCH23390 for 15 DAP differential macroelectrode recordings.....	117
Figure 6-11: Levinson algorithm applied to 6 and 25 DAP microelectrode autocorrelations from data set number 2 (Section 5.4).	120
Figure 6-12: Levinson algorithm applied to 5 and 35 DAP macroelectrode autocorrelations, from data set number 1 (Section 5.3),	121
Figure 6-13: Levinson algorithm applied to 15 DAP micro-macro-electrode autocorrelations, from data set number 3 (section 5.5). Macroelectrode signal is the red tracing and microelectrode is the blue tracing.	122
Figure 6-14: Levinson algorithm applied to to 15 DAP micro-macro-electrode, recordings from data set number 3 (section 5.5). Dose response to 5 mM PH is presented. Macroelectrode signal is the red tracing and microelectrode is the blue tracing.	123
Figure 6-15: Levinson algorithm applied to to 15 DAP differential macroelectrode , recordings presented in section 6.3.1. Response to 50 μ M Sulpiride is presented. Baseline signal is the blue tracing and Sulpiride response is the blue tracing.	124

LIST OF TABLES

2-1: Parameter Definitions for the Model	10
4-1: Physical material characterization of the selected polyphosphazenes	56
4-2: Characterization of the selected polyphosphazenes	56
4-3: T-test results, comparing mean attachment to the polymer films, after 24 and 48 hours in culture.	59
5-1: Summary of the experiments presented in this chapter.....	73
6-1: Population Response to MSG and Promazine Hydrochloride	114

ACKNOWLEDGEMENTS

I wish to thank Dr. Roger Gaumond, for his advice and dedication through out this work and for his emphasis in the quality of the presented results.

I wish to thank Dr. Harry Allcock for providing so much support towards the completion of this work and for sharing some of the costs of the research.

I wish to thank Dr. Byron Jones for providing advice with respect to the pharmacological aspects developed in this research.

I wish to thank Dr. Nandini Vasudevan for providing the cell line and helping initiate this line of research.

I wish to thank Dr. Gong Chen for his help in the electrophysiological aspects of this work.

I wish to thank Dr. Jeffrey Zahn for his advice in micro fabrication that aided in the development of the multi-electrode systems.

I specially wish to thank, my friends Eric W. Barrett and Donald Natale III, who are the greatest collaborators you could expect when developing a new line of research.

I wish to thank the following individuals for their aide and collaboration in completing this research: Miss Jamie Kowal, Mr. Ji-Sun Kim, Mr. Justin Zook and Mr. Jason Moyer, for their undergraduate research in Dr. Gaumond's laboratory. Ms. Elaine Kunze and Ms. Susan Magargee, from the Center for Quantitative Cell Analysis; Mr. Eugene Gerber, from Bioengineering; Dr. William Scheuchenzuber from the Hybridoma & Cell Culture Laboratory and Dr. Mwita Phelps, from Dr. Allcock's laboratory;

I wish to thank Dr. Amit Das, and State of the Art, Inc.; for their collaboration in completing the multi-electrode arrays and their interest in further development of this research.

I wish to thank Dr. John Beard and Dr. Anne Andrews for their independent collaboration in completing HPLC analysis and Ms. Laura Bianco for running all of the HPLC tests.

I wish to thank The Huck Institutes of the Life Sciences, The Department of Bioengineering, The Integrative Biosciences Graduate Degree Program and Universidad Simon Bolivar, for providing me with the education and the resources to complete this research.

I specially want to thank the administrative staff from both the Huck Institutes and the Bioengineering Department. In particular, I would like to thank Dr. Ann Marie Daniels, Ms. Julie Brenneman, Ms. Janice Kennedy, Ms. Doretta Garvey, Ms. Carol Boring and Ms. Rita Kline.

Last but not least, I want to thank my family, my wife Sandra who is always helping me complete the tasks at hand, and supporting my work and research, besides helping me realize all that I am doing wrong and helping me become a better, person, husband and father; my son Miguel and my daughter Isabel, who are the nicest kids that you could possibly dream of; my mom, dad and grand parents who taught me the value of education and of hard work.

I would like to thank the rest of my friends; family; professors; students and all the natural and supernatural forces who have helped me become the person I am today.

Chapter 1

Introduction

The study of spatial-temporal interactions of neural populations, both *in vitro* and *in vivo* is of fundamental interest for neurological research. Extra-cellular monitoring of the electrophysiological activities from neural cell cultures has long been recognized as a valuable tool for neuroscience research (**Novak, 1986**). Effort has been devoted, to develop experimental systems in which populations of neurons are grown in defined patterns, over a physical substrate that allows simultaneous stimulation, visualization and recording from the system.

Thomas, 1972 started experimenting with planar electrode arrays to monitor the activity of cultured cells. Since then, many researchers have developed systems for recording simultaneously from an array of electrodes on the surface of a culture dish (**Gross, 1977; Gross, 1982; Gross, 1985; Gross, 1992; Jimbo, 1993; Borkholder, 1997; Branch, 2000; Heuschkel, 2002**). Microelectrode arrays have become a common solution for many of the technical problems and systems have been developed for monitoring the individual action potential response of groups of neurons both *in vivo* (**Novak, 1986; Maher, 1999; deCharms, 1999**) and *in vitro* (**Thiebaud, 1997; Oka, 1999; Cunningham, 2001**). These systems are aimed to provide recording of individual neurons over a planar array of evenly distributed electrodes, and simultaneous optical microscopic observations.

There are many ways to process the individual signals from neurons in a neural network (**Jimbo, 2000**). Much of the attention in analysis of action potential waveforms has been on finding individual spikes in a noisy record (**Fee, 1996; Stitt, 1998; Gaumond, 1993; Zouridakis, 2000**) or in developing systems for analyzing the interrelationship between the neurons recorded and a particular stimulus (**Gaumond, 1982; Gaumond, 1983; Gross, 1992**). There are cases where the "summed" signal may be of greater interest than single spike analysis (**Gaumond, 2004**). Neurons do not function in isolation but are organized in collective action of groups of neurons, or cell assemblies (**Hebb, 1949; Martignon, 2000**). In order to gain experimental evidence for cell assembly activity in the brain, the activation of many separate neurons has to be recorded simultaneously (**Martignon, 2000**). Correlational measures (**Schiff, 1996**), advanced cross correlation techniques (**Martignon, 2000; Golmeh, 2002**), and different types of clustering (**Fee, 1996; Zouridakis, 2000; Baker, 2000**) are examples of approaches to the data processing problems posed by such systems.

While much effort has been devoted to recording large numbers of individual neurons, the amount of information extracted so far is limited. The aim of this research is to develop a system to study a signal recorded from a population of neurons without distinguishing individuals in the population. Analysis of the summed neuronal signal provides useful information about the "average" response of neurons to an applied stimulus. In some applications, such as high throughput drug screening this "average" response is appropriate. In other applications, such as cell-cell communication the "average" response may prove to be a useful adjunct to standard techniques, which monitor individuals within the population.

There are potential advantages in using such a system to monitor electrical activity in cell cultures. For example, coupling of individual neurons to individual microelectrode pads is problematic and may be transient. There are applications where characterization of group behavior or tendencies is inherently required. For instance, it might be important to determine what percent of neurons in a culture dish responded to the introduction of neural stimulant and how this is related to the physiology of the system.

Some examples of situations where applications of the summed neural signal may provide useful measures of neural behavior are:

- In a neural biosensor application, the detection of an increase in summed neural discharge from a group of sensitized neurons might provide a useful way of detecting biohazards, especially neurotoxins (**Bousse, 1996**).
- In characterizing the stability of any multielectrode "system" (*in vitro* or *in vivo*) it may be useful to monitor the summed signal to see if the spectrum is decreasing in bandwidth over time, suggesting movement of neurons away from the electrodes due to encapsulation or protein deposition.
- In studies of synapse formation, the emergence of signal energy different from prerecorded baseline, and occurring several ms after the peak of an "averaged waveform" signal could provide a progressive quantitative characterization for synaptogenesis *in vivo*, and so add a new dimension to *in vitro* studies.
- In studies of neural degeneration, such as Parkinson or Alzheimer disease, if a fully synaptic network is allowed to degenerate, and cell-to-cell communication

becomes weakened, this system could provide a useful tool to measure the level of neural/synaptic degeneration.

The author of this dissertation seeks to validate the utilization of a summed neural signal as a powerful technique for neuroscience research. Multiple aspects were studied and integrated in order to provide such validation:

- A mathematical model was developed to study the expected behavior of a summed electrical response for a group of non-synaptic neurons.
- A human derived neuroblastoma cell line was studied and characterized to serve as a substrate for neurophysiologic research and confirm the mathematical model.
- An electrophysiological platform was developed, to measure the level of electrical activation and communication of the neuroblastoma cell line.
- A collaboration was established to develop novel polyphosphazene based biomaterials to guide and maintain the spatial localization of the cells in the electrophysiological platform.
- The macroelectrode approach was validated by its use in characterizing the electrical response of the neuroblastoma cell line.

1. Chapter 2

Stochastic Model for Summed Neural Activity

Information derived from an electrode that records activity of many neurons discharging nearby is considered in this chapter. As a first approximation, neurons are assumed to be non synaptic and the relationship between individual events is completely stochastic. A model was developed to calculate the discharge probability of a set of uncorrelated non-synaptic neurons. The model computes the signal generated by the additive response of a population of neurons in the vicinity of an electrode. This is equivalent to recording Field Potential signals (FP) from a group of neurons grown on the surface of an electrode or in a volume, surrounding an implanted electrode Figure 2-1. Results discussed in this chapter have previously been presented in ([Gaumond, 2002](#); [Silva, 2003](#) and [Gaumond, 2004](#)).

Figure 2-1

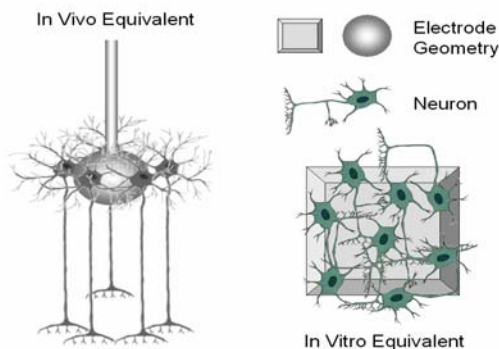


Figure 2-1: Neural cells on an electrode substrate. The electrode sums the neural activity of all cells. Currents produced by Action Potentials from cells contribute minute voltage fluctuations at the electrode surface

Figure 2-2

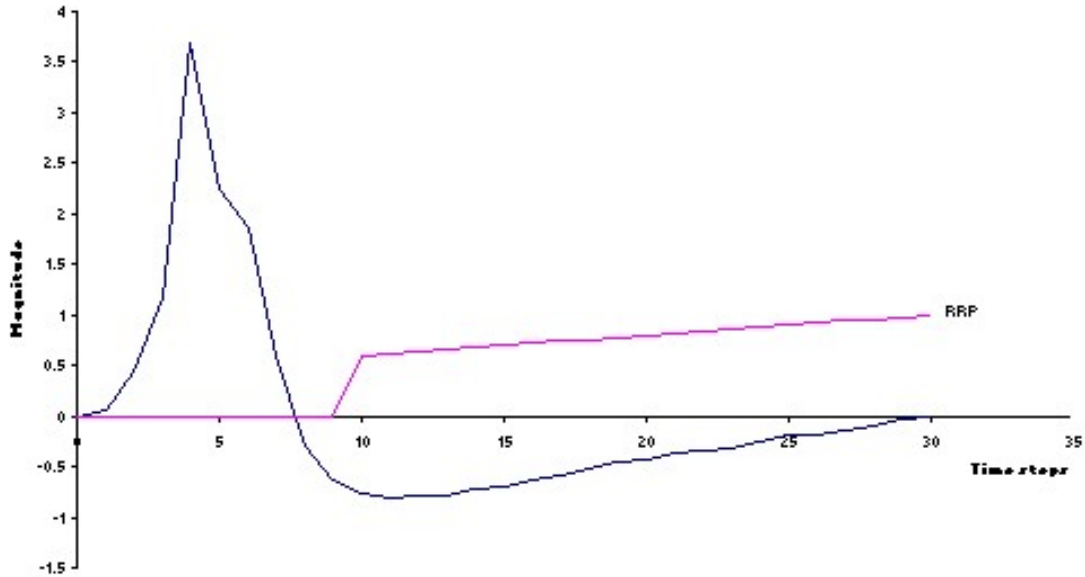


Figure 2-2: The AP waveshape of the extracellular voltage waveforms recorded in the vicinity of the polymodal nociceptor (modified from Pancrazio, 2003). Also shown is a hypothesized refractory "recovery" function R taking on values from 0 to 1 during the AP.

Spontaneous neuronal field potentials vary according to multiple factors, such as the type of neuron, distance to the electrode, electrode geometry, etc.; however the field potential from a particular neuron is fairly consistent. A neural system with a well characterized field potential is the polymodal nociceptor (pain receptor) found in the dorsal root ganglion. These cells have a distinct AP waveshape, with "plateau" region, as shown in Figure 2-2 . A waveform (Gold, 1996; Pancrazio, 2003) was digitized and artificially extended to reflect the absolute refractory period. Two rules were followed: first, the total integrated area of the waveform had to be zero and second, the duration of the action potential waveform should be approximately thirty milliseconds, $K = 30$ and Δt

$= 1$ ms. A current vector \mathbf{C} of length K , such that $\|\mathbf{C}\| = 1$ can be associated with the temporal course of the extra cellular current generated by the neuron.

A K state Markov chain representation of a single neuron was developed, **Figure 2-3** such that each state is associated with the corresponding value of \mathbf{C} (**Gaumond, 2002**). There is a resting state K , and there are $K-1$ states during which the neuron is considered "refractory", i.e., has a diminished firing probability. A neuron whose transmembrane potential is at its resting potential is in the state labeled K . At each time increment $i\Delta t$, a neuron in state K either discharges (transits from K to 1) or remains at K . Once the cell discharges it moves to state $k+1$, until it is "fully recovered" by reaching state K again.

Figure 2-3

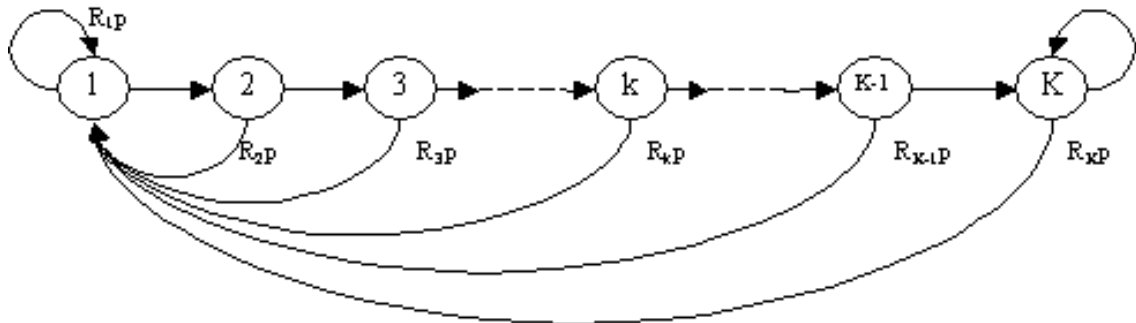


Figure 2-3: *Markov Chain stochastic model for a single neuron, firing randomly a constant mean rate. There is a recovered state (K) and $K-1$ refractory states associated with recovery of the neuron following an action potential.*

The recovery process can be described by vector \mathbf{R} (recovery) and constant p (transition probability), so that a neuron is completely described by the set of 1-step transition probabilities from state k to state k' .

Eq. (2.1)

$$\begin{aligned} P_{k,k'} &= R_{kp} \quad \text{for } k=K \\ &= 1-R_{kp} \quad \text{for } k= k+1, k =1,2,3...K-1 \end{aligned} \quad \text{Equation 2.1}$$

Setting $\mathbf{R} = [0, 0, 0, \dots, 0, 1]$ yields a neuron which is absolutely refractory until it reaches stage K where it has a constant firing probability of p.

For a finite-state Markov chain, there exists a Steady-State occupation probability associated with each state, and this set of steady state probabilities is related algebraically by the state transition probabilities between states. Let Π_k be the Steady State probability of occupying state k. The average firing rate (FR) of the neuron is $\Pi_1/\Delta t$, and

Eq. (2.2)

$$\Pi_1 = p \sum_{k=1}^K R_k \Pi_k = \sum_{k=1}^{K-1} R_k \Pi_k + p R_K (1 - \sum_{k=1}^{K-1} \Pi_k) \quad \text{Equation 2.2}$$

Eq. (2.3)

$$\Pi_1 = \frac{p R_K}{1 - p \sum_{k=1}^{K-1} (R_k - R_K) \prod_{k'=1}^{k-1} (1 - p R_{k'})} \quad \text{Equation 2.3}$$

For example, in the case of a neuron with an absolute refractory property, we let $\mathbf{R} = [0, 0, \dots, 0, 1]$ and

Eq. (2.4)

$$FR = \frac{\Pi_1}{\Delta t} = \frac{p / \Delta t}{1 + (K - 1)p} \quad \text{Equation 2.4}$$

If instead of assuming an absolute refractory property, we modify the \mathbf{R} vector to account for a relative refractory period, then the case will be that depicted on **Figure 2-3**,

where the transition probabilities to state 1, increase linearly by a factor 0.6 to 1 beginning with the 10th state of the Markov Chain (10 ms for this simulation).

2.1 Summation of Currents at the Electrode

The discharge activity of several neurons contributes to the signal monitored at the electrode, as shown in Figure 2-4 . A current vector \mathbf{C} is associated to each neuron and there are many of such neurons with identical characteristics. Each neuron's contribution to the total current entering the electrode is weighted by a factor accounting for cell geometry and for variations in conductive pathway between cell and electrode surface. Let this weighting be characterized by vector \mathbf{W} of length L. Elements of \mathbf{W} correspond to a Gaussian distribution of randomly assigned magnitudes.

Figure 2-4

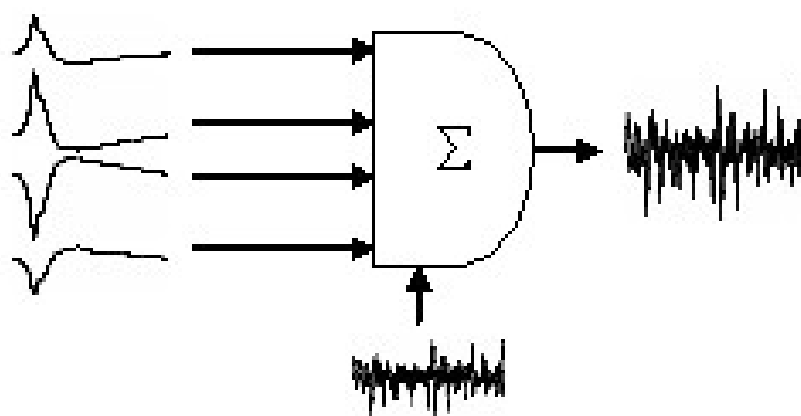


Figure 2-4: *The model sums the action potentials from many randomly oriented, and randomly weighted neurons plus noise into a single composite signal.*

The total electrode current at $i\Delta t$ is

Eq. (2.5)

$$Y_i = N_i + \mathbf{W}^T x S_i x C$$

Equation 2.5

N_i is an electrode current "noise" signal at time $i\Delta t$. S_i is the state matrix of the system, where a 1 at position (n, k) indicates that neuron n occupies state k at time $i\Delta t$.

The total contribution of neural currents at the electrode can be denoted $AP_i = \mathbf{W}^T x S_i x C$

At this point a summary of the previously defined variables is convenient (Table 2-1).

Table 2-1

2-1: Parameter Definitions for the Model

Variable	Definition
C	Current vector that characterizes the temporal response of individual neurons
K	Length of the current vector C
p	Transition probability from state k to k'
R	Recovery vector that defines the step transition probabilities of the system
FR	Average Firing Rate for the system
W	Weighting factor accounting for variations in conductive pathway between cell and electrode
L	Number of neurons
Si	State matrix indicating the state of each neuron at any particular time $i\Delta t$
Ni	Current "noise" signal at any particular time $i\Delta t$
APi	Total contribution of neural currents at the electrode
Yi	Total electrode current at $i\Delta t$

2.2 RMS of the Electrode Signal

The root mean square (RMS) value of the signal Y_i recorded at time interval $I\Delta t$ is:

Eq. (2.6)

$$RMS_Y = \sqrt{\frac{1}{I} \sum_{i=1}^I (N_i + AP_i)^2} \quad \text{Equation 2.6}$$

If signal and noise are uncorrelated, and noise \mathbf{N} is zero-mean, then the expected value of RMS_T is:

Eq. (2.7)

$$E(RMS_Y^2) = \sigma_N^2 + E\left(\frac{1}{I} \sum_{i=1}^I (AP_i)^2\right) \quad \text{Equation 2.7}$$

If we fully expand the Eq. (2.7) then at time $I\Delta t$ the expression will reduce to:

Eq. (2.8)

$$\sigma_N^2 + E(RMS_Y^2) = \sigma_N^2 + \frac{L \times FR \times K \times I \times \Delta t}{I} E(\|\mathbf{W}\|^2) E(\|\mathbf{C}\|^2) \quad \text{Equation 2.8}$$

So in the limit, RMS_Y will be determined as the square root of the sum of a noise term σ_N^2 , and a term which grows linearly with the summed firing rate for all neurons ($L \times FR \times K \times \Delta t$). Because K is a constant intrinsic to the action potential length and Δt depends on the sampling rate, then the driving term will be the product of the number of neurons times the firing rate. Consider the "low firing rate" condition where the probability of simultaneous firing from multiple neurons is vanishingly small, then the RMS_Y will be dominated by noise and the number of neurons being sensed; on the other

hand, if $LxFR$ is big, then this will control the response of the system and the effect of the noise could be neglected, even in the case when the signal to noise ratio is equal to 1.

In practice, as neural firing rate increases in response to applied stimuli, the term WxS_ixC will not grow linearly with the number of firings/sec, because action potential currents from one neuron may cancel those from adjacent neurons either because of geometrical factors, or because discharging neurons are at differing portions of the AP. Simulations are used to compare the growth of RMS signal with $LxFR$ to the "low rate" prediction of a square root relation.

2.3 Simulation: Signal RMS versus Firing Rate

Counting processes for neuron counts L of 5, 10, 15, 20 and 25 were simulated. The neurons themselves were identical with shape **C** and refractory recovery **R** as shown in Figure 2-1 :

Eq. (2.9)

$$\begin{aligned} R &= 0 \text{ for } k = 1, 2, \dots, 9 \\ &= .6 + .4(k-10)/20 \text{ for } k = 10, 11, \dots, 30 \end{aligned} \quad \text{Equation 2.9}$$

This function was chosen to provide an absolute refractory period during the positive portion of the AP and a slow recovery of activity during the after potential.

The relation of Eq. (2.3) was inverted numerically to find a value of p corresponding to each firing rate simulated, FR of 5, 10, 15, 20, and 25.

The elements of the L -dimensional weight vector **W** and those of I -dimensional noise vector **N** were chosen to have elements with a zero mean, normal Gaussian

distribution truncated at 2 standard deviations, with a RMS value of 1. For each value of L and each value of FR, 5 simulations of 60 seconds of discharge activity were carried out and the results plotted separately for increasing FR and for increasing L and then for the product FR x L as shown in Figure 2-5, Figure 2-6 and Figure 2-7. The simulations were of 5, 10, 15, 20, and 25 absolutely refractory neurons, with firing rates of 5, 10, 15, 20, and 25 per second.

Figure 2-5

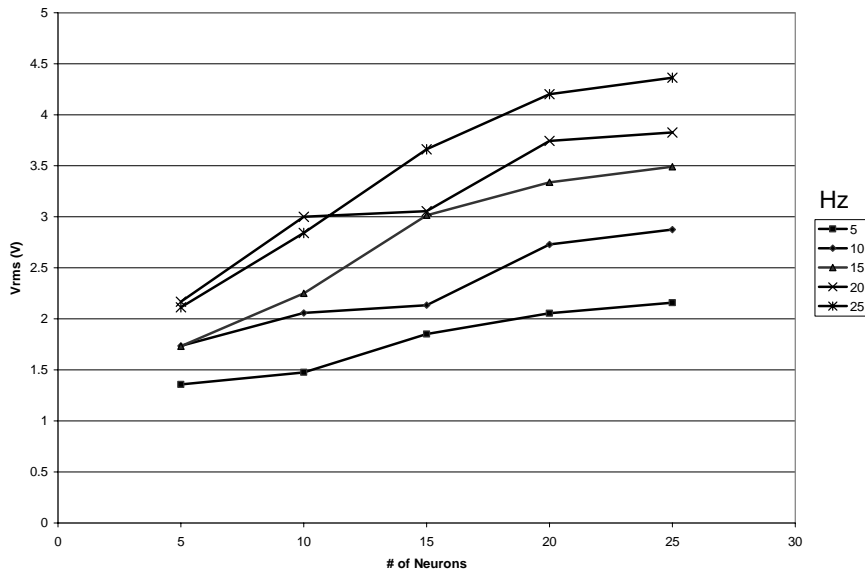


Figure 2-5: V_{rms} vs. Number of Neurons for Firing Rates of 5-25 Hz with Absolute Refractory Period

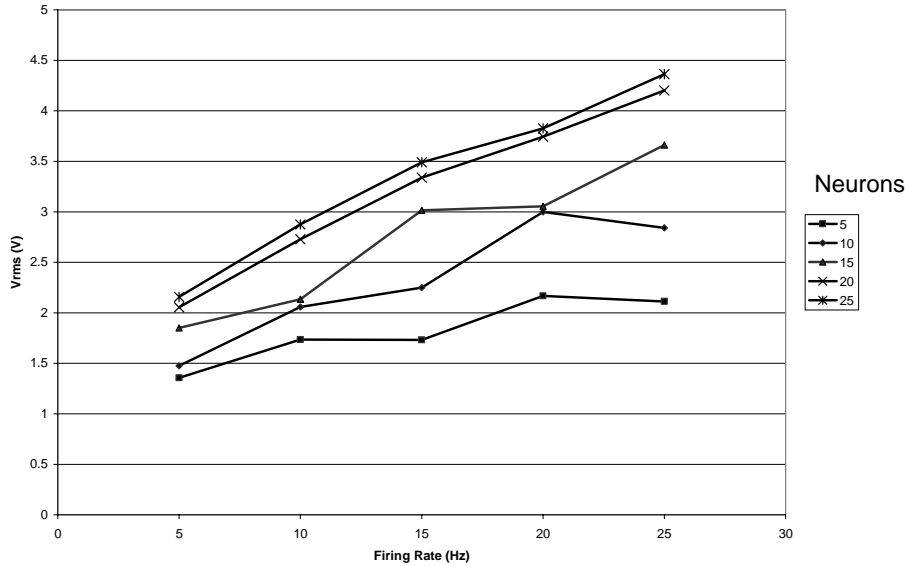
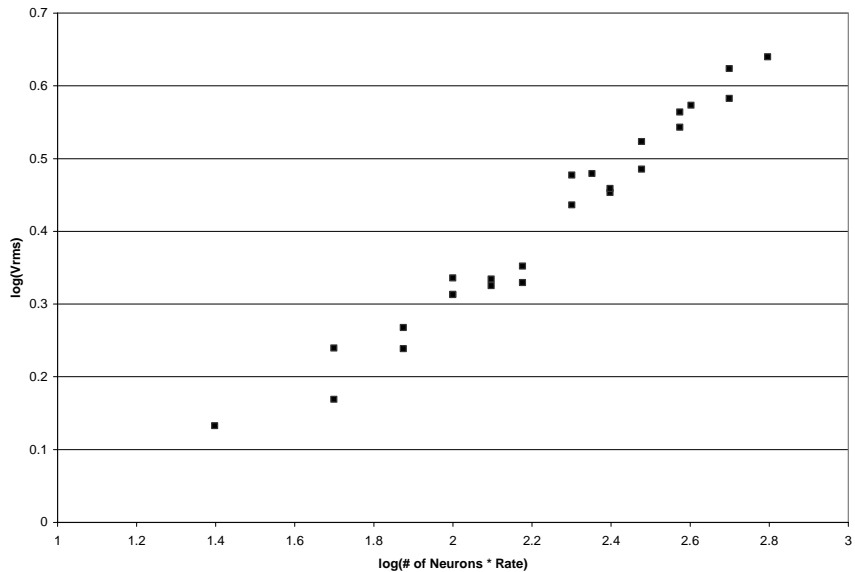
Figure 2-6Figure 2-6: *Vrms vs. Firing Rate for 5-25 Neurons with Absolute Refractory Period***Figure 2-7**Figure 2-7: *$\log(V_{\text{rms}})$ vs. $\log(\# \text{ of Neurons} * \text{Firing Rate})$ with Absolute Refractory Period*

Figure 2-5 shows the RMS value vs. number of neurons at each firing rate. Figure 2-6 shows the RMS value vs. firing rate at each number of neurons. Finally, Figure 2-7 combines the two graphs with a log-log plot of the RMS value vs. the product of the number of neurons and the firing rate. The plots indicate a general increase in RMS value as the number of neurons increases and as the firing rate increases. However, the slope of the points in log-log plot in Figure 2-7 is 0.39, slightly under the calculated slope of 0.5 from Equation 12. This result is expected because there is significant noise added to the signal and because of the assumption of a low firing rate.

2.4 Action Potential Waveform Recovery

$\text{AR}(1)$, the zero-lag value of the autocorrelation function $\text{AR}(j)$ is the variance, and provides a measure of the strength of signal response as described in section 2.3. $\text{AR}(j)$, $j=1,2,\dots,M$ can also provide an indication of shape of the action potential. This follows from the argument that the signal T_i can be thought of as originating from the convolution of an integer-valued signal corresponding to the number of neurons ($1,L$) firing in each time interval Δt , with current vector \mathbf{AP} . For independent neurons, the count of firings in each Δt is Poisson-distributed, with a high probability of zero-counts. This spectrum of such a signal is broad-band, approaching that of white-noise in the limit $\Delta t \rightarrow 0$.

The convolution of a broadband noise with vector \mathbf{AP} yields a signal whose spectrum is that of \mathbf{AP} . A vector \mathbf{AP}_R can then be recovered from $\text{AR}(j)$ using the Levinson algorithm, which solves the Yule-Walker Eq. (2.10). \mathbf{AP}_R should resemble \mathbf{AP}

with the intrinsic limitations from the system, that is, the scaling factor is lost, since the low frequency components of the signal are filtered and the quality of the \mathbf{AP}_R increases as the number of averaged AP's increases, hence as the length of the simulation increases. This will slow the process, since more points would have to be computed and analyzed.

Eq. (2.10)

$$\begin{pmatrix} R(1) & R(2)^* & \dots & R(M)^* \\ R(2) & R(1) & \dots & R(M-1)^* \\ R(M-1) & R(M-2) & \dots & R(2)^* \\ R(M) & R(M-1) & \dots & R(1) \end{pmatrix} \begin{pmatrix} C(2) \\ C(3) \\ \vdots \\ C(M) \\ C(M+1) \end{pmatrix} = \begin{pmatrix} -R(2) \\ -R(3) \\ \vdots \\ -R(M) \\ -R(M+1) \end{pmatrix} \quad \text{Equation 2.10}$$

Using the Levinson-Durbin recursion and the original waveform (Figure 2-2) as a template, we can quantify the effectiveness of the algorithm in recovering the AP shape Figure 2-8. Since the scaling factor is inherently lost from the process, the recovered AP is scaled in such a way as to make the maximum value match that of the original waveform. A moving window was used to correlate the peak of the recovered waveform with that of the original one to the account for the maximum likelihood (Silva, 2003). The wave forms were compared and the recovery error computed for different number of simulation points (Silva, 2003).

At 1 ms time steps, the recovered waveform follows the original relatively closely, including the small perturbation in the downward slope of the AP. As the time step decreases, the resolution of the AP waveform increases, but the quality of the recovered waveform decreases (Zook, 2003). Because the AP contains more points at higher resolutions, it becomes more difficult for the algorithm to resolve all of the details of the waveform. The Levinson algorithm therefore appears to be most effective at

recovering the AP shape at a resolution of 1 ms, when length of the AP is 30 ms (**Zook, 2003**).

Figure 2-8

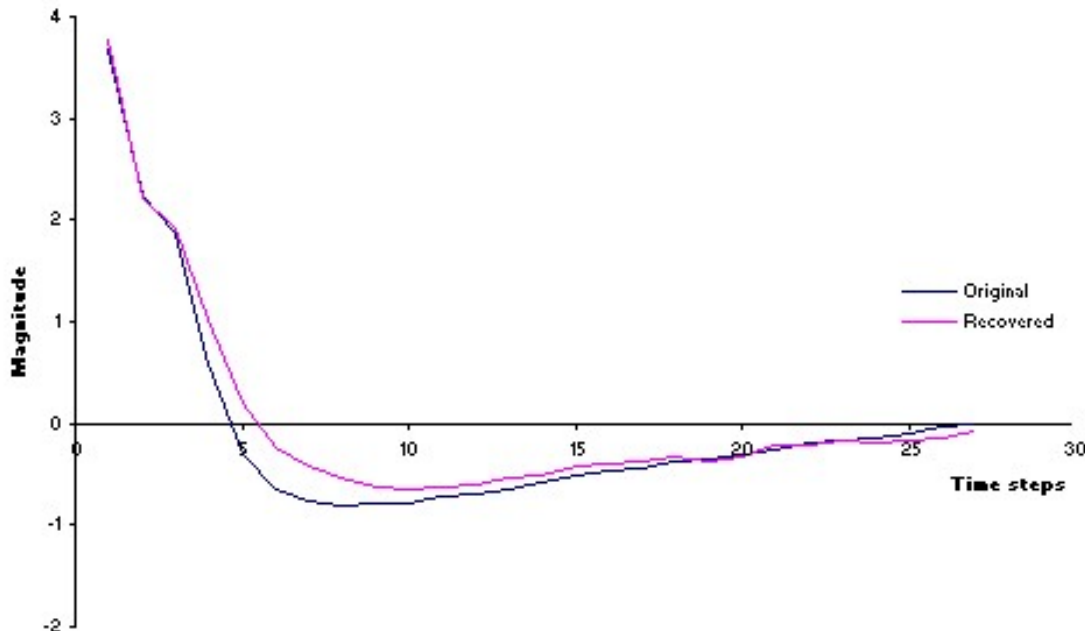


Figure 2-8: *Original and recovered waveforms.*

The term temporal correlation has been used to indicate chains of associated firing events at specific temporal intervals (**Martignon, 2000**). Terms like couple and triplet have been used to denote spatiotemporal patterns of two or three neurons firing simultaneously or in sequence (**Martignon, 2000**). The simulation protocol can be modified in order to account for the case of activity trains, where one neuron firing modifies the firing probability of one additional cell. In this case 5 out of 25 neurons where chained in such a way as for that the firing of the first neuron in the chain will force the firing of the second neuron with a 10 ms delay and successively until all five

fired in a temporal sequence. If we recover the signal from this new case, we can identify the coupled trains by observing a second peak in the recovered waveform Figure 2-9.

Figure 2-9

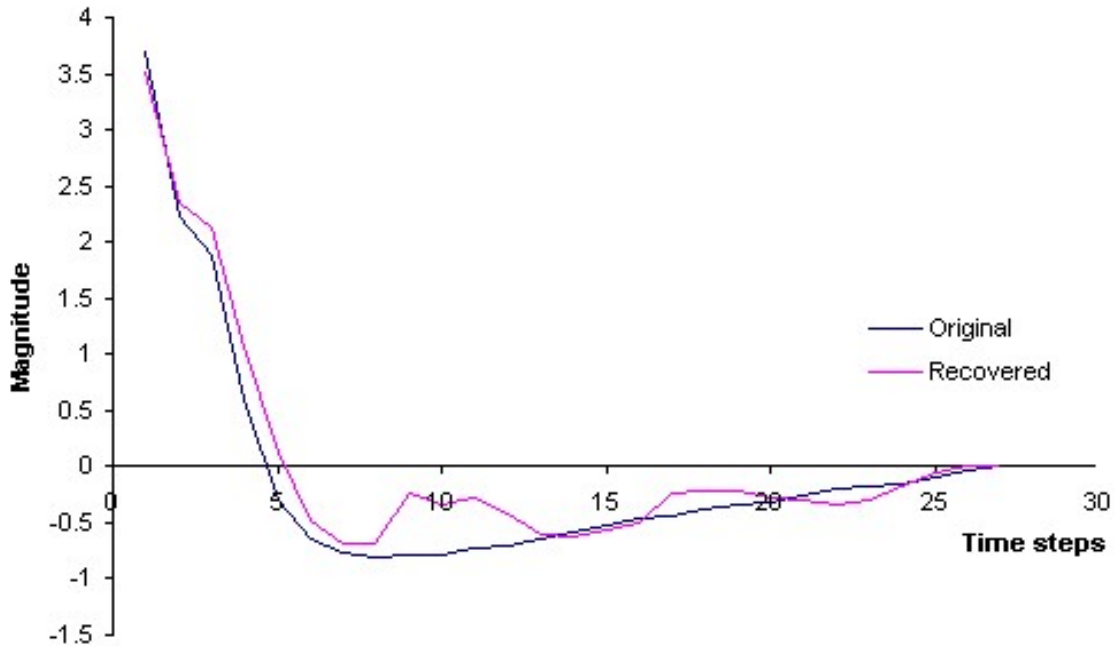


Figure 2-9: : *Original waveform with second spike and Recovered AP Waveforms with uniform weights*

With all neurons given equal weight, the recovered waveform contained diminished second and third spikes after the initial spike (Figure 2-9). The second spike is actually only about 8-9 ms after the initial spike in the recovered waveform, in contrast to the 10 ms delay that should exist. Similarly, the third spike is about 8-9 ms after the second spike. The second spike is approximately one-fifth as high as the initial spike because only 5 out of the 25 neurons are interconnected. The recovered waveform cannot be compared directly with the original waveform, due to the second and third

firings. However, it should be similar to the original with a second spike of one-fifth the amplitude, 10 ms after the initial spike.

2.5 Chapter Summary

Information recovery from a single electrode that sums the currents of a population of neurons is mathematically feasible. The root-mean-square value of the summed input voltage increases monotonically as neural activity increases, even though, the input signal is zero-mean. Sensitivity - that is, fractional change in voltage for fractional change in neural population - increases monotonically with neural population; accordingly, the larger the neural culture, the more sensitive the device.

In addition the average AP wave form for the system can be recovered using the Levinson-Durbin recursion. This approach also serves to recover spatiotemporal patterns of activity trains, where one neuron firing modifies the firing probability of one additional cell. In this case the coupled trains can be identified by observing secondary peaks in the recovered waveform.

Chapter 3

Characterization of the SK-N-BE(2c) Neuroblastoma Cell Line

3.1 Introduction

Validation of the stochastic model for summed neural activity (**2.1**) required a model cell. Such a cell needed to be stable, electrogenic and easy to manipulate. Multiple cell lines and primary cultures were considered for this purpose: Primary dorsal root ganglion neurons were originally considered as an ideal model for this research; however failure in extracting and isolating these cells opened the door to other possibilities. Primary cortical and hippocampal neurons from neonate rats are routinely extracted at Dr.Gong Chen's laboratory, however they are clearly synaptic cells and a non synaptic model was thought to be convenient for validation purposes. Rat pheochromocytoma (PC12) is a very popular dopaminergic cell line, utilized for neurotransmitter release research; however it does not produce overshooting action potentials (**Gribkoff, 1995**). The pluripotent murine embryonal carcinoma P19 is electrogenic and commonly used cell for neuroscience research, however it is highly heterogeneous and multiple phenotypes are co-expressed in the same culture (**McPherson, 1995**). In that sense, neuroblastoma cell lines seemed like a reasonable candidate for this research. Various neuroblastoma cell lines have been reported to produce action potentials and to be nonsynaptic (**Biedler, 1978; Standifer, 1994; Cheng, 1995; Ryan-Moro, 1996; Mathis, 2001**).

3.2 Background

Neuroblastoma (NB) is the most common extra-cranial childhood cancer, originating from the autonomic nervous system or the adrenal medulla (**Haase, 1999**). NBs account for 80% of pediatric cancers under the age of 5 years, being the most prominent solid cancer of this age group (**Haase, 1999; van Noesel, 2004**). NBs are neuro-ectodermal tumors of embryonic neural crest-derived cells with a complexity of genetic alterations (**van Noesel, 2004**). The neural crest in normal development gives rise to nerve cells of the sympathetic nervous system. NBs are considered to be embryonal tumors, which originate from a developmental defect that prevents normal cellular differentiation and locks cells in a state of increased division (**van Noesel, 2004**).

NB cell lines have been isolated both from primary tumors and from metastases. These cell lines do not generally show features associated to mature neurons, instead they show features characteristic of early embryonic and autonomic cells. They lack extensive arborisation and sprout short neuritic projections, unless they are induced to differentiate (**Biedler, 1978; Standifer, 1994; Cheng, 1995; Ryan-Moro, 1996; Mathis, 2001**).

The SK-N-BE(2c) Human Neuroblastoma Cell line was established by Dr. June Biedler, from the Laboratory of Cellular and Biochemical Genetics of the Sloan-Kettering Cancer Center (New York, NY) in November 1972 (**Biedler, 1978; Standifer, 1994; Cheng, 1995; Ryan-Moro, 1996; Mathis, 2001**). The cell line was developed *in vitro* from a bone marrow biopsy of a 2-year-old male patient with disseminated Neuroblastoma (**Biedler, 1978**). This cell line was the second line

established from the patient, since a prior biopsy (June 1972) also gave rise to an immortal cell line, the SK-N-BE(1n).

Figure 3-1

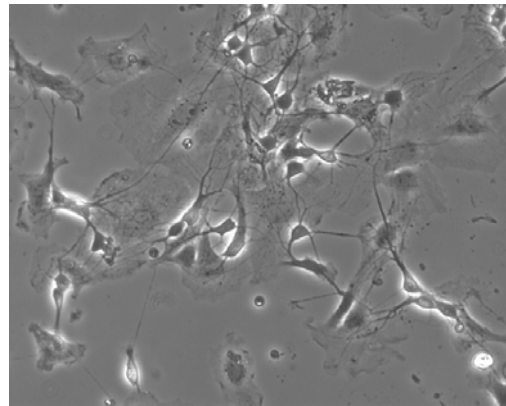


Figure 3-1: Typical SK-N-BE(2c) cell cluster after 10 days in culture.

SK-N-BE(2c) is considered to be an I-type (I) neuroblastoma: morphologically intermediate between neuroblastic (N) cells, which exhibit neurite-like properties, and substrate-adherent (S) cells having properties of Schwann/glial/melanocytic cells (**Ciccarone, 1989; Jori, 2001; Ross, 2003**). This I-type neuroblastoma can be induced into the N lineage with all-trans retinoic acid (RA) or into the S lineage with bromodeoxyuridine (BrdU) (**Jori, 2001**).

The SK-N-BE(2c) is tumorigenic (**Biedler, 1978**) and expresses the tumor necrosis factors receptors p55 and p75 (**Chambaut-Guerin, 1995**). The cells prefer tissue culture polystyrene rather than glass for attachment and that when grown over plastic replicates with an average population doubling time of 27 hr (**Biedler, 1978**). If left alone it will proliferate indefinitely, however, RA inhibits cell proliferation and induces morphological differentiation (**Chambaut-Guerin, 1995**). Before differentiation,

the SK-N-BE(2c) cells tend to grow in tight aggregates, consisting of cells with short neurite-like processes (**Biedler, 1978**). When differentiated with RA, SK-N-BE(2c) cells acquire a neuronal phenotype, with small cell bodies and long neurite-like processes with varicosities along their length (**Jori, 2001**).

Vitamin A and its derivatives retinal and retinoic acid, play an important role in normal cellular differentiation. Treatment of neuroblastoma cell lines in vitro with RA can mimic differentiation (**Sidell, 1983**). The cells change in morphology, biochemical activities and gene expression. The morphological changes include sprouting of thin dendrites, terminal arborisation, and axonal swelling (**Sidell, 1983; Chambaut-Guerin, 1995**). These changes are similar to those of maturing neural crest cells (**Sidell, 1983**).

SK-N-BE(2c) cells have been used extensively as a model system to study the role of estrogens on neural cells (**Agrati, 1997; Patrone, 2000**); and the differentiation of neural cells upon treatments with estrogens (**Maggi, 2000; Ciana, 2003**); retinoids (**Ponthan, 2001; Ponthan, 2003**) and Dehydroepiandrosterone (**Silvagno, 2002**). In addition, they have been used to study the pharmacological properties of the delta-opioid receptors, which are endogenously expressed in this cell line (**Namir, 1997; Hasbi, 1998; ; Hasbi, 2000; Allouche, 2000**). They are also considered a convenient model for studies of neural crest progenitor cells (**Jori, 2001**) and for the antiproliferative effects of Iron Chelators (**Richardson, 1997**).

3.3 Patch Clamp Recordings

Overshooting action potentials from the SK-N-BE(2c) neuroblastoma cell line have not been reported; however they have been reported from patch clamp recordings of other human SK-N derived neuroblastoma lines. Of particular interest are results presented by (**D'Amico, 2003**) from the 21S neuroblastoma sub-clone. The 21S displays the surface adherent (S) cell phenotype, appearing large flattened and highly adherent. This phenotype has traditionally been associated with the astrocytic lineage (**Ciccarone, 1989**), however the S cells proved capable of generating overshooting action potentials (**D'Amico, 2003**). Also, the 21S cells proved more electrogenic than their parent cell line, the SKN-SH-SY5Y which is an I type neuroblastoma (**D'Amico, 2003**). The prior research suggests that the electrogenic component in the SK-N-BE(2c) cell line could reside in the S, rather than the N cells. In order to confirm that hypothesis patch clamp recordings were performed in both the S and N cells 15 days after plating.

SK-N-BE(2c) cells were seeded on 15 mm #1 (0.13 to 0.16 mm thick) round cover slips at a density of 8×10^6 cells/ml and maintained in Ham's F-12: Minimal Essential Media (MEM, Gibco BRL) supplemented with 15% fetal bovine serum (Bioreclamation), 100 units/ml penicillin, and 50 µg/ml streptomycin. The cells were studied using the patch-clamp technique in the whole-cell configuration. Patch clamp recordings were performed at Dr. Gong Chen's laboratory with the invaluable assistance of Dr. Jinshun Qi.

Microelectrodes (3-5 MΩ in bath solution) were made from borosilicate glass capillaries (1 mm in diameter) pulled to a final internal diameter of about 1 µm using a P-

97 Micropipette puller (Sutter Instruments, CO). Electrophysiological measurements were made using a patch-clamp amplifier (MultiClamp, 700A, Axon Instruments, CA) and computer interface (Digidata 1322A, Axon Instruments). Clampex 9.0 software (Axon Instruments) was utilized for data acquisition and Matlab version 6.5.1.199709 Release 13, Service Pack 1 (The Mathworks, Inc.) for signal processing.

The extracellular bath contained (mM): NaCl 128, KCl 5, CaCl₂ 2, MgCl₂ 1, Hepes 25, and glucose 30, pH was adjusted to 7.3 with NaOH. The pipette solution contained (mM): K⁺ gluconate 125, KCl 10, EGTA 5, Hepes 10, MgATP 4, Na₂ ATP 0.5, pH 7.3 achieved with KOH. Cells were patched inside a Faraday Cage using a Nikon Eclipse TE 2000-S microscope. Voltage clamp recordings where performed in the whole cell mode using the following protocol: Cells were maintained at a polarized resting potential of -70 mV. Depolarizing potentials of -40, -30, -20, -10, 0, 10, 20 and 30 mV were sequentially applied, sustained for 1.5 s and followed by 1.5 s at the resting potential. Each experiment was repeated 6 times and the average response was obtained.

Figure 3-2

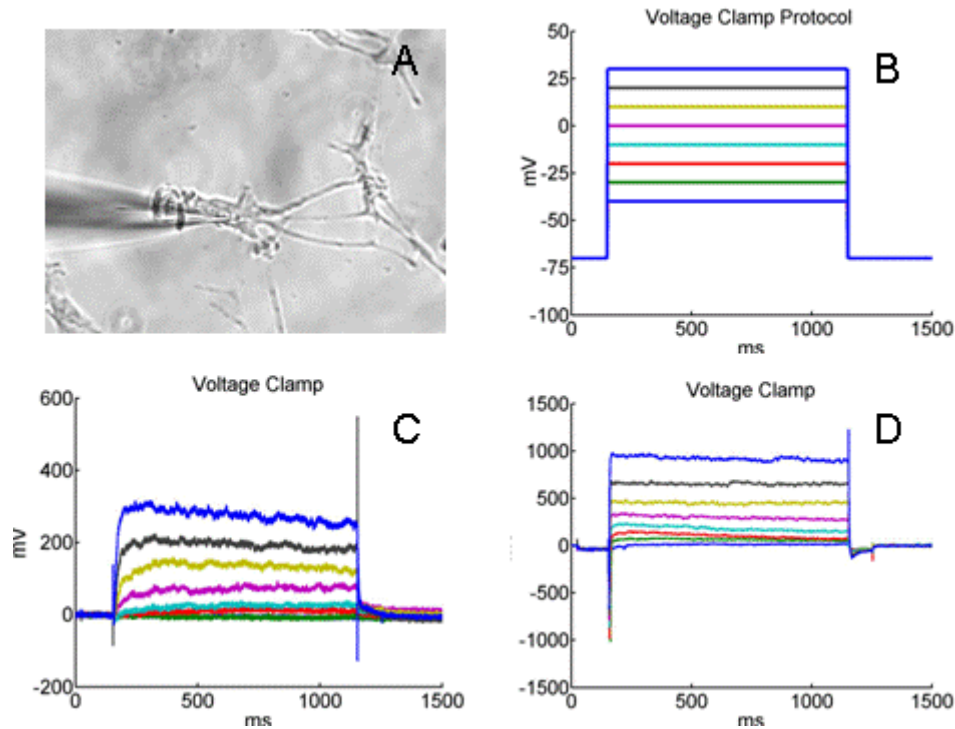


Figure 3-2: (A) shows a 15 day after plating microphotograph of a surface adherent (S) cell being patched. (B) shows the voltage clamp protocol utilized to stimulate the cells; a sequential depolarizing potentials of -40, -30, -20, -10, 0, 10, 20 and 30 mV were applied from -70 mV and sustained for 1.5 s. (C) Membrane response for an electroactive S cell, note the large activation events. (D) Membrane response for a non electrogenic cell, note the absence of activation events.

Figure 3-2 shows the patch clamping results for an electrogenic S cell and a non electrogenic N cell. In the case of the non electrogenic cells, the inward activation potentials are not present, indicating the absence of voltage gated sodium channels. The inward potentials for the electrogenic cell are achieved with depolarizing potentials greater than -30 mV, suggesting we are in the presence of a voltage activated sodium channel with a threshold in the order of 30 mV. By magnifying the activation and deactivation of the electrogenic cell, Figure 3-3 we can appreciate that the activation

kinetics are very slow, between 5 and 10 ms. Regarding the inactivation, recovery of the action potential for the SK-N-BE(2c) cell line is mediated by an Inward Rectifying Potassium Channel (IRK) similar to IRK1 and consistent with the inactivation currents seen in Figure 3-2 (Tonini, 1999).

Figure 3-3

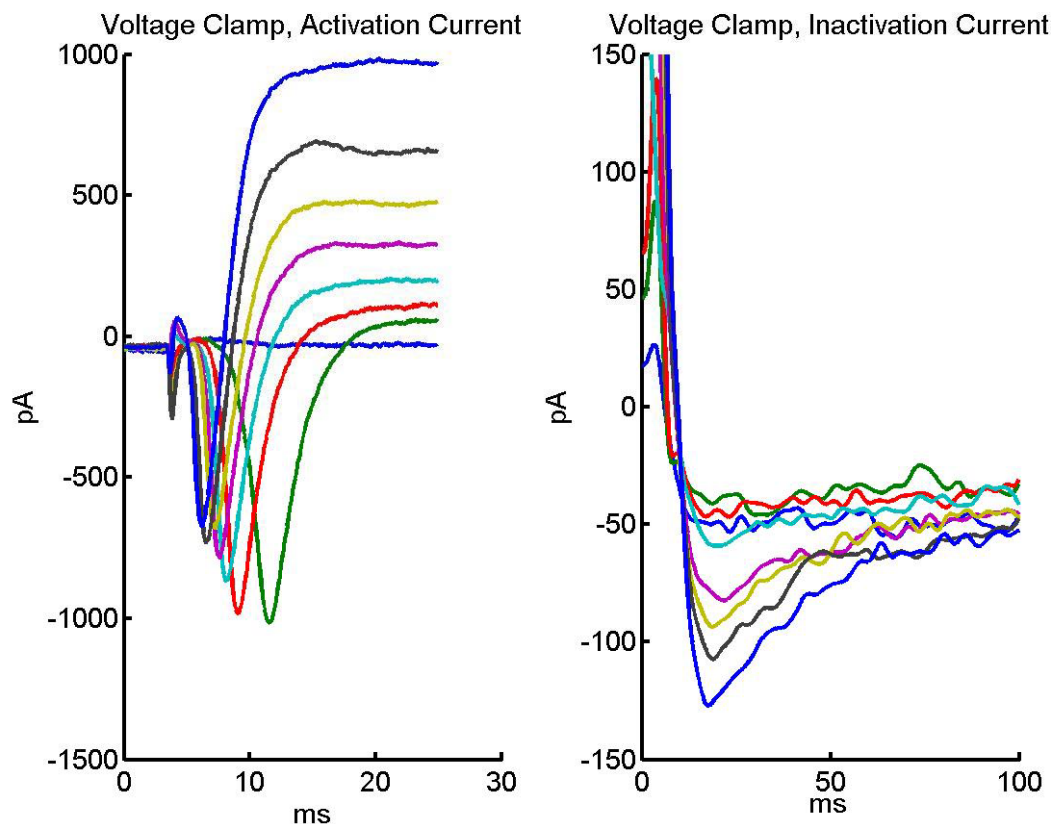


Figure 3-3: Membrane response for an electroactive SK-N-BE(2c) S cell 12 days after plating, showing the activation and inactivation currents. Each trace corresponds to sequential depolarizing potentials of -40, -30, -20, -10, 0, 10, 20 and 30 mV from -70 mV baseline.

Based on the experiments performed, the electrical properties of the SK-N-BE(2c) are characterized by a long lasting (5 to 10 ms) depolarization event, followed by an even

longer (around 50 ms) hyperpolarizing potential resulting from the IRK channel present in the cell line.

3.4 Analysis of Neurotransmitter Release

The SK-N-BE(2c) cell line expresses several neurotransmitter related enzymes, such as tyrosine hydroxylase (converts tyrosine to L-DOPA) and dopamine- β -hydroxylase (converts DA to NE), being extremely efficient in DA production (**Biedler**,). Tyrosine is hydroxylated into L-DOPA, subsequently, aromatic amino acid decarboxylase (dopa-carboxylase) catalyses the conversion of L-DOPA to dopamine (DA) (Figure 3-4).

Figure 3-4

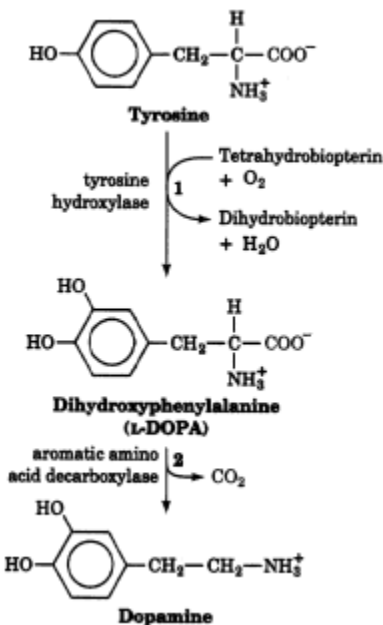


Figure 3-4: *Dopamine Synthesis (Modified from Molson, 2000)*

Dopamine is an unstable molecule that is rapidly metabolized by enzymatically active cells. The main enzymes metabolising DA are monoamine oxidase (MAO), catechol-O-methyltransferase (COMT) and aldehyde dehydrogenase (AH), and the main metabolites of DA are 3,4-dihydroxyphenylacetic acid (DOPAC), 3-methoxytyramine (3-MT) and homovanillic acid (HVA). Dopamine (DA). DA via COMT is degraded into 3-MT and via MAO is degraded into DOPAC. 3-MT, is formed from released DA by COMT and is further metabolised to HVA by MAO and AH. These two byproducts, are again degraded into HVA being the last step of the degradation process (Figure 3-4). Thus, tissue contents, as well as extracellular concentration of 3-MT, HVA and DOPAC can be used as an index of DA release.

Figure [Figure 3-5](#)

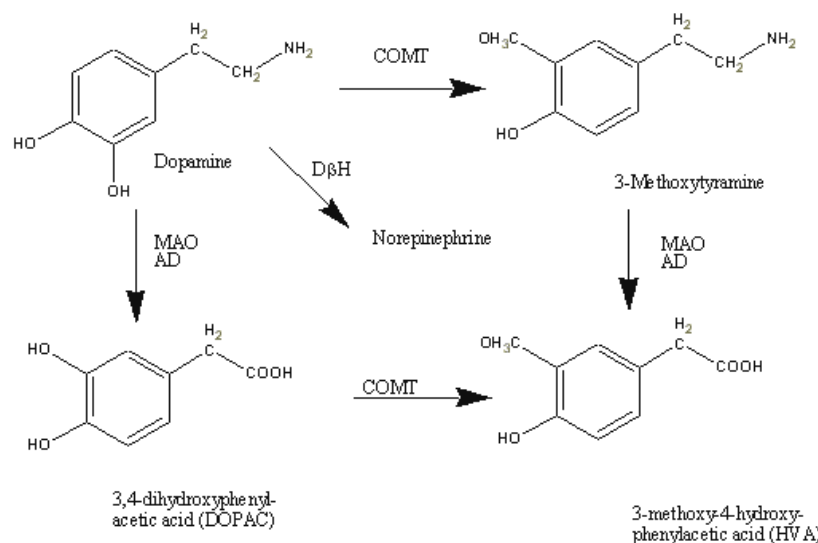


Figure 3-5: Dopamine Metabolic Pathways (Modified from [Okereke, 2002](#))

To verify the production of DA by the cell line high performance liquid chromatography with electrochemical detection (HPLC-EC) at 0.24 V was utilized, in

collaboration with Ms. Laura Killinbeck from Dr. Anne Andrews' Laboratory. A technique modified from (**Andrews, 1993, A; Andrews, 1993, B**): 50 µl of media was injected onto a 10 cm x 4.6 mm Spherisorb 3 µM ODS reverse-phase chromatography column (Thomson Instruments, Springfield, VA) in a mobile phase containing 0.1 M citric acid, 8% acetonitrile, 0.5 g/l octanesulfonic acid, 0.3% triethylamine, and 10 mM EDTA at a flow rate of 0.7 ml/min. The standards used and their elution times (min) are as follows: NE, 3.367; Epinephrine, 4.183; DOPAC, 4.561; DA, 6.323; 5-HIAA, 7.698; HVA, 10.014; 3-MT, 14.015; 5-HT, 15.456 and 5-N-Me-5HT, 19.322.

SK-N-BE(2c), were plated at a density of 8×10^6 cells/ml over tissue culture polystyrene and maintained in Ham's F-12: Minimal Essential Media (MEM, Gibco BRL) supplemented with 15% fetal bovine serum (Bioreclamation), 100 units/ml penicillin, and 50 µg/ml streptomycin. Cells were grown at 37 °C, 5% CO₂ and after three days media was changed to Minimal Essential Media (MEM, Gibco BRL) without serum. Cells were left to develop over an additional three day period after media was changed.

Figure 3-6

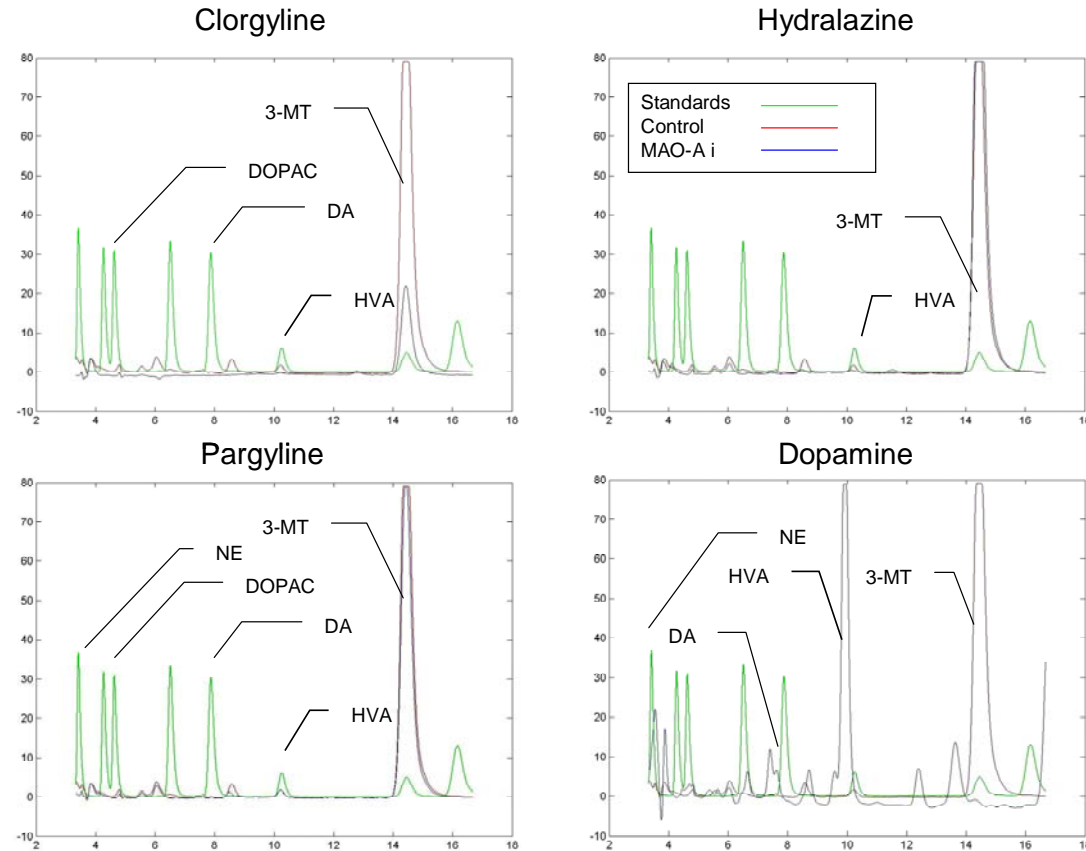


Figure 3-6: HPLC-EC of the cell culture media and its response to a selective MAO-i inhibitor and Dopamine, as compared to the elution standards.

HPLC-EC was obtained for the serum free media and DI water as mobile phase, elution controls. Serum free media signal was digitally subtracted from that obtained for each treatment using Matlab version 6.5.1.199709 Release 13, Service Pack 1 (The Mathworks, Inc.). Various Monoamine Oxidase Inhibitors (MAO i) were added to the cell culture at a final concentration of 0.5 μ M. The selected inhibitors were: Clorgyline (N-methyl-N-propargyl-3(2,4-dichlorophenoxy)propylamine) hydrochloride a MAO-A

inhibitor; Hydralazine a nonspecific MAO-A/B inhibitor and Pargyline, a MAO-B inhibitor. Media was extracted from the cell cultures after 24 hr.

As expected from the metabolic pathways, by selectively blocking the MAO enzyme, there should be a decrease in the dopamine metabolites, and this is consistent with the results found from the HPLC-EC analysis. It can be noticed (Figure 3-6) that Clorgyline effectively decreased the measured amount of 3-MT, HVA and DOPAC, while Hydralazine and Pargyline, reduced the concentration of HVA but not that of 3-MT or DOPAC. In consequence, by artificially adding dopamine to the culture media, there should be an increase in the quantity of expected metabolites. In figure 3-6-D, the corresponding DA peak in the HPLC-EC is observed, plus there is a clear increase in the amount of HVA produced. This indicates that the addition of DA favors the metabolic degradation to the DOPAC pathway, whose quantity is increased, and disfavors the 3-MT pathway, whose quantity is diminished. The presence of NE was also observed, consistent with the existence of the dopamine- β -hydroxilase enzyme in the cell line (**Biedler, 1978; Ishiguro, 1993**).

Additionally, Mono Sodium Glutamate (MSG) was added to the cell culture and the response was again analyzed via HPLC-EC (Figure 3-7). In this case, there is a clear increase in the amount of DA, DOPAC and HVA, suggestive of a glutamate mediated dopamine response.

Figure 3-7

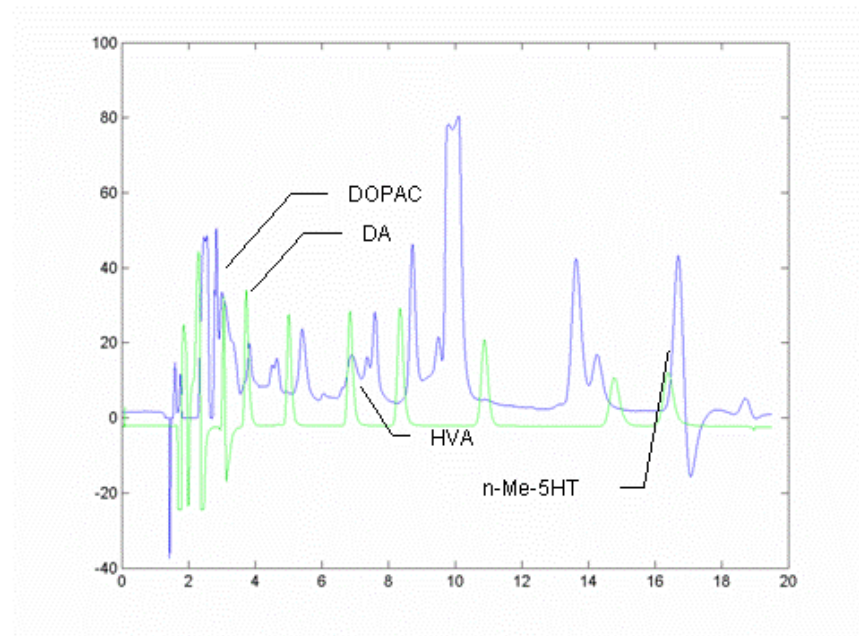


Figure 3-7: HPLC-EC comparing the response to MSG of the cells in culture, versus several standards. Notice that the matching peaks correspond to DOPAC, DA, HVA and n-Me-5HT

3.5 Imaging Studies

Several sets of experiments were performed with the aim of analyzing the synaptic properties of the cell line. Microphotography was used to show the presence of globular engrossments of the neurite processes that resemble synaptic bouton (Figure 3-8). Cells were cultured over cell friendly materials for 35 days and were stained with Cell Tracker Green® (5-chloromethylfluorescein diacetate), (Cambrex Bio Science Walkersville, Inc.), following the manufacturers instructions (Cambrex, 2005). Cell Tracker Green® crosses the plasma membrane of intact cells and is retained

intracellularly after reacting with cytoplasmic thiols (**Cambrex, 2005**). Is colorless and nonfluorescent until the acetate groups are cleaved by intracellular esterases (**Cambrex, 2005**). Microphotographs were obtained using an Olympus BX-60 epi-fluorescent upright microscope.

Figure 3-8

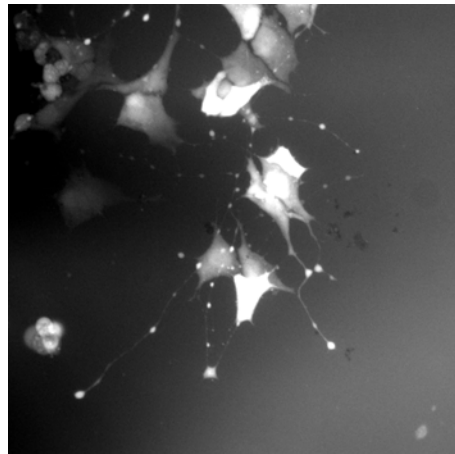


Figure 3-8: *Digital microphotograph of cells after 35 days in culture, stained with Cell Tracker Green®. Notice the globular structures (bright “dots”) present in most of the neurite-like processes. Microphotographs were obtained using an Olympus BX-60 epi-fluorescent upright microscope.*

To further characterize the cell line, immunofluorescence was used to show the presence of pre and postsynaptic markers. Non specific dopamine receptor antibody was selected as post synaptic marker, because DA production has been measured and D2-dopaminergic receptors have previously been reported in the cell line (**Namir, 1997**). Cells cultured over cell friendly materials were fixed after various days in culture. Cells were fixed in 4% paraformaldehyde in 0.1 M phosphate buffer for 10 min at room temperature (RT), washed twice with PBS and incubated for 20 min at RT with the primary antibody. Anti-synaptophysin (Sigma) was used as presynaptic marker while

nonspecific anti-Dopamine Receptor (Sigma), was used as postsynaptic marker. Secondary, ALEXA 555 goat anti-mouse and ALEXA 496 donkey anti-rabbit (Molecular Probes) were used for fluorescence. Microphotographs were taken using an Olympus Fluoview 300 Confocal Laser Scanning Microscope. Sequential scanning was utilized to avoid “bleed through” of one wavelength to the other.

Figure 3-9

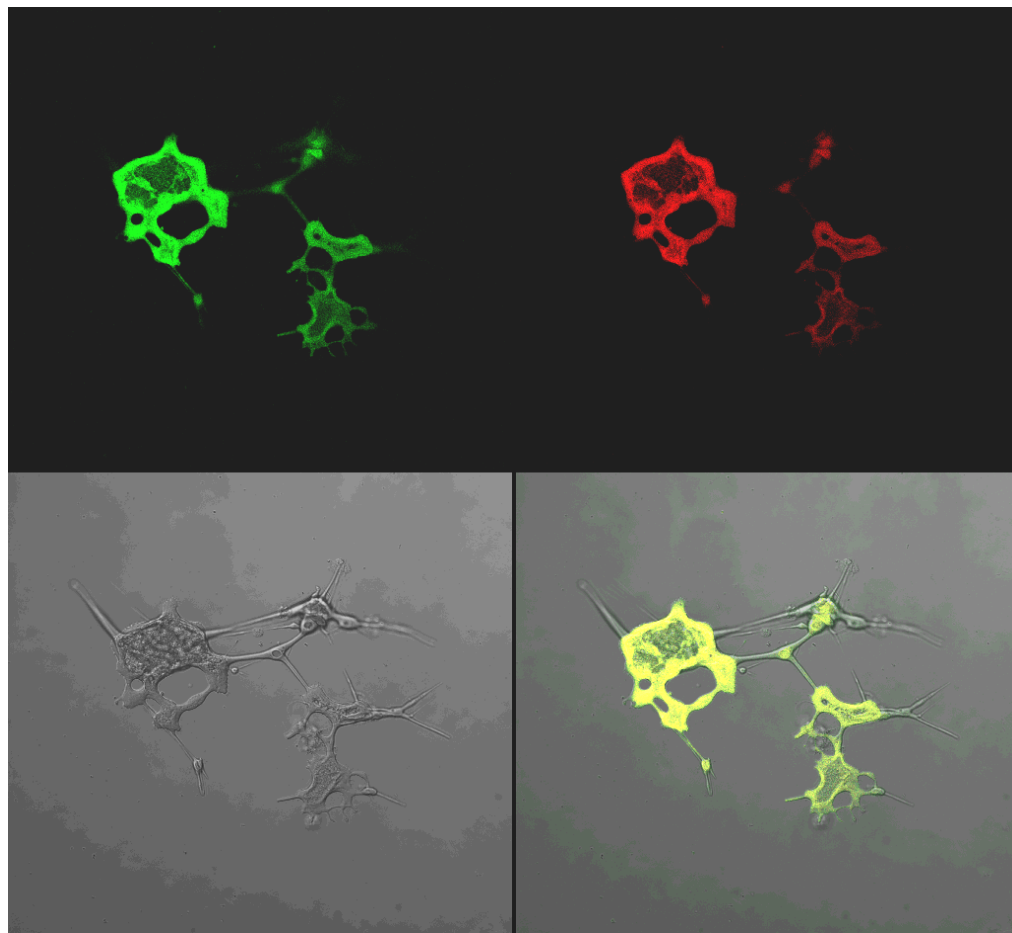


Figure 3-9: 40 X Digital microphotograph of a group of cells after 6 days in culture, immunostained with anti-synaptophysin (green) and anti-dopamine receptor (red). The bottom right image shows the composite of the prior three panels overlaid. Yellow color in the bottom left panel implies colocalization of the fluorescent markers.

After 6 days in culture, cells have extended projections and have contacted neighboring cells, while the pre and post synaptic markers appear widely distributed throughout the cellular surface (Figure 3-9). After 20 days in culture, synaptic markers are concentrated in very specific areas along the neural surface and, in particular, the anti-dopamine receptor markers are only present in specific spots, while occupying thin layers of the volume (Figure 3-10).

Figure 3-10

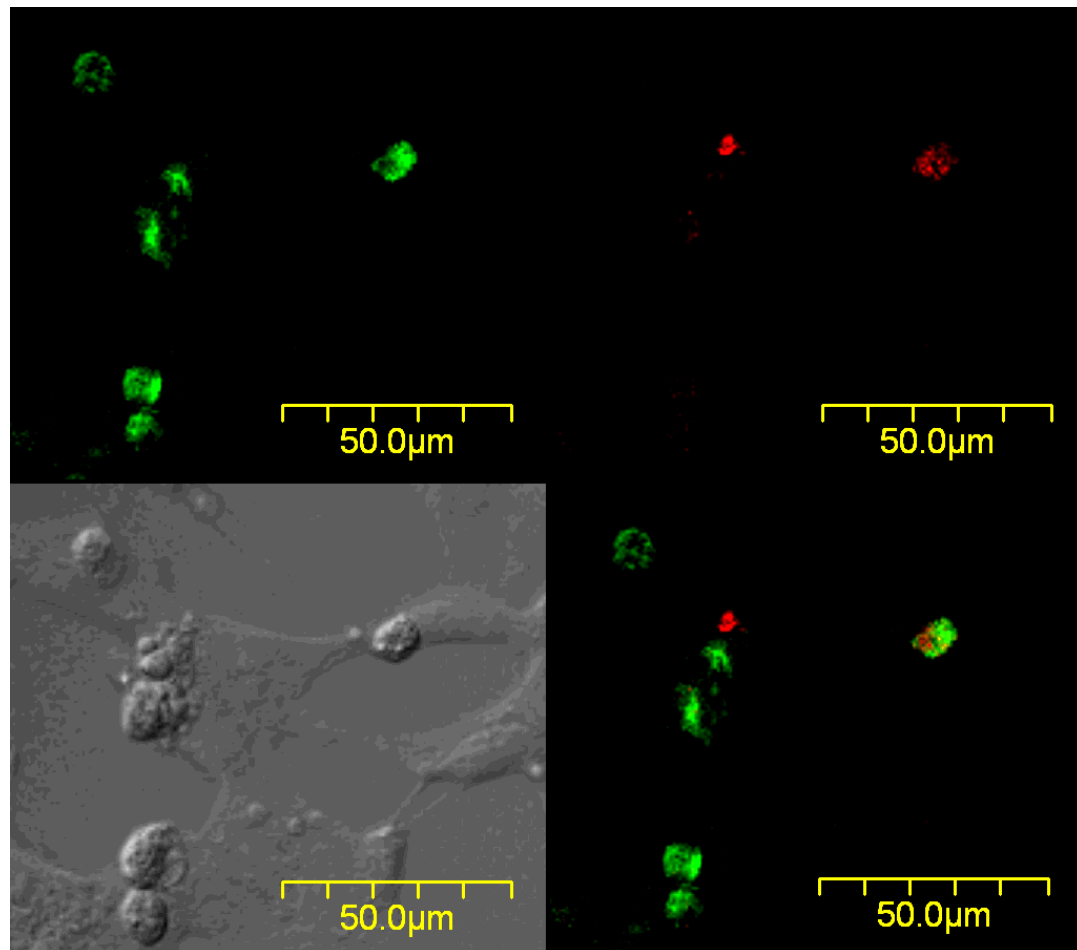


Figure 3-10: 60 X Digital microphotograph of cells after 20 days in culture, immunostained with anti-synaptophysin (green) and anti-dopamine receptor (red). The bottom right image shows the composite of the top two panels overlaid.

3.6 Additional Characterization

In order to use the cell line to study non-native proteins, the cell line needs to be transfectable. To corroborate the transfectability, cells were maintained in Ham's F-12: Minimal Essential Media MEM (1:1) (Gibco BRL) supplemented with 15% fetal bovine serum (Bioreclamation), 100 units/ml penicillin and 50 µg/ml streptomycin (Vasudevan, 2001, A). For transient transfections, SK-N-BE2C cells, where plated on the cell friendly coated ITO glass slides, placed in 6-well plates (Falcon) at a density of $0.3 * 10^6$ cells/well and transfected using Effectene (Qiagen) following the manufacturer's instructions. Forty-eight hours after plating, the cells were transfected with Green Fluorescent Protein (GFP) based expression plasmids (**Glusman, 2000;**, **Glusman, 2000,** and **Zozulya, 2001**) to a total of 400 ng/well.

Figure 3-11

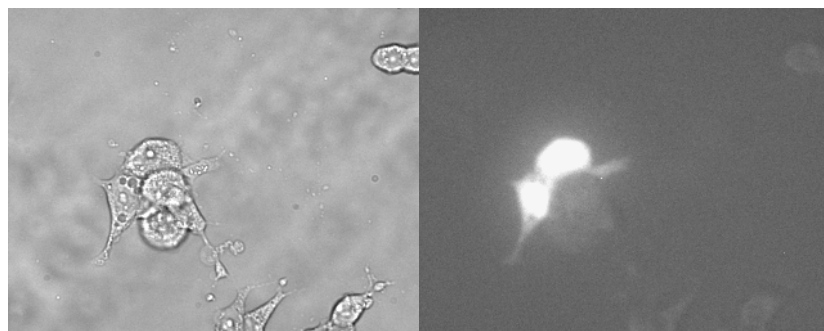


Figure 3-11: Bright field and fluorescent image of GFP transfected SKN-B-E(2)C cells. Transfection efficiency above 30% is commonly accomplished.

Transfection efficiency was quantified by comparing the number of transfected (fluorescent) neurons with respect to non-transfected cells grown on each slide (Figure 3-11). To achieve this, the slides where divided into grids of 250 mm², and the number of

neurons in each of 20 such squares was counted, using a Nikon Eclipse TE 2000-S microscope. Efficiency greater than 30% was achieved, which is consistent with the results presented by (Vasudevan, 2001, A; Vasudevan, 2001, B; Vasudevan, 2001, C; Vasudevan, 2001, D) using the same technique.

Experiments are normally performed at room temperature, so an important aspect to consider is the viability of the cell culture outside of the incubator. In order to determine this a 7 day culture plated under standard conditions was stained with a live-dead assay FDA-PI. FDA, fluorescein diacetate is a non-fluorescent molecule which can pass through the cell membrane whereupon intracellular esterases cleave off the diacetate group releases the highly fluorescent product fluorescein. The fluorescein will accumulate in cells which possess intact membranes and green fluorescence serves as a marker of cell viability. This stain is used in combination with PI (Propidium Iodide) staining because non-viable cell nuclei will take up the PI and stain red whereas viable cells will not take up the PI and should only stain green.

Stock solutions of Propidium Iodide (100 mg/ml PI [Sigma] in PBS) and Fluorescein Diacetate (5 mg/ml FDA [Sigma] in ethanol) were diluted 100x and 40x respectively to produce the working solution. Culture media was washed twice with PBS and replaced with the working solution. Cells were incubated at room temperature for 3 min and viability was observed under an Olympus Fluoview 300 Confocal Laser Scanning Microscope. A 12 well tray was used and cells were screened for viability every 20 minutes. After 3 hours at room temperature (21 °C), over 50% of the cells were still viable (Figure 3-12).

Figure 3-12

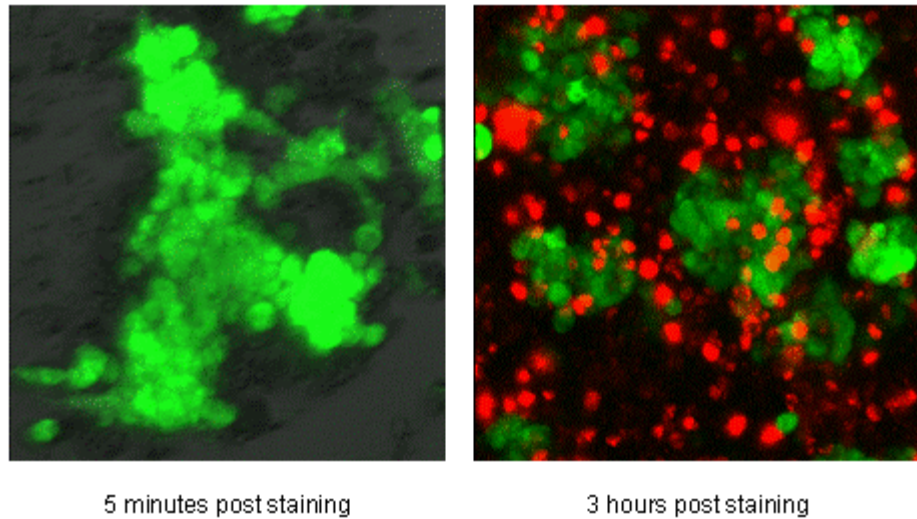


Figure 3-12: *SK-N-BE(2c)* cells, 7 days after plating, screened with live-dead assay: Fluorescein Diacetate (FDA), green fluorescence, serves as a marker of cell viability - Propidium Iodide (PI), red fluorescence, stains the nuclei of non-viable cells.

3.7 Chapter Summary

The SK-N-BE(2c) cell line is an I-type neuroblastoma: morphologically intermediate between neuroblastic (N) cells, and substrate-adherent (S) cells. The cell line shows features characteristic of early embryonic and autonomic cells and can be induced to differentiate and extend projections with retinoic acid. Patch clamp recordings from the cell line show the presence of large depolarizing sodium currents, as well as hyperpolarizing inward potassium currents, similar to those of the **IRK** channel. Overall the electrical properties indicate long lasting (5 to 10 ms) depolarization event, followed by an even longer (around 50 ms) hyperpolarizing recovery. Further characterization is

important to determine the percentage of electrogenic cells and if this percentage varies with time after plating and with the induction of neural growth factors.

The SK-N-BE(2c) cell line expresses several neurotransmitter related enzymes, and HPLC-EC analysis was performed to determine the type of neurotransmitter produced. Dopamine (DA) was found as the main product of the cell line. An increase in DA production was found with the addition of Monosodium Glutamate suggesting that there is a Glutamate induced response from the cells in culture. Immunofluorescence imaging studies provide strong evidence, suggesting the formation of functional dopaminergic synapses in vitro.

The SK-N-BE(2c) cell line is robust, easy to transfect, electrogenic, synaptogenic and polymorphic and could serve as a model system for the study of developing neural cell populations. For example, they could be utilized as a model for studies of neural crest progenitor cells. They could also serve as a model for the study of synapse formation and networking. Besides, the robustness of the cell line could provide an ideal substrate for the development of cell based biosensor systems.

Chapter 4

Development of a Multiunit Cell Based System

4.1 Introduction

As described in the introduction, a main drawback to single cell recordings is that a good electrical signal requires a good electro-neural coupling and a good electro-neural coupling requires good localization and selectivity of the electrode-neuron interface. The proposed solution is to couple hundreds to thousands of cells on top of large electrode pad and measure the response of the cellular ensemble. This is mathematically equivalent to recording from individual neurons and then adding the output signals to measure the level of integration.

The concept can be illustrated as 2 electrodes with cells growing on one of them (Figure 4-1). The amount of current contributed by each cell's response is "added" at the summing electrode and amplified via a differential-amplifier. Much of the neuron's current is shunted through the extracellular fluid pathway, but the contributions of many neural elements sum. The geometry of the cell-electrode system such as distance from the electrode will vary the magnitude of the extra cellular current contribution, but according to the mathematical model the total energy of the system should be the geometric sum of the individual contributions.

Figure 4-1

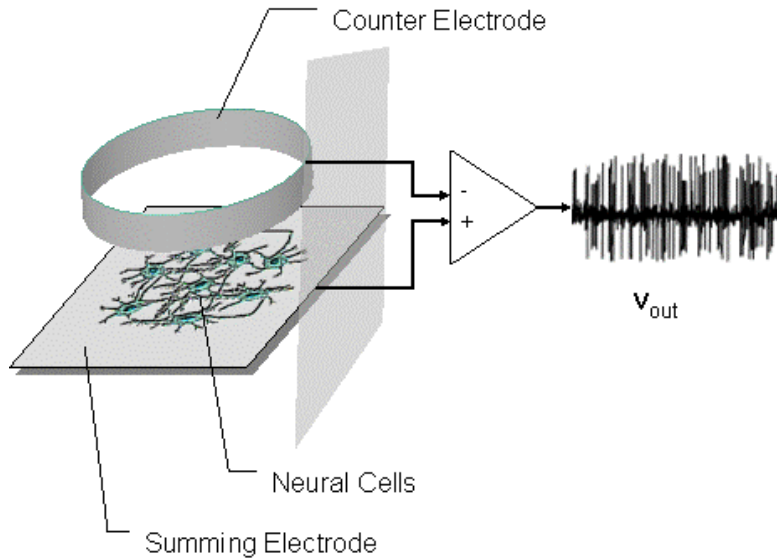


Figure 4-1: Idealized Biosensor Design

A major constraint is the adhesion of cells to the electrodes, because electrical recordings require a good electrical conduction path from the cells to the electrode. If cells are not located on top of the electrodes they do not make a good electrical contact, and the amplitude of the signals is difficult, if not impossible, to separate from the background noise. The solution has been to utilize masking techniques to direct preferential binding of the cells to a particular site within the culture media. For instance, photolithographic and micro contact printing techniques have been used to produce patterns of absorbed proteins and synthetic peptides, on surfaces for patterned cell growth and adhesion on top of electrodes (**Stenger, 1994**).

Materials for cell patterning should ideally be easy to fabricate, hydrolytically stable, non-toxic, chemically inert, synthetically reproducible, scalable, and inexpensive. In order to couple the patterned networks to microscopic observations, the material

should also be transparent and, if electrogenic cellular activity is to be monitored, it is convenient for the material to be electrically conductive.

A simple electrode chamber for recording the sum of extracellular action potential discharge currents from a population of SK-N-BE(2c) cells was developed. The chamber allows tight adhesion of differentiated cells to a surface electrode, via the utilization of novel polyphosphazene based materials.

The whole system consists of a Cell Culture Chamber (CCC) where the recording electrodes are located and a signal processing software, capable of acquiring analyzing the sum of extracellular action potential discharges from a group of neurons. Two independent CCCs were developed and are presented in this chapter. Recordings performed with this systems and the corresponding signal processing is discussed in Chapter **5.2**.

4.2 Cell Culture Chamber # 1

The Cell Culture Chamber #1 (CCC #1) was the first working model for a simple integrated system that could be used for cell population research, while being inexpensive, dependable, transportable and even, disposable. The system consists of a macroelectrode substrate plate, where cells can grow and adhere plus a reusable cell culture chamber that can be loaded with the macroelectrode plates. Cells can be grown on many such slides, and conveniently placed one at a time into the chamber. In order to enable the cells to be observed, and to correlate the cell positions with the position of the electrodes the substrate plate consisted of standard glass microscope slides, 1×1.5 cm,

sputtered on one side with the transparent conductor indium tin oxide ITO (Evaporated Coatings Inc. Willow Grove, PA).

The CCC #1 was made from Teflon® in order to be reusable, cleanable and biocompatible. The chamber developed consisted of two parts, the bottom provides a groove for the placement of the ITO coated slide and a mechanical support for the top. The top of the chamber holds the electrical connections, consistent of an adjustable copper connector attached to the central pin of a female BNC and a silver-silver-chloride (Ag/AgCl) ring that serves as a counter electrode (Figure 4-2).

The chamber was built in the Penn State Engineering Machine Shop according to the blueprints provided by the author. The silver ring was manufactured by a local jeweler and chlorinated inside the chamber. A piece of conductive rubber (Zoflex®, CD45.1), serves as the interface between the ITO base plate and the copper connector.

Figure 4-2

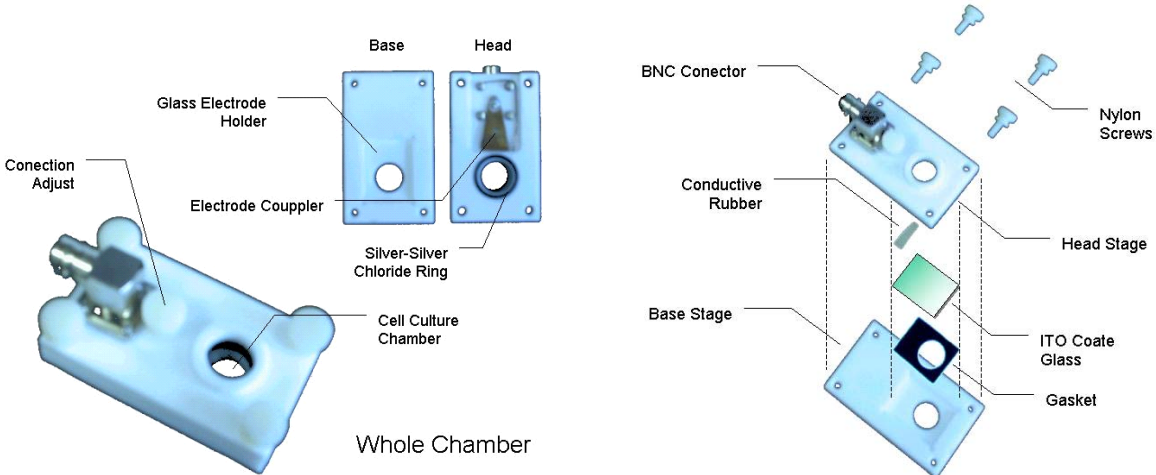


Figure 4-2: *Cell culture chamber # 1, machined from Teflon®, incorporates ITO-coated glass, and Ag/AgCl ring electrode in an open chamber which can be covered during cell incubation, or when carrying out repeated measurements over time, but opened when access to the cell surface is required.*

When properly assembled, the arrangement provides good immunity from thermal electrical noise via the low-conductivity ($1 \text{ K}\Omega$, typical) pathway between the ITO and Ag/AgCl electrode. The chamber arrangement permits viewing of the surface on which the cells are growing via inverted-stage microscopy and allows the introduction of a stimulant-containing fluid via a small flow controlled device. The electrophysiological recordings presented in Chapter 5.3 were performed with this device.

4.3 Cell Culture Chamber # 2

In order to provide a multiple macroelectrode array system a new culture chamber was required (CCC #2). The two part chamber with the removable electrode pad proved to be valuable from the CCC #1 design, so such configuration was maintained. To

provide increased functionality a full 2.5 x 7.5 cm standard microscope slide was to be utilized as base plate and multiple connectors where to be provided at both sides of the chamber. A flow regulator with bubble reduction was to be incorporated in order to reduce artifacts produced by bubbles in the flow.

The top of the chamber was again made out of Teflon®, however, the base of was made out of aluminum, to provide increased mechanical strength. The BNC connector used in CCC #1 was replaced by dual DB9 connectors at both ends of the chamber. An additional fluidic chamber was connected to the main cell culture chamber, in order to better regulate the flow and reduce the formation of bubbles, produced by the aspirating system. The main culture chamber is surrounded by a large O-ring (Dash 029) that maintains a waterproof seal so that cell culture media can be maintained and exchanged through access ports within the chamber. **Figure 4-3** shows a 3D rendering of the CCC#1, the top of the chamber was manufactured by the Penn State Engineering Machine Shop. The bottom part was manufactured in house at the Bioengineering workshop out of $\frac{1}{4}$ " aluminum sheath using a JET JVM-836 milling machine (Jet Equipment & Tools, Burnaby, Canada).

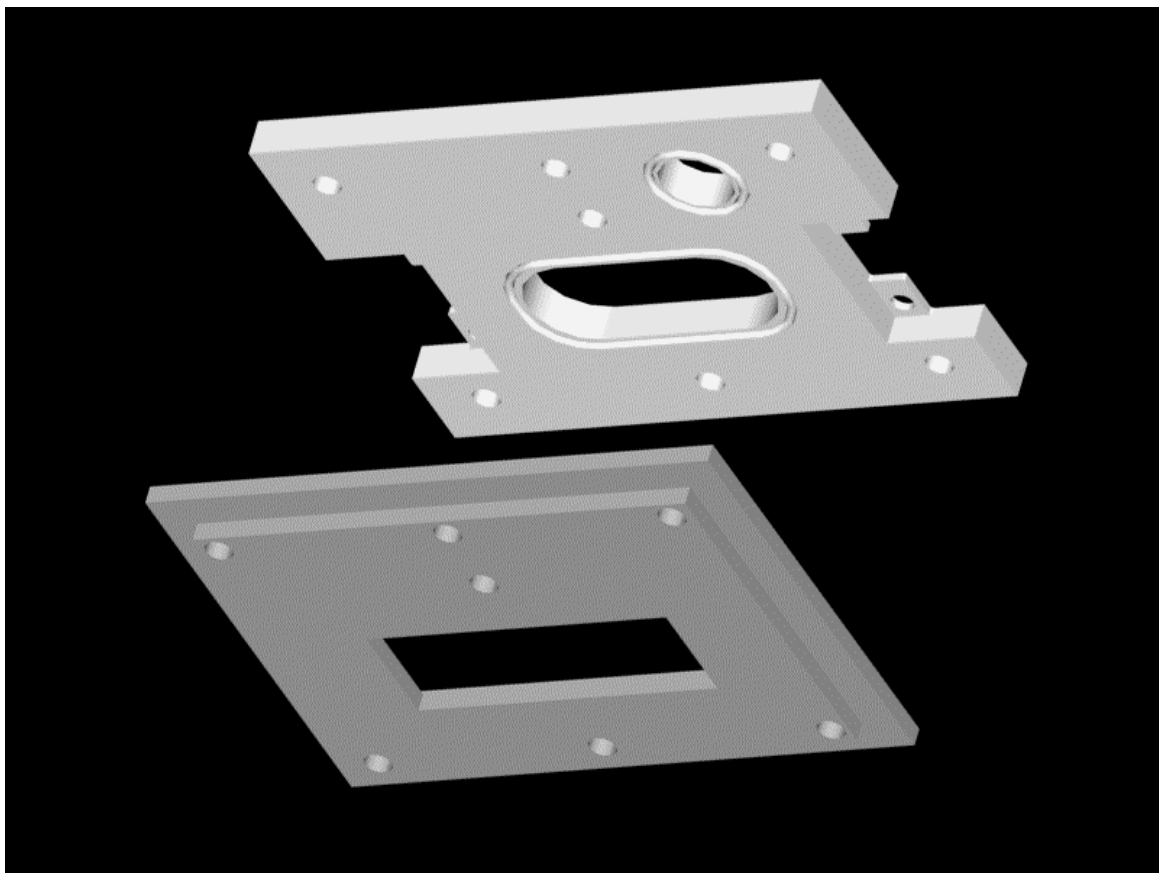
Figure 4-3

Figure 4-3: 3D rendering for the CCC #2 (Artwork by Donald Natale III.) This 3D model was utilized by the Penn State Engineering Machine Shop to manufacture the chamber out of Teflon®.

The base plates provide a high degree of versatility and can be designed with multiple electrode pads for stimulation and recording of cell signals. Cell friendly polyphosphazenes (**4.4.4**) allow the desired cells to grow, and also serve as a bridge between the conductive areas. These conductive areas are each connected via conductive wires to the edge of the microscope slide where they are interfaced to signal acquisition setup via the DB9 connectors and ZEBRA® elastomeric connectors specially manufactured for this application by Fujipoly America Corporation (Carteret, NJ). The

microscope slide with the assembled CCC #2 is positioned within a custom manufactured fixture that secures the slide, to the microscope stage. A special DB9 to BNC adaptor provides electrical connections to the signal acquisition setup. Cells can be grown on top of the base plates and then introduced independently in the chamber or they can be cultured inside the chamber so that long term electrical measurements can be performed.

Figure 4-4 shows a picture of the fully assembled CCC #2.

Figure 4-4

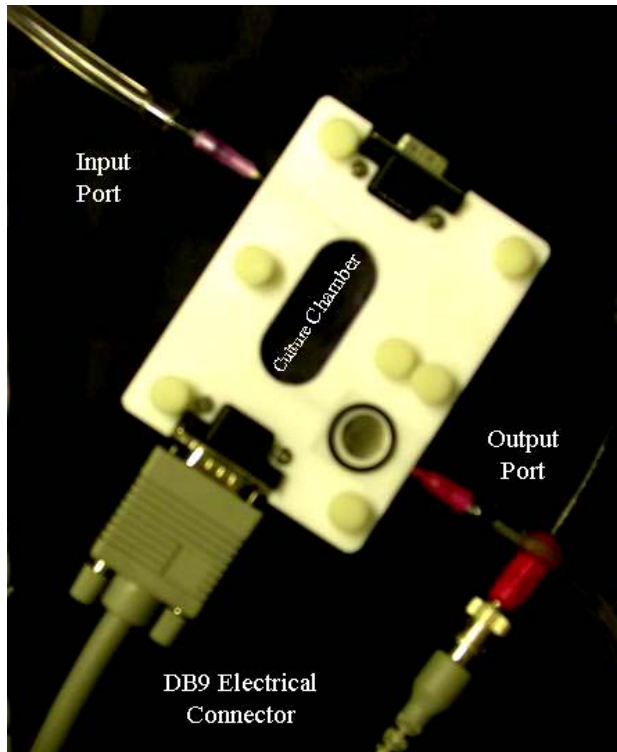


Figure 4-4: Assembled CCC #2 showing the special DB9 to BNC adaptor in one side and fluidic connections to the input and output ports.

Two multi-microelectrode base plate masks were designed (**Figure 4-5**). Such designs were patterned over standard glass microscope slides, coated with ITO (Evaporated Coatings Inc. Willow Grove, PA), by State of the Art (State College, PA)

using the mask designs provided by the researchers. ITO utilized was ECI #949 with a resistivity $< 100 \Omega/\text{square}$ and $> 80\%$ white light transmission. Patterns were ion-milled and the results were within the expected resolution. Transparency of the film was not affected by the milling process and only minor defects were observed towards the edge of the circular patterns.

Figure 4-5

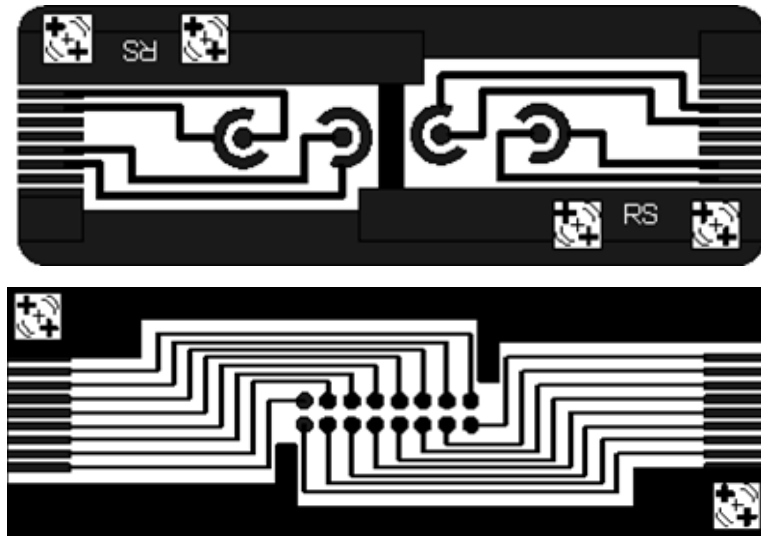


Figure 4-5: Multi-microelectrode designs: Both panels represent independent masks for standard microscope slides, 2.5 x 7.5 cm. The top corresponds to a differential electrode arrangement; cells are grown in the central circular pads and recordings will be performed between the central electrode and the surrounding ring. The second corresponds to a stimulus/record setup, where cells can be grown between electrode pairs and one electrode can be used for stimulation and the second one for recording.

Impedance of the electrodes measured in air ranged between 1.1 and 3.8 K Ω depending on the electrode. Noise was measured under standard experimental conditions with saline solution. Electrical recordings were performed in a Faraday cage using a high input impedance, high gain AC-coupled amplifier (Data Inc, Fort Collins, CO) band pass filtered between 150-2000 Hz, with a gain of 12,000 and sampled at 10,000 samples/sec

(Biopack Systems, Inc. Santa Barbara California). Noise without polymer coating was in the range of $10.68 \pm 0.02 \mu\text{V}$.

Electrodes were spin coated with 1 to 3 μm film of Poly[bis(trifluoroethoxy) phosphazene], (See **4.16.3**). Material around the electrodes was removed by physical abrasion and coated with Poly[(methoxyethoxyethoxy)_{1.0}(p-cresoxy)_{1.0} phosphazene]. Coated ITO slides were inserted in the cell chamber and in the presence of culture media, have impedances of $1.2 \pm 0.4 \text{ K}\Omega$ as measured at 1 KHz. Noise measured with this configuration was in the order of $2.19 \pm 0.02 \mu\text{V}$, a noted improvement as compared to noise without the polymer coating.

Coated electrodes were autoclave sterilized and neither the material nor the ITO delaminated. Also cell deposited debris, was successfully removed without affecting the patterned electrodes. Overall, the patterned substrates fulfill all of the expected requirements, providing a good opportunity for the development of advanced population-based biosensor systems.

4.4 Novel Polyphosphazene Based Materials for Differential Cell Adhesion

Polyphosphazene based materials were developed in collaboration with two graduate students from Dr. Harry Allcock's laboratory at The Pennsylvania State University: Mwita Phelps, and Eric Barrett. Many of the aspects mentioned in this document comprise research jointly developed with those students and published in (**Barrett, 2005**).

Polyphosphazenes form a broad class of inorganic-organic polymers with a phosphorus-nitrogen backbone and two organic side groups covalently attached to each phosphorous. Dr. Harry Allcock, developed the technique to synthesize all of the different polyphosphazene derivatives originating from the same macromolecular intermediate. The procedure involves the nucleophilic replacement of chlorine atoms in the highly reactive macromolecular intermediate, poly(dichlorophosphazene) (**Figure 4-6**), by alkoxides, aryloxides, and/or amines. This polymeric intermediate can be obtained by a ring-opening polymerization reaction (**Figure 4-6**). The final properties of the polymer are governed by the nature of the side groups.

Figure 4-6

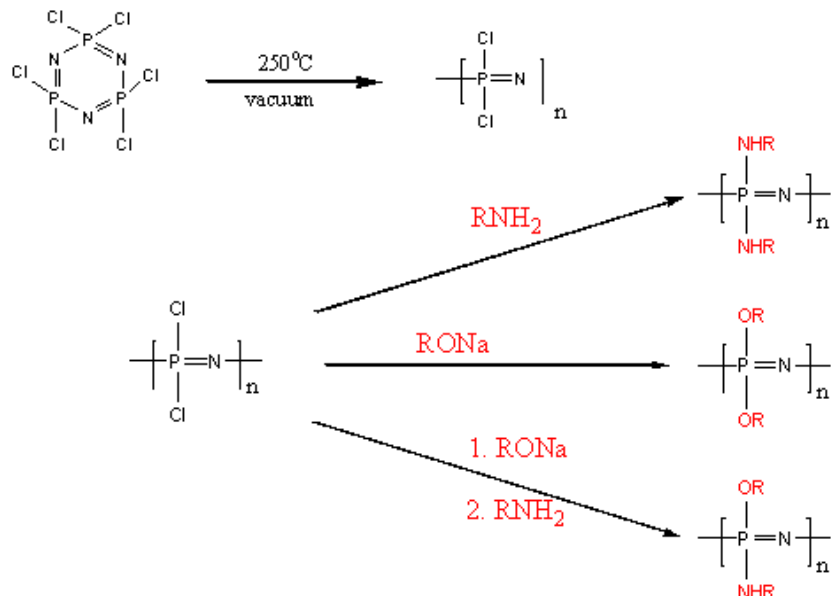


Figure 4-6: *Synthesis of poly(organophosphazenes) via macromolecular substitution. The procedure involves the nucleophilic substitution of the highly reactive intermediate, poly(dichlorophosphazene), by alkoxides and/or amines*

4.4.1 Polymer Selection Criteria

It has been found that several hydrophobic side groups linked to a polyphosphazene chain promote good cellular adhesion if cosubstituted with methoxyethoxyethoxy (MEE) side group. These include phenoxy, benzyloxy, arylalkoxy, as well as p-cresoxy, ethylphenoxy, and alkylphenoxy. With this in mind, three hydrophobic and two hydrophilic side groups were selected: These are the hydrophobic trifluoroethoxy, p-methylphenoxy, cinnamyloxy groups and the hydrophilic methoxyethoxyethoxy and carboxylato phenoxy units.

The hydrophilic methoxyethoxyethoxy (MEE) side group was selected because, when covalently bonded to the phosphazene backbone, it produces a water-soluble, transparent polymer. Following exposure of the solid to ultraviolet (UV) radiation or gamma radiation, MEEP crosslinks covalently and forms a very stable hydrogel ([Allcock, 1998; Nelson, 1991; Allcock, 1994](#)). Cinnamyloxy was chosen as a co-side group because this species is especially photosensitive to UV radiation. Exposure to UV radiation induces 2 + 2 cycloaddition which crosslinks the polymer. Cinnamyloxy is also very hydrophobic compared to MEE. By adjusting the co-substitution ratios of these two side groups on the polyphosphazene backbone, both the hydrophilicity and the UV exposure time can be controlled.

4.4.2 MEEP Biocompatibility

To determine the biocompatibility of the MEEP side group, cell viability in the presence of aqueous solutions of MEEP was examined with three cell lines. Human

cervical carcinoma cells, Hela (ATCC), dog kidney cells, L929 (ATCC) and mouse fibroblast cells, MDCK (ATCC) were screened in the presence of MEEP for cell growth and proliferation. Cytotoxicity experiments were performed at the Hybridoma and Cell Culture Laboratory at The Pennsylvania State University. The cells were grown in Dulbecco's Minimum Essential Medium (DMEM) with 10% fetal calf serum, and gentamicin (10 µg/ml). At near confluence the cells were dissociated by trypsinization, counted and adjusted to a concentration of 1.5×10^5 viable cells/ml in growth medium.

A stock solution of polymer was prepared at a concentration of 50 mg/ml in growth medium. The stock solution was placed in a 96-well flat-bottomed cell culture plate. Serial dilutions (0.5 X) were made such that each well contained 50 µl of polymer solution. The 96-well plate was incubated in a CO₂ atmosphere at 37°C for 24 hours. The supernatant solution was removed from the wells by decantation and cell viability was determined using an MTT 3-(4,5-dimethylthiazol-2-yl)-2,5-diphenyltetrazolium bromide assay (**Mossmann, 1983**). **Figure 4-7** shows that approximately 60% or greater cell viability was detected in the presence of MEEP polymer solutions at or below a concentration of 6.25 mg/ml. This is comparable with the FDA-approved tissue culture PEG, whose structure and properties are similar to those of MEEP.

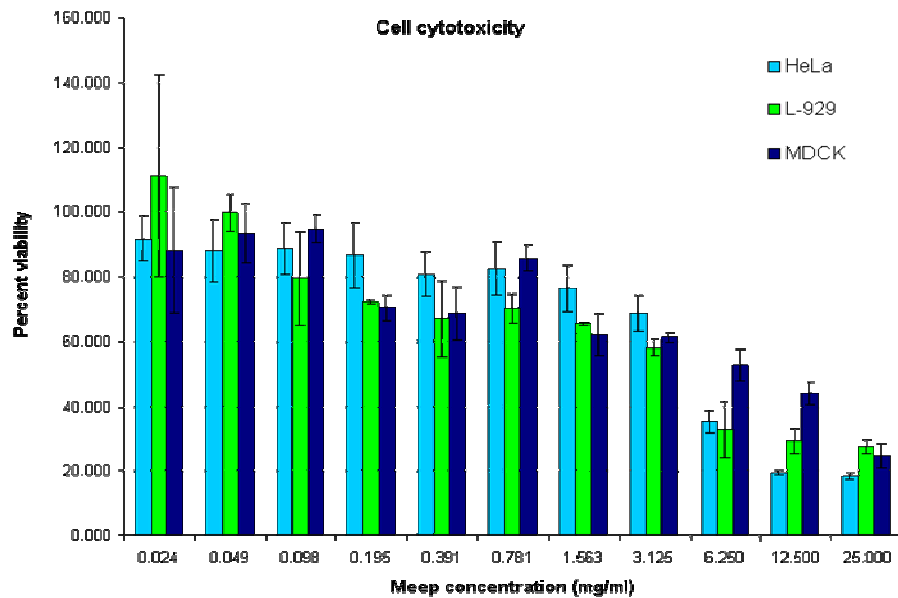
Figure 4-7

Figure 4-7: Cytotoxicity experiments using commercially available cell lines: Hela (ATCC), L929 (ATCC) and MDCK (ATCC) cells in the presence of aqueous solutions of MEEP at various dilution factors.

4.16.3 Polymer Characterization

All polyphosphazene candidates (Figure 4-8) were synthesized by the macromolecular substitution approach (Allcock, 2003). Each polymer was characterized by multinuclear NMR (Bruker AMX-360) to confirm the structure and side group ratio (Table 4-1). Molecular weights were determined using gel permeation chromatography (GPC) (Hewlett-Packard HP 1090 equipped with an HP-1047A refractive index detector and Phenomenex Phenogel 10 μm analytical columns calibrated using polystyrene

standards) (Table 4-2). Thin films ($<20\ \mu\text{m}$) of these materials are transparent, hydrolytically stable and adhere well to glass.

Figure 4-8

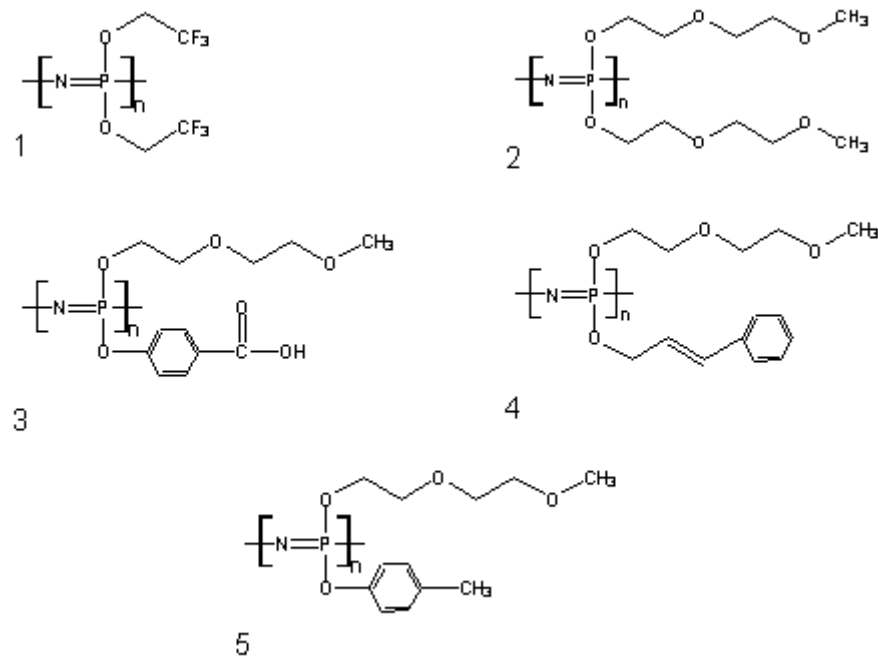


Figure 4-8: The top panel shows the structure of the synthetised polymers:

1. *Poly[bis(trifluoroethoxy) phosphazene]* (TFE)
 2. *Poly[bis(methoxyethoxyethoxy) phosphazene]* (MEEP)
 3. *Poly[(methoxyethoxyethoxy)_{1.0}(carboxylato phenoxy)_{1.0} phosphazene]* (PMCPP)
 4. *Poly[(methoxyethoxyethoxy)_{1.0}(cinnamyl oxy)_{1.0} phosphazene]* (PMCP)
 5. *Poly[(methoxyethoxyethoxy)_{1.0}(p-methylphenoxy)_{1.0} phosphazene]* (PMMP)
-

Table 4-1

4-1: Physical material characterization of the selected polyphosphazenes

Polymer	1H NMR (ppm)	31P NMR (ppm)
TFE	4.2 (br CF3), 3.3 (m etheric)	-8.0
MEEP	4.0 (m etheric), 3.6 (m etheric), 3.5 (m etheric)	-8.2
PMCPP	8.0 (m aromatic), 6.9 (m aromatic), 4.3 (m etheric), 4.0 (m etheric), 3.6 (m etheric), 3.5 (m etheric) 1.8 (m alkane), 1.0 (m alkane)	-8.3, -14.2
PMCP	7.1 (br aromatic), 6.4 (br aromatic), 4.1 (m alkene) 3.3 (m etheric)	-7.8
PMMP	7.0 (br aromatic), 6.8 (br aromatic), 4.0 (m etheric), 3.6 (m etheric), 3.5 (m etheric), 2.1 (m CH3 on aromatic)	-11.0, -15.9, -21.0

Table 4-2

4-2: Characterization of the selected polyphosphazenes

Code	Acronym	Cell Selectivity	Contact	Mw	Mn	PDI
Angle						
1	TFE	-CAP	113°	8.56×10^5	2.24×10^5	3.83
2	MEEP	-CAP	57°	1.71×10^5	6.55×10^5	2.61
3	PMCPP	+CAP	0° (hydrogel)	3.00×10^6	1.48×10^6	2.03
4	PMCP	+CAP	0° (hydrogel)	6.87×10^5	5.54×10^5	1.24
5	PMPP	+CAP	67°	2.25×10^5	9.47×10^4	2.37

4.4.4 Differential Cell Adhesion

In order to study differential cell adhesion and pattern stability of the polymer samples, SK-N-BE(2c) cells were plated at a density of 8×10^6 cells/ml and maintained in Ham's F-12: Minimal Essential Media (MEM, Gibco BRL) supplemented with 15 % fetal bovine serum (Bioreclamation), along with 100 units/ml penicillin, and 50 $\mu\text{g}/\text{ml}$ streptomycin. Measurements and photographs were taken using a Nikon Eclipse TS100 inverted microscope with a 10X objective lens and a 4 M Pixel Nikon Coolpix 4500 digital camera. Slides were divided into $250 \mu\text{m}^2$ grids where the number of cells were counted. Three slides and 5 randomly selected grids per slide were used for every measurement ($N=15$).

Cells were cultured over the various polyphosphazene-coated slides, and compared to various controls. Polylysine (PL) is a widely accepted cell friendly and transparent substrate for cell culture applications and was used as positive control. PL has been shown to allow patterned cell adhesion and growth (**Stenger, 1994; Chang, 2003; Qian, 2004**). Poly(ethylene glycol) (PEG) is the preferred cell-unfriendly polymer, being transparent, inexpensive and biocompatible (**Stenger, 1994; Chang, 2003; Qian, 2004**). The combination PL and PEG has been used extensively for cell patterning (**Stenger, 1994**). A major limitation for this system, is that PL dissolves in cell culture media within a few days and patterns are inherently lost and PEG needs to be UV or radiation treated to remain stable. The other controls were glass, ITO coated glass, cell culture treated polystyrene, and collagen coated cell culture dishes (BD, BioCoatTM). PL was

solution casted and slightly baked over the surface of previously hydroxylated glass slides to promote stability.

Development of the cultures over the materials was followed for 48 hours (**Figure 4-9**) and a one sided t-test (Table 4-3) was used to determine significance. Glass and ITO are not shown in the significance table since they are not polymer films; however they are shown on **Figure 4-9**, for completeness.

Figure 4-9

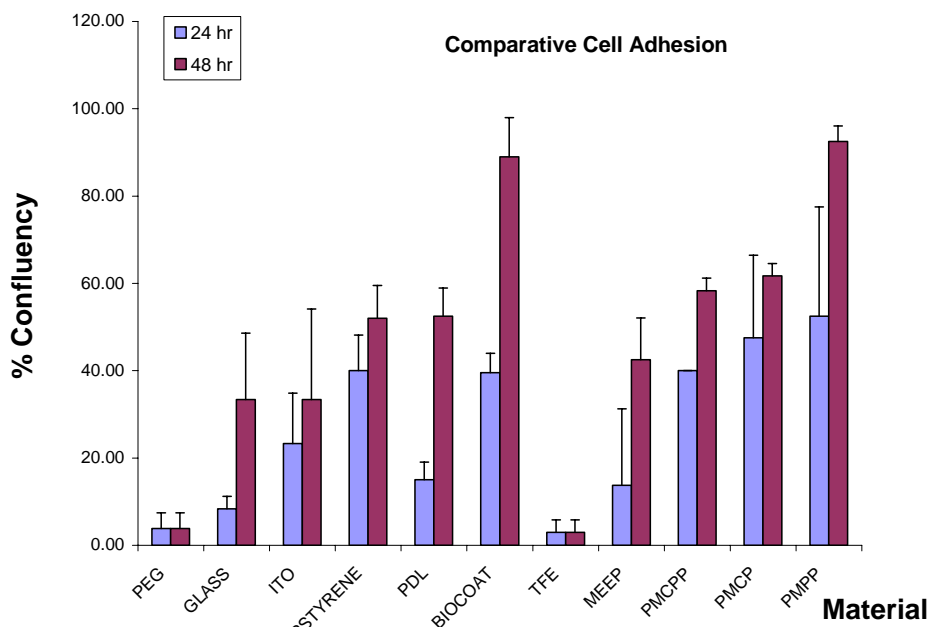


Figure 4-9: Confluence after 24 and 48 hours in culture, expressed in a percent basis for the tested materials. The whole cell culture substrate was coated with the specific cell culture material and the confluence measures were performed under a microscope with a 10x objective. N = 15 for each material tested.

Table 4-3

4-3: T-test results, comparing mean attachment to the polymer films, after 24 and 48 hours in culture.

24 hr	PSTIRENE	PDL	BIOCOAT	TFE	MEEP	PMCPP	PMCP	PMPP
PEG	*0.01	*0.04	*0.01	0.31	0.25	*0.00	*0.03	0.06
PSTIRENE		*0.04	0.50	*0.01	0.11	0.50	0.40	0.22
PDL			*0.01	0.05	0.46	*0.01	*0.05	0.08
BIOCOAT				*0.01	0.10	0.50	0.41	0.21
TFE					0.18	*0.00	*0.04	*0.04
MEEP						0.09	0.19	*0.01
PMCPP							0.40	0.21
PMCP								0.34
48 hr	PSTIRENE	PDL	BIOCOAT	TFE	MEEP	PMCPP	PMCP	PMPP
PEG	*0.01	*0.00	*0.00	0.31	*0.01	*0.00	*0.00	*0.00
PSTIRENE		0.35	*0.00	*0.00	*0.01	0.37	0.11	*0.01
PDL			*0.03	*0.00	0.19	0.21	0.10	*0.00
BIOCOAT				*0.00	*0.00	*0.02	*0.02	0.35
TFE					*0.00	*0.00	*0.00	*0.00
MEEP						*0.03	*0.02	*0.00
PMCPP							0.21	*0.00
PMCP								*0.00

Of the polyphosphazene materials, TFE and MEEP were not significantly different from PEG at 24 hr and TFE was still not significantly different at 48 hr therefore they are classified as cell-repulsive materials (-CAP). Regarding MEEP is important to state that the cells that proliferated after 48 hr appeared rounded and non-adherent (**Figure 4-9**). The other 3 materials were significantly more adherent than TFE, after 24

and 48 hr, therefore they are classified as cell adhesive (+CAP). After 36 hours, cells cultured over +CAP materials were adhesive with multiple neural projections and 100% confluent. If the culture is not differentiated with RA by day 3, cells overpopulate and begin to detach from the surface. However if the cell excess is removed, the cells will rapidly reattach.

4.4.5 Differential Cell Patterning

The possibility of attaining differential cell patterning on the surface of the polymers was explored. Several combinations of +CAP or -CAP microfeatures were patterned over a spun cast layer of polymer to determine if mammalian cells would grow preferentially on the +CAP (**Figure 4-10**). Photolithographic or microstamped features were produced and cells were cultured as in the differential cell adhesion experiments for one week. After 3 days in culture, the culture medium was exchanged for serum free media, to avoid further expansion of the culture.

Two sets of experiments were performed: Photholithographically patterned circles (250 μm in diameter) of MEEP were patterned onto PMCP, and nonspecific angular patterns of PMCPP were microstamped onto TFE. With these two experiments, we intended to test if similar results could be achieved with different materials and distinct microfabrication techniques and if selectivity is material specific and technique independent. As seen in figure 7, cells grow predominately on the +CAP micropatterned regions, and avoid the -CAP with over 60% selectivity for the MEEP-PMCP and over 80% selectivity for TFE-PMCPP.

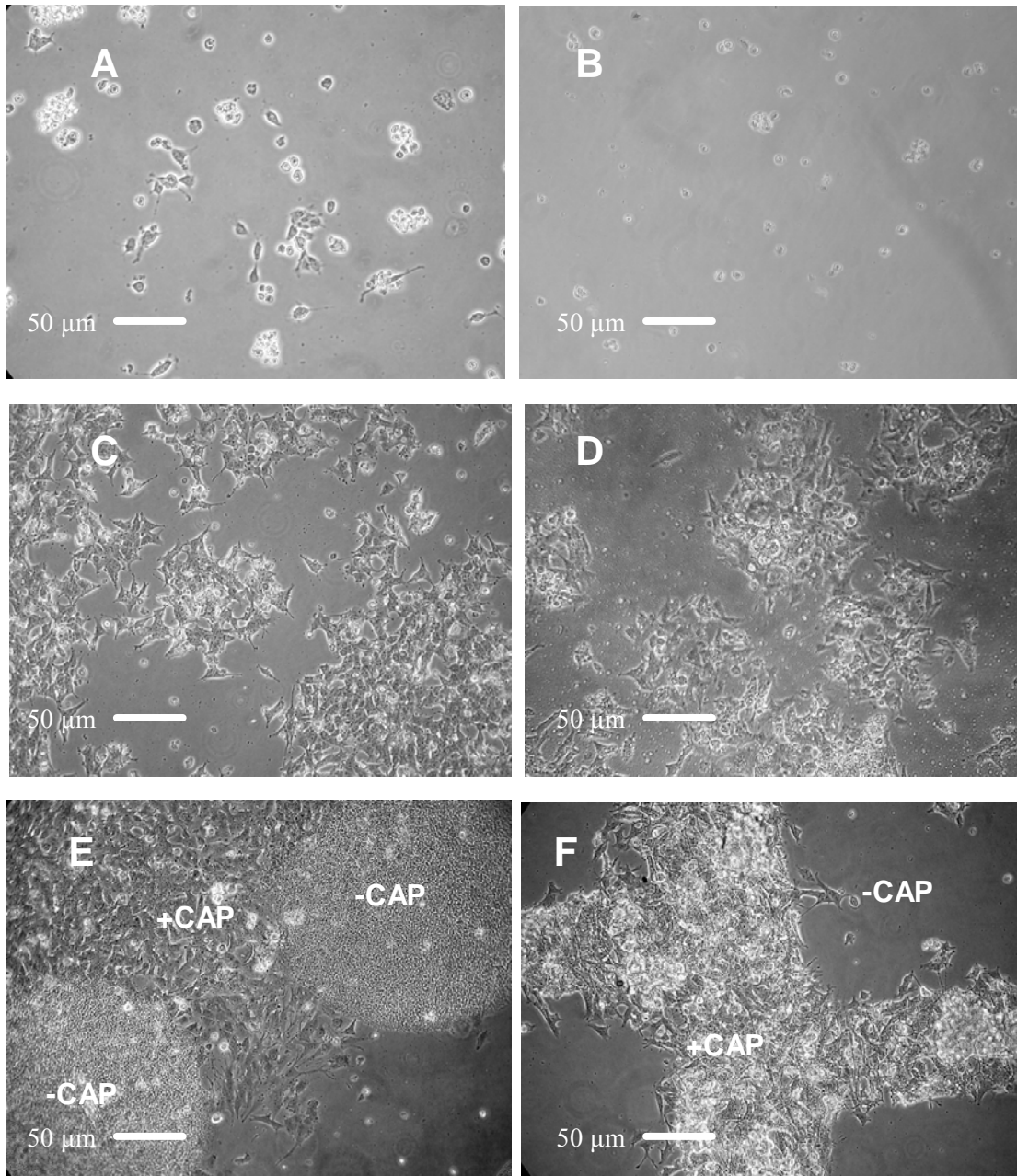
Figure 4-10

Figure 4-10: Differential Cell Adhesion after 3 days in culture: A) 2 (MEEP), B) 1 (TFE), C) 4 (PMCP), D) 3 (PMCPP), E) Photolithographically patterned circle of 2 onto 4, F) Microstamped pattern of 3 onto 1.

Another aspect that has been suggested as a potential cause of differential cell adhesion is the presence of topographical features. Recently it has been shown that feature size and the distance between neighboring features may have a significant effect on cellular adhesion and orientation (**Dowell-Mesfin, 2004**). In this work axonal and dendritic projections grew preferentially on the surface of polymeric features if the gaps between them were smaller or close to the size of the projections. If the features were further apart, selectivity was diminished. This is also the case for cell body adhesion if the feature sizes and gaps between features are comparable or smaller than the size of the adherent cell body. 250 μm square PDMS stamps with 50 μm square features and 50 μm spacing were used to stamp TFE over a spun cast layer of TFE. The previously described technique was utilized to quantify the cells, and an increase in adhesion was observed. After 3 days in culture 3 times more cells were seen than on the uniform layer of TFE (**Figure 4-11**). However, adhesion was not uniform and other factors may have influenced the process. If the size of the features was increased to be much larger than the cells (250 μm feature) there was no increase in cell adhesion and the large stamp behaved as before (**Figure 4-9**).

Another explanation for this phenomenon could lie in the apparent or “average” hydrophilicity of the patterned biomaterial as detected by the cells. As the cells rest on the hydrophobic –CAP and bridge the 5 μm gaps between the micropatterned features, regions of the cell body are exposed to the hydrophilic culture media. This “average” hydrophilicity could potentially fall in a range suitable to promote cellular adhesion.

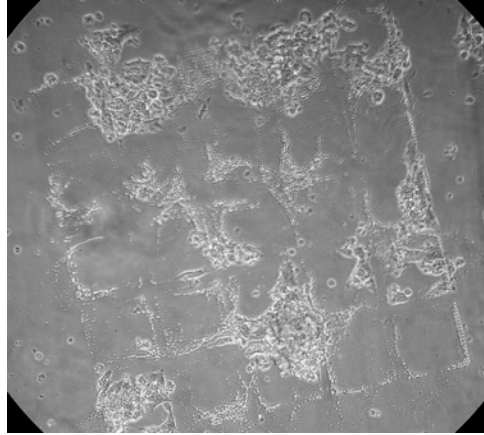
Figure 4-11

Figure 4-11: TFE over TFE, 250 μm square stamps made out 50 μm square features

4.4.6 Impedance Analysis

In addition to the cell adhesive (+CAP) and non adhesive (-CAP) areas for patterned neural networks, when working with microelectrode arrays (MEA), an insulator layer is also required to isolate connections to and from the microelectrodes (**Stenger, 1994**). The material design took into account desired electrical properties. The +CAP should be electrically conductive and should provide a low impedance path between the cells and the microelectrodes. The ideal -CAP would be dielectric and serve as an insulation layer for the connections. Since cells are cultured in a fluid ionic environment, the material should either permit or restrict ionic flow. For that reason all of the +CAP materials were designed to form stable ion permeable hydrogels. With respect to the -CAP species, TFE is not only hydrophobic, but due to its similarities with Teflon®, it was expected to be a good insulator.

As shown previously (Differential Cell Patterning), TFE and PMCPP produce stable patternable substrates with large cell selectivity. To measure the ionic impedance of these materials a parallel plate chamber was designed, such that two copper electrodes, 5 mm in diameter were separated by 5 mm in a 1 mM KCl solution. One of the electrodes was spin coated with a 1 to 3 μm film of the polyphosphazene and the whole system connected to an HP 4192A LF impedance analyzer. Magnitude plots for the specific impedance of the materials, as compared to the chamber are shown in **Figure 4-12**.

Figure 4-12

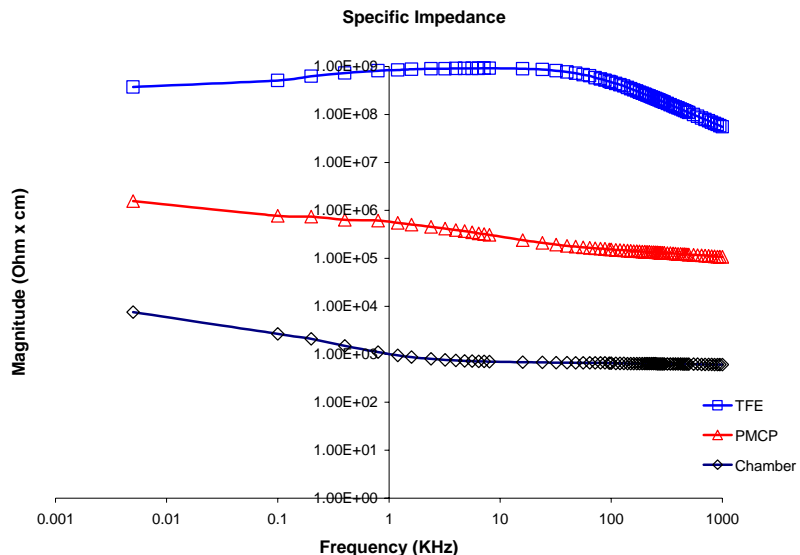


Figure 4-12: Magnitude plot for the specific impedance of TFE (1) and PMCPP (3) as compared to the test chamber.

From **Figure 4-12** it is clear that TFE shows a high resistance with a magnitude in the order of $10^9 \Omega\text{cm}$ while PMCPP has an average magnitude of $10^6 \Omega\text{cm}$, 3 orders of magnitude difference. At frequencies higher than 10 KHz, TFE behaves like a capacitor.

Impedance measurements for PL, were attempted but the material dissolved quickly in the ionic solution, and no measurement was possible.

4.4.7 Cell Adhesion Mechanism

Well-supported evidence exists that indicates that one of the initial steps of the cellular adhesion mechanism is the deposition of a biomacromolecule film. This film may be comprised of polysaccharides and proteins and is deposited by a cell before adhesion (**Nivens, 1993; Bryers, 1994**). This film is deposited only if the cell finds a substrate that is compatible to biofilm binding and hence “compatible” with the cell. In the work presented here it was shown that plated SK-N-BE(2c) neuroblastoma cells, adhere directly to PMCP showing normal axonal sprouting and neural morphology.

Fibronectin is a glycoprotein of high molecular weight that occurs in fibrillar form in the extracellular matrix of animal tissues. It has multiple domains that confer the ability to interact with various elements such as collagen, fibrin and cells. Cells specifically bind to fibronectin by the means of integrins. Integrins are specific membrane receptors that bind to an RGD (ArgGlyAsp) sequence in the fibronectin protein. Interaction of integrins with fibronectin results in adhesion and spreading of the cell.

In order to determine the adhesion mechanism a collaboration with Dr. Winograd was established and collaborative research was performed with Ms. Abigale Marcus. Time-of-flight secondary ion mass spectrometry (ToF-SIMS) was utilized to obtain molecular identification from the surface of a sample. ToF-SIMS uses a primary ion

beam which impinges on the surface of a sample. The impacting ion creates a collision cascade which causes sputtering from the surface. Secondary ions which form during that sputtering process evolve from the sample surface into the vacuum chamber and are detected. The secondary ions are detected in parallel and a mass spectrum or a total ion image is generated. Secondary ion yields can dictate how much of a surface is seen, so a higher ion yield while keeping the chemical integrity intact is advantagous.

The substrate used for this experiment was comprised of 200 nm Au on 10 nm of Cr on a Si wafer. This substrate was cleaned in a nitric acid – hydrogen peroxide piranha etch for 30 sec, rinsed three times in 18 MΩ H₂O. The substrate was left in 18 MΩ H₂O until polymer sample preparation was done on the substrate. Prior to polymer sample preparation, the substrate was rinsed in acetone.

A 10 mg/ml solution of PMCP in acetone was spin coated onto the substrate at 3000 rpm for 30 seconds. The PMCP coated substrate was rinsed in 3 times in PBS before plating the cells. Cells were plated at a density of 8×10^6 cells and maintained in Ham's F-12: Minimal Essential Media MEM (1:1) (Gibco BRL) supplemented with 15% fetal bovine serum (Bioreclamation), 100 units/ml penicillin and 50µg/ml streptomycin.

The secondary ion mass spectrometry studies and images were performed on a custom built (Dr. Winograd Laboratory) Biotof Tof-SIMS instrument. The vacuum inside the analysis chamber was maintained at 5×10^{-9} Torr. Two independent ion sources were utilized for analysis:

- First source consisted of a pulsed 15 keV Ga⁺ ion beam with a beam current of between 3-4 nA, a spot size of 100 nm, a pulse width of 40 ns at 3 kHz. The stage, reflect, retard and extract lens voltages were the following respectively: 2500 V, 2550

V, 1175 V, and 4300 V. The polarity of these voltages depended on whether spectra were collected for positive or negative ions. The ion fluence was kept below 1.0×10^{12} ions/cm², so the fluence stayed below the static SIMS limit. Charge compensation was not required for any of these experiments. Samples were detected using post acceleration of 17 kV applied to the front plate of the detector.

- A second source was comprised of blanked pulsed 25 keV Au ion beam with a spot size of 100 nm, a pulse width of 40 ns at 3 kHz. The ion fluence was kept below 1.0×10^{12} ions/cm², so that it stayed below the static SIMS limit. This Au source has several different primary ions which were selected out using a magnet field ion selector. The currents for Au+, Au++, Au2+, and Au3+ were as follows: 4 nA, x, y and z. These experiments were also kept below the static SIMS limit.

The ToF-SIMS images were taken by rastering the beam over the surface area of 1168 μm x 1168 μm with a primary ion fluence of less than 10^{12} ions/cm² using 256 x 256 pixels with 41 counts/shot.

Before cell imaging experiments were performed, the control spectrum of PMCP was taken with ToF-SIMS to determine the characteristic peaks for this polymer. The characteristic peaks in the low mass region from m/z 0-400 of the negative SIMS for PMCP are the following: m/z = 16 (O⁻), m/z = 17 (OH⁻), m/z = 117 (C₅H₉O₃⁻), m/z = 162 (C₅H₉NO₃P⁻), m/z = 270 (C₁₂H₁₇NO₄P⁻), m/z = 349 (C₁₂H₁₉N₂O₆P₂⁻). The characteristic separation between high mass peaks is 165 Daltons which corresponds to a structure of (C₅H₁₀O₃NP). This loss corresponds to the loss of a MEEP side chain. These negative peaks clearly showed that PMCP was present on a surface. The characteristic peaks in positive SIMS for PMCP were the following: m/z = 62 (HNOP⁺), m/z = 111

($^{+}\text{C}_4\text{H}_2\text{ONP}^+$), , m/z = 113 ($^{+}\text{C}_4\text{H}_2\text{ONP}^+$), m/z = 168 ($\text{C}_7\text{H}_7\text{O}_2\text{NP}^+$), and m/z = 305 ($^{+}\text{C}_{15}\text{H}_{16}\text{NO}_4\text{P}^-$).

Five days after plating, cells were extracted from the incubator. Media was removed and washed twice with PBS. 45 μl of Ag nanoparticles (30-70 nm) were added to the cell preparation to help boost the signal. Samples were placed in a glass Petri dish and soaked with liquid nitrogen. After half the nitrogen had evaporated, the samples were introduced in a turbo molecular pump (Pfeiffer Vacuum Technology AG, Germany) at 1×10^{-8} Torr overnight.

Figure 4-13 shows a ToF-SIMS image of the culture discriminated for specific molecular weights. The first panel (a) illustrates all the ions collected during an experiment. Panel (b) depicts the 184 characteristic phoshatidylcholine (cholesterol) image which is indicative of the lipid bilayer of a cell. c) The green image shows the polymer pentamer at m/z 1355 Daltons. The significance of this particular image is that it does not map to where the 184 maps indicating that there is a layer of polymer underneath and cells are not growing in that particular area. d) The polypeptide GlyHisTyrArgGlyAsp with an m/z of 686 maps to an area not localized to the cellular lipid bilayer. This result implies that this particular polypeptide is located in the extra cellular matrix. f) The ProValAlaLeuPheArgGlyAsp with an m/z of 856 maps to an area not localized to the cellular lipid bilayer. This result implies that this particular polypeptide is located in the extra cellular matrix.

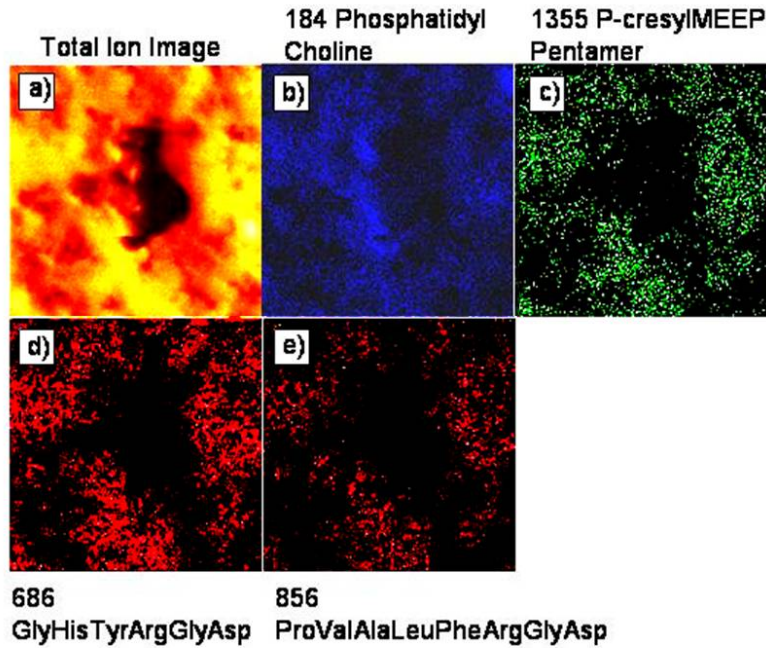
Figure 4-13

Figure 4-13: *ToF-SIMS image of cells cultured over PMCP indicating: a) Total ions collected. b) m/z 184 phosphatidylcholine characteristic fragment c) m/z 1355 PMCP pentamer d) m/z 686 GlyHisTyrArgGlyAsp e) m/z 856 ProValAlaLeuPheArgGlyAsp*

Considering the fact that no extraneous protein was put down on the surface of the polymer, and that the polypeptides were not present in control spectrum of PMCP, the finding of the two polypeptide sequences with the ArgGlyAsp domain imply that the cells are growing their own biomacromolecule film to facilitate adhesion to the polymer surface.

4.5 Chapter Summary

Two independent cell culture and recording chambers were designed and built for the study of population based macroelectrode recordings. CCC #1 served as the proof of

concept for the design and CCC #2 was improved to provide greater macroelectrode functionality and reduced noise. Two macroelectrode base plates were designed and built for the CCC #2 systems. These macroelectrodes are transparent, and reusable, making them a cost effective solution for cell population research.

Various polyphosphazenes were designed synthesized and characterized in collaboration with Dr. Allcock's laboratory. Materials were classified as "cell-compatible" (+CAP) or cell-repulsive (-CAP) polymers. Based on the material properties various microfabrication strategies were utilized and this showed that cell selectivity can be attained when cells are cultured over +CAP and -CAP patterns. The results of this study demonstrate the potential for polyphosphazenes for directed growth of mammalian cells.

It was also shown that cells are growing their own biomacromolecular (protein) film to facilitate adhesion to the polymer and that the polymers are biologically friendly. Some authors suggest that not only the surface chemistry but also the topography characteristics of the material affect the adhesions of cells. Therefore; the potential for an increase in cell adhesion was explored by patterning -CAP microfeatures on -CAP, and showed that adhesion is increased.

It was also shown that TFE can be used as a -CAP and isolative layer and PMCPP as a conductive +CAP layer. This means that a substantial reduction can be achieved in the number of patterning steps required to manufacture multielectrode arrays, by combining the insulation and -CAP properties into a single material. It is also possible to increase the electrical coupling between the cell and the electrode by use of the

hydrogel layer. Moreover, patterning of these two materials is compatible with silkscreen technologies that are suitable for batch manufacturing of cell selective arrays.

Although little or no attention has previously been placed on the micropatterning of polyphosphazenes for biological applications, this family of polymers could provide an efficient and cost effective platform for batch manufacturing of patterned cell culture systems. Secondly, the system utilizes water swollen hydrogels, which potentially could be used to entrap biologically relevant molecules to further aid and control cellular adhesion. Third the polymer promotes the deposition of extracellular matrix proteins by the cells that should further aide in the biocompatibility of the system. The thick profile of such a pattern may also limit cellular migration into undesired regions of a pattern.

Chapter 5

Electrophysiology of Neuroblastoma Cell Clusters

5.1 Introduction

Section 3.3 presented patch clamp recordings for the SK-N-BE(2c) neuroblastoma cell line, suggesting the viability of utilizing such a system as a model for population based research. This chapter presents population potentials obtained from SK-N-BE(2c) cells and compares them to the results found in chapter 2.

All of the recordings were obtained from SK-N-BE(2c) cells plated over the cell friendly PMCP (Section 4.5.3) and amplified by means of a high input impedance, high gain AC-coupled amplifier (Data Inc, Fort Collins, CO). Signals were digitally sampled with a Pentium II based PC computer equipped with a Biopack MP100, ISA100B communication adapter (Biopack Systems, Inc. Santa Barbara California), running Windows 98 operating system (Microsoft Corporation) and Acqknowledge version 3.5.7 (Biopack Systems, Inc. Santa Barbara California). Signal processing was performed using Matlab version 6.5.1.199709 Release 13, Service Pack 1 (The Mathworks, Inc.)

Three independent data sets are presented:

- **Data Set Number 1:** Macroelectrode recordings using the Cell Culture Chamber #1 (CCC #1 section 4.2).
- **Data Set Number 2:** Microelectrode recordings using tungsten-parylene 50 μm electrodes (TPE).

- **Data Set Number 3:** Combined Macroelectrode + Microelectrode recordings using the Cell Culture Chamber #2 (CCC #2 section **4.4**) and the TP electrodes.

A summary of the experiments performed for each data set is presented in Table **5-1**.

Table **5-1**

5-1: Summary of the experiments presented in this chapter

Data Set	Type	Electrode	DAP	Samples	Files	BPF (Hz)	SR (KHz)
1	M	CCC#1	5,10,20,35	20	>200	150 2000	10
2	m	TPE	3,6,9,12,25	12	160	0.05 5000	10
3	M+m	CCC#2+TP	10,15,20	3	100	0.05 3000	6

Type: Macroelectrode (M), microelectrode (m)

DAP = Days after Plating

CCC#1 = Cell Culture Chamber Number 1

CCC#2 = Cell Culture Chamber Number 2

TPE = Tungsten-Parylene 50 μ m electrodes

DAP = Days After Plating

Samples = Number of independent samples for the data set

Files = # of 30 s files recorded for the data set

BPF = Band Pass Frequency

SR = Sampling Rate

The first data set was used to characterize the population response from the cell line and to validate the macroelectrode approach. The second data set was utilized to characterize the field potentials in the vicinity of small cell clusters. The last data set was utilized to correlate simultaneous microelectrode and macroelectrode recordings and further validate the use of the macroelectrode approach.

The model presented in Chapter 2 was derived for discrete time. Therefore some modifications need to be made, to account for continuous time. The continuous time signal processing strategy was previously presented in (**Gaumond, 2004**) and will be discussed in the following section.

5.2 Continuous Time Signal Processing Strategy

In Chapter 2, a discrete time approach for the simulation of summed neural activity was presented. Signals analyzed in this chapter are continuous time signals so certain modifications are required. If signal and noise are uncorrelated, then the total current can be expressed as follows:

(Equation 5.1)

$$y(t) = ap(t) + n(t)$$

Equation 5.1

Where $ap(t)$ is the sum of all the action potential waveforms contributing to $y(t)$ and $n(t)$ is the "noise" from all sources, for example, thermal and shot noise components. In general, $y(t)$ is obtained through a series of amplification and filtering steps, in both the analog and digital domains. It is assumed that these are linear operations acting independently on the components of $y(t)$.

A useful way of characterizing $y(t)$ is via the autocorrelation $AR_y(\tau)$

(Equation 5.2)

$$AR_y(\tau) = E[y(t)y(t+\tau)] \approx \frac{1}{T} \int_0^T y(t)y(t+\tau)dt$$

Equation 5.2

The $E[]$ denotes the "expectation" operation, estimated in practice (assuming a well-behaved "ergodic" random process) by calculating the average of the quantity over some finite time interval T . $AR_y(0)$ is the power of signal $y(t)$, equal to the variance of $y(t)$ if $E[y(t)]$ is zero. This follows directly from the definition of $R_y(\tau)$, setting $\tau=0$. The Fourier Transform of $AR_y(\tau)$ is the power spectral density of $y(t)$, written $G_y(f)$:

(Equation 5.3)

$$Gy(f) = \int_{-\infty}^{\infty} AR_y(\tau) e^{j\omega\tau} d\tau \quad \text{Equation 5.3}$$

Substituting 5.1 into 5.2 and assuming that noise “n(t)” is independent of signal “ap(t)”, the autocorrelation of the total signal is the autocorrelation of the signal plus the autocorrelation of the noise:

(Equation 5.4)

$$ARy(t) = ARap(t) + ARn(t) \quad \text{Equation 5.4}$$

Due to the linearity of the integration, the same is true for the power spectrum and:

(Equation 5.5)

$$Gy(f) = Gap(f) + Gn(f) \quad \text{Equation 5.5}$$

5.3 Data Set Number 1

A population of SKN-B-E(2c) neuroblastoma cells, was plated in CCC #1 (See section 4.2). The developing cell culture was followed for a period of 35 days and both photographs, and electrical measurements were taken. Over 200 independent, 30 s recordings were obtained from over 20 independent samples. Cells were plated at a density of 8×10^6 cells/ml, over glass slides 2×2.5 cm, sputtered on one side with a transparent indium-tin-oxide (ITO) electrode and spun cast with a layer of a cell friendly PMCP. The cells were maintained in Ham’s F-12: Minimal Essential Media MEM (1:1) (Gibco BRL) supplemented with 15% fetal bovine serum (Bioreclamation), 100 units/ml

penicillin and 50 μ g/ml streptomycin. Cells plated over the transparent electrodes were placed individually into the CCC #1 and recordings were performed. At the end of each recording session the cells were discarded to avoid contamination of the remaining culture.

All electrical recordings were performed in a Faraday cage using a high input impedance, high gain AC-coupled amplifier (Data Inc, Fort Collins, CO) band pass filtered between 150-2000 Hz, with a gain of 12,000 and sampled at 10,000 samples/sec (Biopack Systems, Inc. Santa Barbara California). PMCP coated ITO slides inserted in the cell chamber and in the presence of culture media, has impedance in the range of 1 K Ω as measured at 1 KHz measured between the ITO and Ag/AgCl electrodes. This configuration is very robust and cells survived electrically active for over 40 days.

Deflections of varying shapes (bi-phasic, tri-phasic, etc.) of around 5 microvolts amplitude and 6 ± 2 ms in duration were observed, in all of the recordings. These signals were generally similar through time as shown in the two upper panels of Figure 5-1. In these two panels recordings from 5 and 35 days after plating (DAP) are compared and both the average magnitude and duration of the events is preserved. An additional signal was also observed in the recordings as shown in the lower panel of Figure 5-1. Notice that the time scale for the lower panel is expressed in seconds while the scale in both of the upper panels is in milliseconds. On day 35, (Lower panel of Figure 5-1), large and slow spikes (30 microvolts in amplitude) separated by 1-2 seconds were detected in the population (Silva, 2003). The hypothesized explanation for such a phenomenon is the following: a small cell cluster acts as a pacer; synaptic mediated transmission allows for the propagation of a two dimensional wave front, and the spatial-temporal summation of

the propagating wave is registered as slow potentials. Experiments presented in this chapter were designed to test this hypothesis.

Figure 5-1

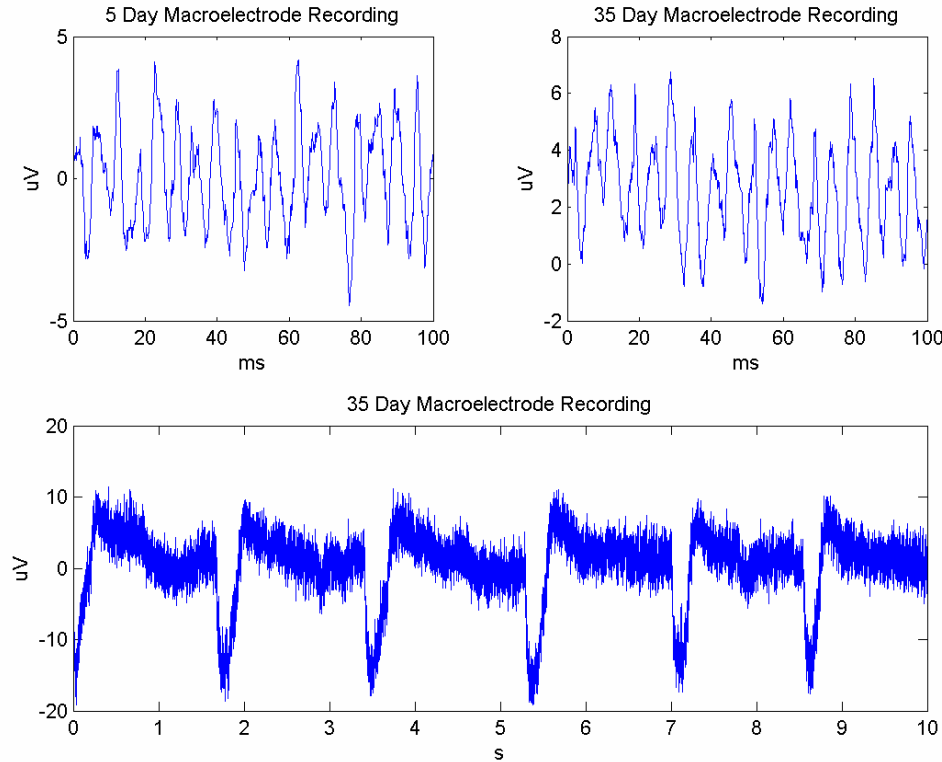


Figure 5-1: *Bio-Electric-Potentials, recorded by means of the CCC #1, for 5 and 35 days after plating. Upper panels show individual field potential waveforms for days 5 and 35 after plating. Lower panel shows pacemaker-like slow potential spikes observed at day 35.*

Potentials, recorded by means of the CCC #1, represent the activity of around 250,000 cells, assuming a confluent layer and an effective radius, that accounts for inter cell separation, of 20 μm per cell. It is assumed that the signal energy is highly correlated, while the noise is broadband and uncorrelated from the signal. In this case, the autocorrelation of the function is expressed as in (Equation 5.1). $ARy(0)$ represents the

total amount of energy in the segment being analyzed and ARy can be normalized by its corresponding $ARy(0)$. The power spectral density $Gy(f)$ defined in Eq. (5.5) is another useful measure of the systems energy that provides information from the frequency domain. By comparing the time response of the signals with its respective ARy and Gy a good characterization of the signal can be obtained. The analysis is focused in distinguishing two signals of interest; “slow” (lasting more than 20 ms) and “fast” (lasting less than 20 ms) potentials; therefore, two time scales are utilized for comparison purposes: 2 s and 200 ms. By comparing time, autocorrelation and power spectral density domains as a function of days after plating, a complete picture of the temporal evolution of the signals can be obtained. Power Spectral Density was estimated via Welch's method with a Hamming window and 50% overlap. This method estimates the average periodogram from overlapping windows, decreasing variance in the overall estimate. Figure 5-2, presents a comparison of the time signal, ARy and Gy for 5, 10, 20, and 35 days after plating. Each row shows traces (red and blue) corresponding to independent experiments performed on the same day. Two time scales are used both in the time domain and in the autocorrelation domain to compare the evolution of slow and fast events.

Figure 5-2

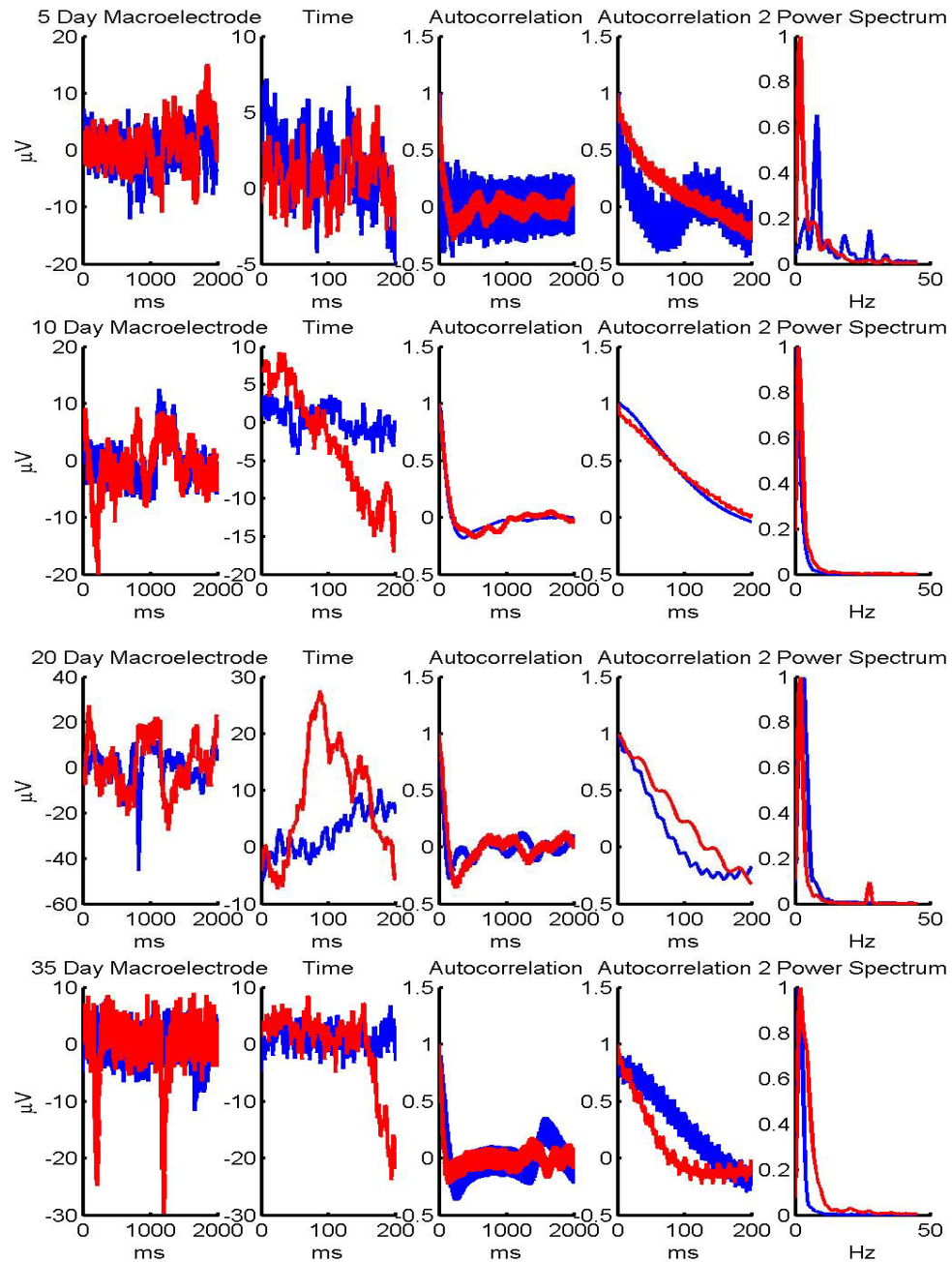


Figure 5-2: Time signals, and normalized ARy and Gy for 30 s recordings obtained using CCC#1; 5, 10, 20 and 35 days after plating. Blue and red tracings correspond to independent experiments performed at the same day. Recordings were performed under identical conditions using the same devices and settings.

From the figure it can be seen that energy from the system is low frequency as shown by the power spectrum domain (last column). The energy spectrum is under 50 Hz for 10 days after plating and under 25 Hz, 15 days after plating and beyond. The 200 ms autocorrelation panel (fourth column from the left) shows the first peak of ARy ranging from 75 ms (blue trace, 5 DAP) to 200 ms (both traces, 10 DAP). This autocorrelation is broader than the fast potentials, estimated to last 6 ± 2 ms and indicate the presence of multiple cells firing within a narrow time window. This effect is the result of spatial-temporal summation of the bioelectric potentials from multiple units that result in enhanced population potentials (slow potentials). A good example of spatial-temporal summation is seen in the 200 ms time panel of the 20 day signal. Here (red trace) a positive slow potential of around 40 mV and 200 ms in duration is shown. Notice how the slow potential is made of smaller subunits (spikes) in the order of 10 ms.

5 DAP slow potentials are erratic and almost absent, at this time, small broadenings of up to 18 μ V and 20 ms in duration randomly appeared in the macroelectrode recordings. Across time the magnitude of the response increases and the large events become dominant, as seen in the first column of Figure 5-2. To confirm this observation, 2 (5 DAP) to 5 (10 DAP and beyond) slow events from 3 to 6 recordings per day at 5,10,15 and 20 DAP were selected and “slow” versus “fast” amplitude ratio was computed (Figure 5-3) (Silva, 2005). From the figure it is clear that there is a linear increase for this ratio and that slow potentials strengthen with time. This observation suggests that the amount of cells firing within a close time window increases with time after plating indicating greater connectivity within cell culture.

Figure 5-1

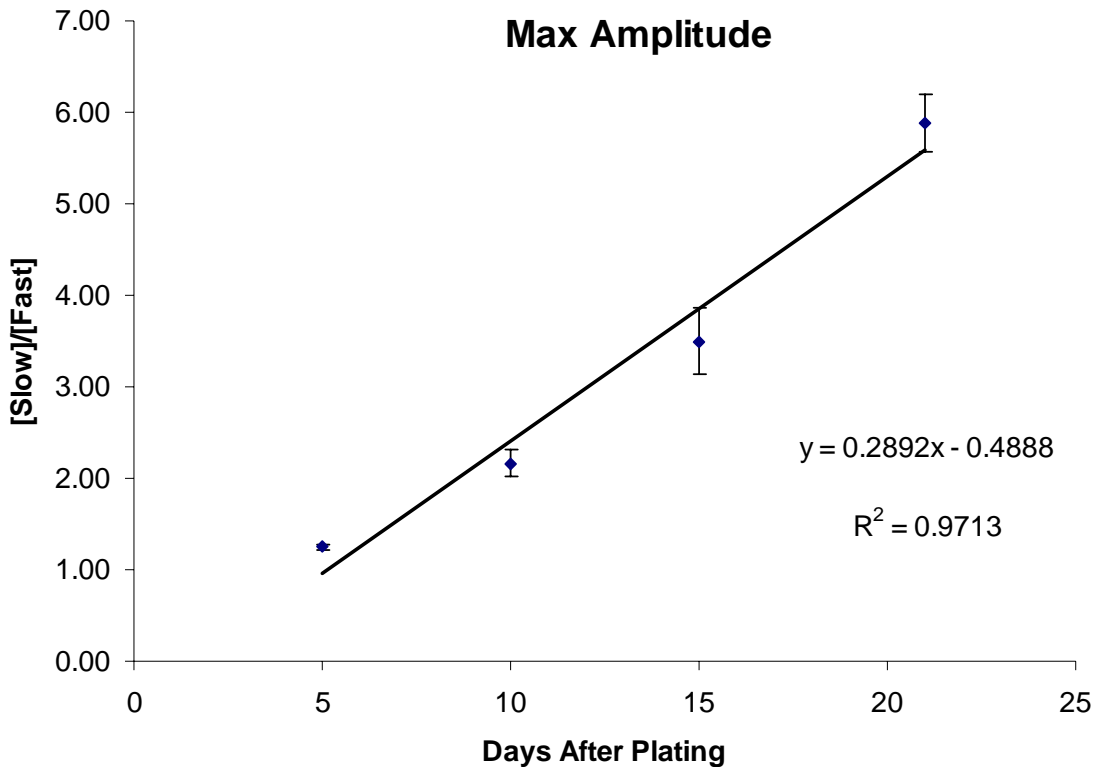


Figure 5-3: Plot of Multiunit Spike amplitude versus Single Unit Spike Amplitude Ratio as a function of time (Silva, 2005).

Besides increasing in size, the time between slow events (Slow-Event Interval) also evolves. The first and third columns of Figure 5-2 indicate that slow events transition from uncoordinated to highly coordinated events as seen in the bottom left panel of the figure (35 day, 200 ms time signal). Coordination of the slow events is clearly observed in the autocorrelation domain. By looking at the 2000 ms autocorrelation column (third from the left) of Figure 5-2 it is clear that cells evolve through three phases:

- **Uncoordinated Phase:** Observed with the 5 day recordings, the appearance of secondary and tertiary peaks in the autocorrelation domain is random and does not indicate coordinated behavior within the cell culture.
- **Transition Phase:** Observed with the 10 day recordings, there is a very sharp primary peak and the amount of secondary firings is almost absent.
- **Coordinated Phase:** Seen in both the 20 and the 35 day recordings, the primary peak is still very sharp but the amount of energy for secondary peaks increases. These secondary peaks are clearly distinguishable and indicate that the spacing between large events not random but happens within a specific time window.

If cells were not communicating with each other, uncoordinated behavior should be expected for all of the recordings and both the transition and the coordinated phase would be absent. The transition phase indicates that groups of cells are starting to communicate with each other and to produce slow potentials; however, there is no pacing behavior and secondary slow potential firings could happen any time. The coordinated phase is the most important finding: Cells are not only firing together, but the time between firing is also dominated by the culture and there is a clear pacing mechanism. In the case of the 20 day culture there could be multiple competing pacers and several secondary rhythms are observed. At day 35 there is a clear single pacer and large population of the cells in culture are firing at a rate of about 0.5 to 2 events per second. In order to understand the process driving the development of the coordinated phase the study of smaller populations is required and therefore the second data set was developed.

5.4 Data Set Number 2

To understand the dynamics of the field potentials at a smaller scale, microelectrode recordings were performed in the vicinity of the cells. Tungsten-Parylene 50 μ m electrodes (TPE) (A-M Systems, Carlsborg, WA) were coupled to a pair of M3301 three-axis fine-controlled manual micromanipulators (World Precision Instruments, Inc., Sarasota, Florida). As previously described (Section 5.1) data was amplified with a high gain AC-coupled amplifier (Data Inc, Fort Collins, CO) and band pass filtered between 0.05 Hz-5 KHz, with a gain of 10,000 and sampled at 10,000 samples/sec (Biopack Systems, Inc. Santa Barbara California). The band width was expanded, in particular towards low frequency, since results from section 5.3 indicate that most of the energy occurs at frequencies below 50 Hz.

Cells were plated over glass slides, coated with the cell friendly PMCP as described in section 4.5.4. Evolution of the cell culture was followed and independent samples were utilized for recordings. Placement of the microelectrodes was performed manually at 10x magnification, using an Olympus IMT-2 inverted stage microscope (Olympus America Inc., Melville, New York), equipped with a COLCAMNTSC-1 (World Precision Instruments, Inc., Sarasota, Florida) video camera and connected to a Dazzle Digital Video Creator 80USB, video transfer connector (Pinnacle Systems, Mountain View, Calif). Images were captured using Microsoft Imaging (Microsoft Corp.). A microphotograph of the TPE in contact with a small cell cluster, 3 DAP is presented in **Figure 5-4**.

Figure 5-4

Figure 5-4: Microphotograph of the Tungsten-Parylene 50 μm electrodes (TPE) in contact with a small cell cluster, 3 days after plating.

Once the TPE was positioned in contact with the cells, multiple sets of recordings were obtained. Once the experimentation was concluded cells were discarded, to avoid contamination of the remaining cultures. The set of microelectrode recordings presented comprises samples taken at 3, 6, 9, 12 and 25 days after plating. Over 160 independent 30 s recordings were obtained from 12 independent samples.

Three days after plating, electrical potentials of various magnitudes and in the order of 10 ± 5 ms, were present in all of the microelectrode recordings. Potentials appeared in bursts of similar spikes, of various sizes, as shown in **Figure 5-5**.

Figure 5-5

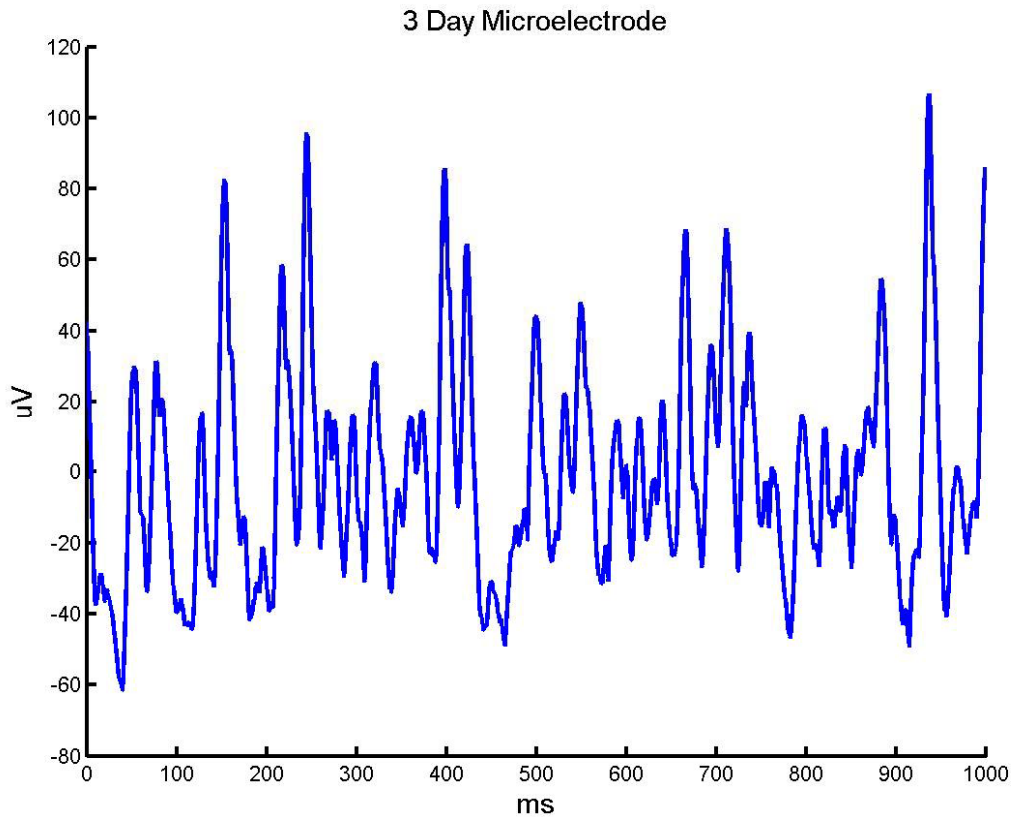


Figure 5-5: Microelectrode recording, from an SK-N-BE(2c) culture 3 day after plating over PMCP coated glass. Recordings were obtained using tungsten-parylene 50 μm electrodes (A-M Systems, Carlsborg, WA). As previously described (Section 5.1).

To confirm that most of the energy comes from signal, rather than noise, a 30 s recording was utilized to obtain the ARy for the 3 day base signal presented in (Figure 5-3). The noise base was obtained by placing a TPE in contact with the cells and recording signals. The microelectrode was then raised from the cell surface at 50 μm steps. At a distance of 100 μm away from the cells ARy had fallen to 1/10 of the original magnitude. Figure 5-6 presents a comparison between ARy, ARn and ARap for a three day recording ARn corresponds to the electrode located 100 μm away from the cells.

Figure 5-6

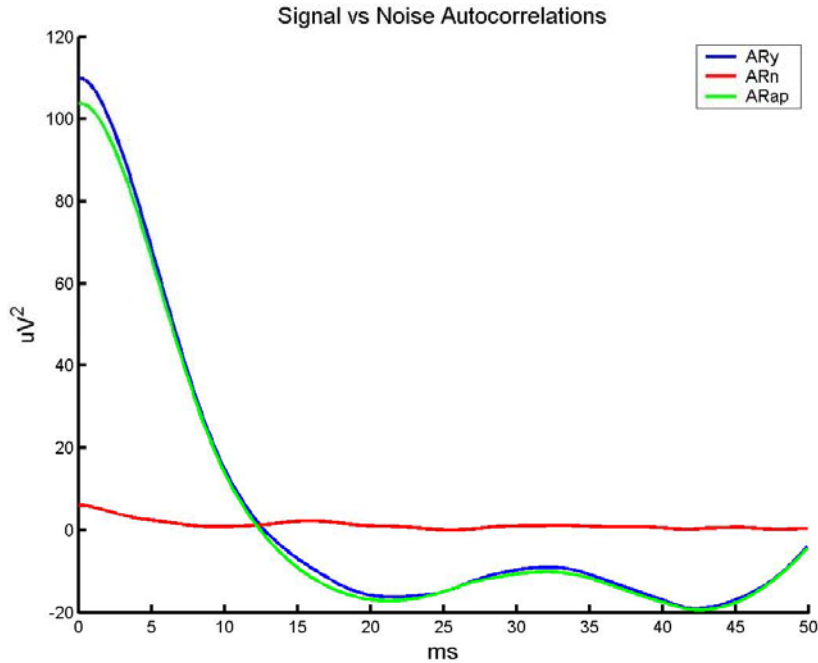


Figure 5-6: Power spectrum for the autocorrelations of signal and noise, as a measure of activity in the vicinity of the cells for a 3 day microelectrode recording. ARn corresponds to the electrode located 100 μm away from the cells ARap was obtained by subtracting ARn from ARy.

From figure 5-6 it is clear that the microelectrode is recording some activity from cells located up to 100 μm away which explains the various magnitudes seen in Figure 5-

5. If the electrode is further separated from the cell substrate the signal drops drastically and the noise base floor for the culture dish can be found. Figure 5-7 shows ARn for the microelectrode at 150, 200 and 250 μm away from the cells. Notice that 250 μm away from the cells there is no cell signal and the base floor is broadband.

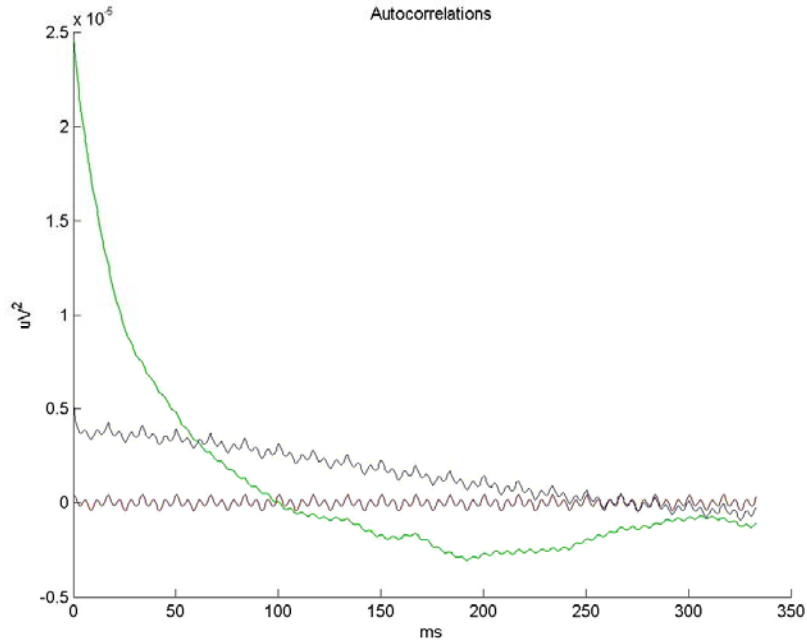
Figure 5-7

Figure 5-7: *ARn* for the TPE microelectrode at 150, 200 and 250 μm away from the cells.

The width of the first peak of ARy represents the duration of the most correlated events, and in this case the most correlated events are the bioelectric potentials present in the recordings. Notice that the width of the first peak of ARy in Figure 5-6 is in the order of 10 ms, which is in the same order as the depolarization events obtained from the patch clamp recordings Figure 3-3. To analyze the evolution of the microelectrode response the same approach utilized in section 5.3 is presented. Figure 5-8, shows a comparison of time, ARy and Gy for 3, 6, 9, 12, and 25 days after plating. The red and blue traces in each panel represent two independent microelectrode recordings for each day. Recordings were performed in identical conditions using the same devices and settings.

Figure 5-8

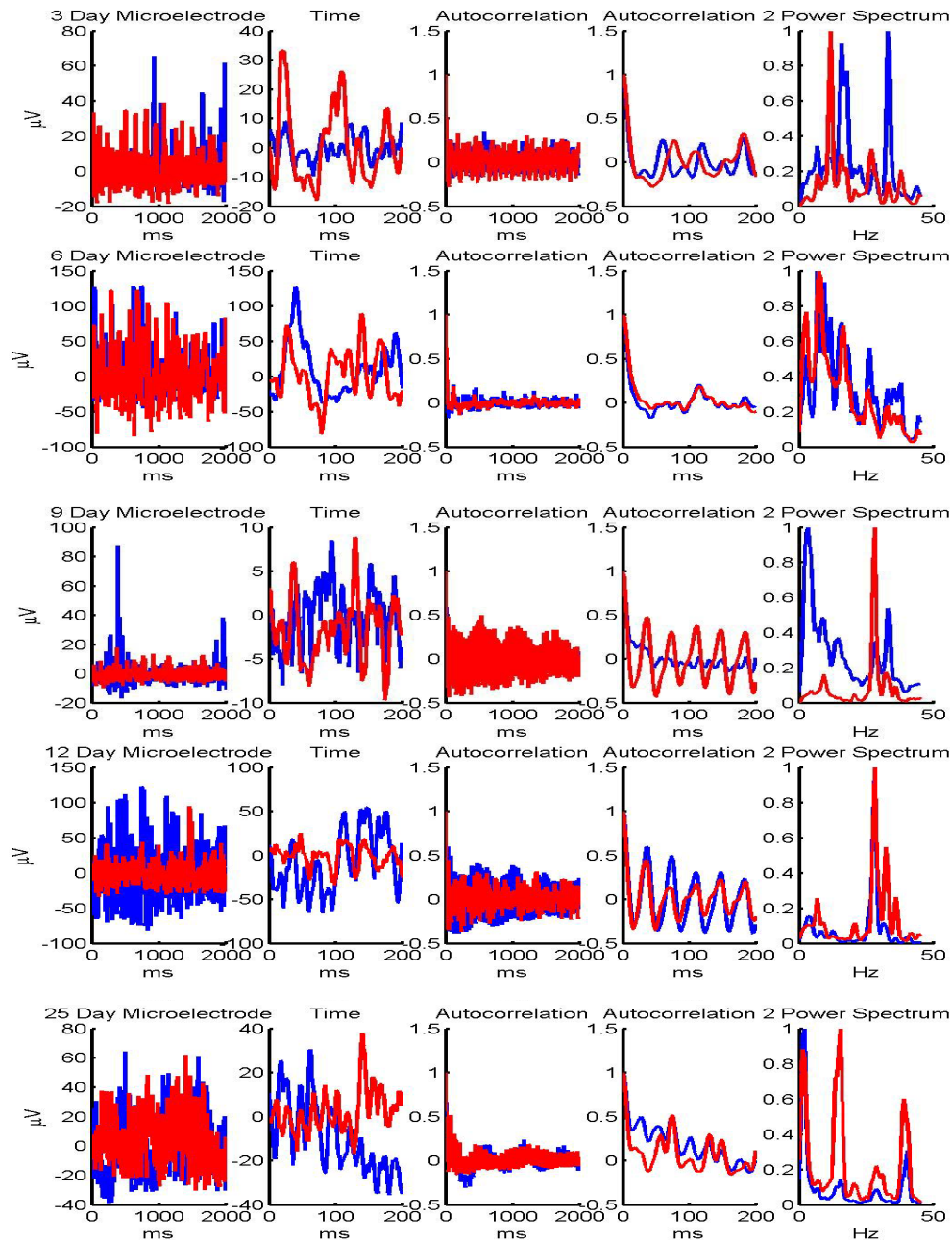


Figure 5-8: Time signal and Normalized ARy and Gw for 3, 6, 9, 12 and 25 days after plating using the TPE microelectrode. Blue and red tracings correspond to independent experiments performed at the same day.

The first relevant aspect from Figure 5-8 is that the width of the first peak in the 200 ms autocorrelation (fourth from the left) is conserved throughout the recordings. This is consistent with the fact that the microelectrode is recording single cell events and that the autocorrelation of single cell waveforms is conserved through time. This observation indicates that the development of the slow potentials observed in the data set number 1 (sect. 5.3) is not the result of broadening of the depolarization event of cells in the population, but rather a summation of many similar events within a window of time.

Consistent with the idea of temporal summation is the fact that the three phases previously discussed in section 5.3 are again visible in the data set. By looking at the 2000 ms autocorrelation column (third from the left) it is clear that 3 DAP both traces show activity consistent with the **Uncoordinated Phase**: Large secondary and tertiary peaks in the autocorrelation domain indicate bursts of similar events from the more active cells in the circuit but do not necessarily indicate coordinated behavior within the cell culture.

9 to 12 DAP (blue trace for the 12 DAP 200 ms autocorrelation) cells are clearly in the **Transition Phase**. There is a very sharp primary peak and the amount of secondary firings is almost absent. This indicates that networks are being established but synapses are not strong enough and dominant connective delay has not been reached.

12 and the 25 day recordings are clearly in the **Coordinated Phase**. Energy in the primary peak is still very sharp but the amount of energy for secondary peaks increases. These secondary peaks are clearly distinguishable and indicate that the spacing between large events is not random but happens within 20 ms of a primary firing cell for the 12 day recordings. In a population of millions of cells these offset time delayed circuits

would generate a broader potential. In fact by looking closely at the 200 ms autocorrelation for the 25 day signals it is clear that the energy from the first peak does not return to zero after 10 ms, but rather temporal summation has occurred and the energy returns to cero after a longer period of time. This indicates cells firing within a closer time window such that an average summed, wider potential is generated. These results are consistent with the idea of slow potentials being the result of a propagating wave front, through synaptically coupled cells, where the mean time between spikes is shorter than the duration of a single spike and spatial-temporal summation is expressed as a slow potential.

To couple the results from the prior two data sets, a new set of experiments was designed. In this case simultaneous micro and macro electrode recordings were performed to determine the relation between both approaches. This will serve to validate the significance of the macroelectrode approach.

5.5 Data Set Number 3

From data sets 1 (sect. 5.3) and 2 (sect. 5.4), there is a clear trend towards coordinated behavior that progresses with time. The data set number 2 (sect. 5.4), indicates that transition from random to correlated behavior (transition phase) occurs between days 9 and 12. In order to understand the nature of the correlated behavior a final set of recordings was performed. In this case, a slightly modified version of the CCC #2 (section 4.4) was utilized. The DB9 connector was replaced by a single electrode attachment, connected to a BNC port. In this way a single electrode with an

approximate area of 13 cm² was created. A standard microscope slide, plated with ITO, was coated with cell friendly PMCP as in the prior experiments and cells were plated and maintained in standard conditions. An Ag/AgCl ring served as counter electrode. Microelectrode recordings were obtained via tungsten-parylene 50 µm electrodes (A-M Systems, Carlsborg, WA), as previously described. Recordings were performed at 3, 6, 10, 15 and 20 days after plating. data was amplified with a high gain AC-coupled amplifier (Data Inc, Fort Collins, CO) and band pass filtered between 0.05 Hz-3 KHz, with a gain of 10,000 and sampled at 6,000 samples/sec (Biopack Systems, Inc. Santa Barbara California). Recordings with the micro and macro electrode were performed simultaneously, using the Ag/AgCl ring as counter electrode. One slide was used per day and discarded after experiments were performed; additional slides were used for calibration and noise recordings. Over 100 independent 30 s recordings were acquired.

Figure 5-9 shows a 20X microphotograph of the microelectrode in contact with the cell substrate, 10 days after plating. At this time the culture is already mature; cells are highly adherent and have extended projections within the substrate. The distance separating the microelectrode from the macroelectrode is of the order of the thickness of a cell layer. The thickness of a cell layer is less than 10 µm as seen from the confocal fluorescent image of a 10 DAP culture shown in Figure 5-10. Microphotograph was taken using an Olympus Fluoview 300 Confocal Laser Scanning Microscope. Cells were stained with Cell Tracker Green (5-chloromethylfluorescein diacetate), (Cambrex Bio Science Walkersville, Inc.).

Figure 5-9

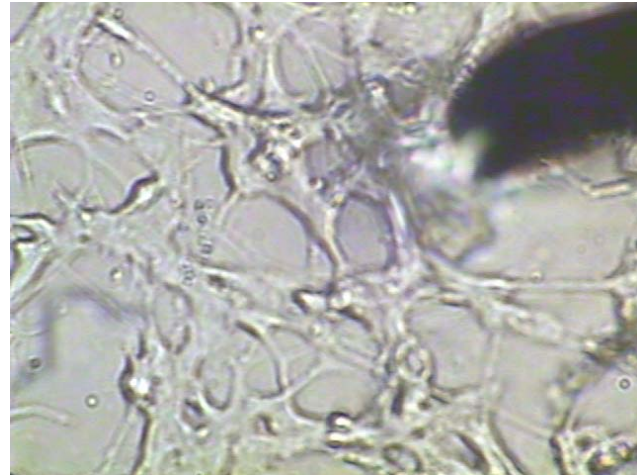


Figure 5-9: 20X microphotograph of the microelectrode in contact with the SK-N-BE(2c) cell substrate, 10 days after plating. There is a lensing effect in the area surrounding the electrode due to the displacement of fluid.

Figure 5-10

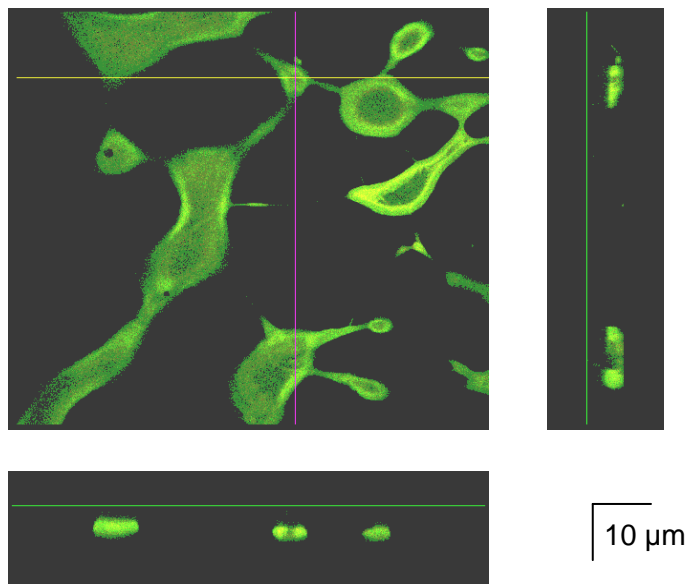


Figure 5-10: Confocal Microphotograph of a 10 DAP culture stained with Cell Tracker Green, (Cambrex Bio Science Walkersville, Inc.), showing vertical and horizontal cross sections.

Figure 5-11

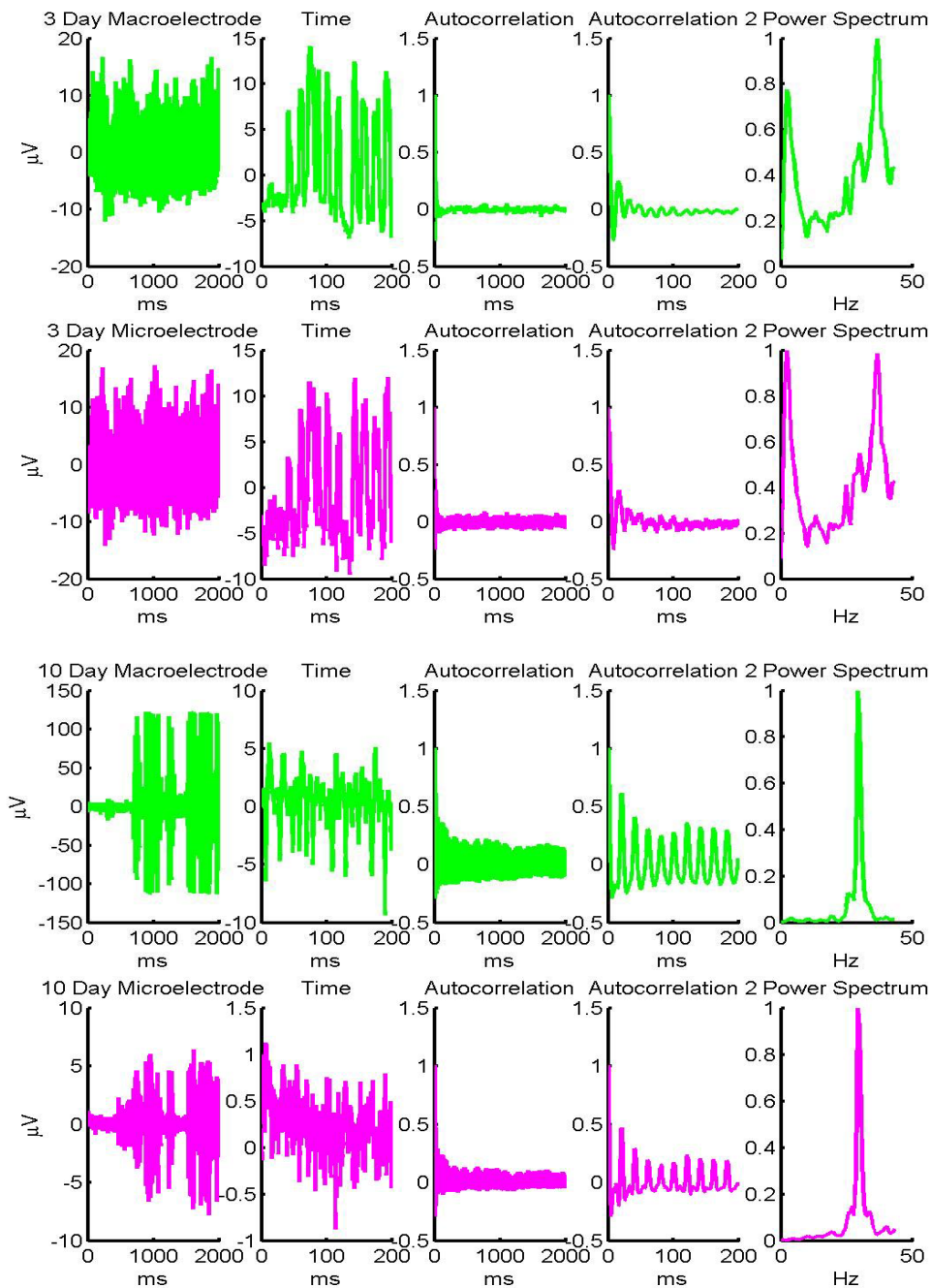


Figure 5-11: Normalized ARy and Gw for 3 and 10 days after plating recordings. Green tracings correspond to the macroelectrode signal and magenta tracings correspond to microelectrode recordings. Recordings were performed simultaneously under the same experimental conditions and using the same Ag-AgCl counter electrode.

Figure 5-12

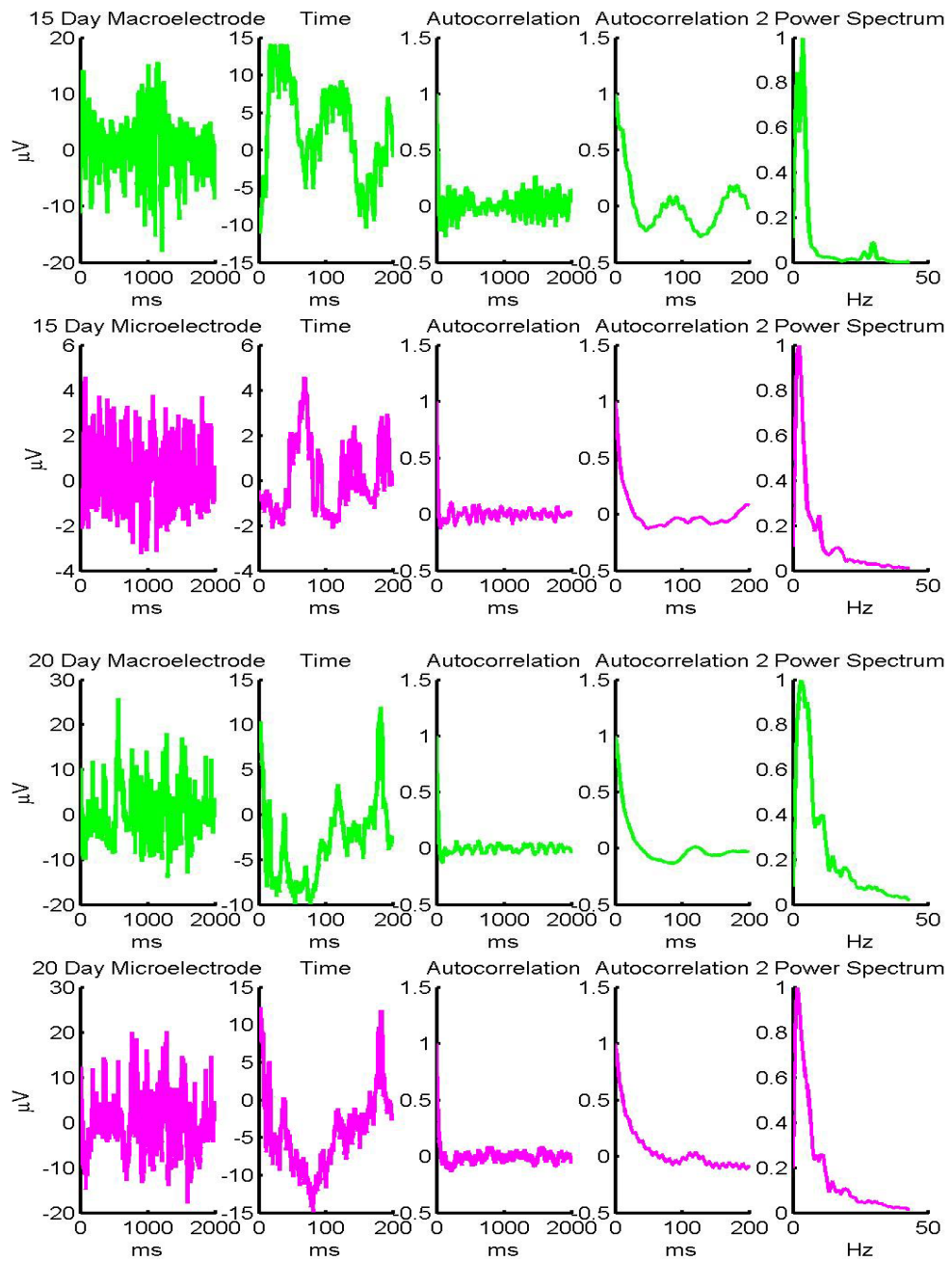


Figure 5-12: Normalized ARy and Gw for 15 and 20 days after plating recordings. Green tracings correspond to the macroelectrode signal and magenta tracings correspond to microelectrode recordings. Recordings were performed simultaneously under the same experimental conditions and using the same Ag-AgCl counter electrode.

As before, time signals, AR_y and G_w for the recordings are presented. Figure 5-11 and figure 5-12 show signals for 3, 10, 15 and 20 days after plating. It is important to distinguish a slight variation from this image as compared to Figure 5-2 and Figure 5-8. Here (Figures 5-11 and 5-12) microelectrode and macroelectrode recordings from the same day are presented in consecutive rows (Green and Magenta Tracings). The energy signature for both traces is similar; but that of the microelectrode tends to have less energy and to be noisier than that of the macroelectrode, except for the 3 DAP where both electrodes have about the same amount of energy.

The Uncoordinated Phase is present in both the micro and the macroelectrode tracings for the 3 day recordings. At day 10, cells are already in a fast pacing post transitional phase, equivalent to that observed for the 12 DAP 200 ms autocorrelation panel of Figure 5-8. It is interesting to observe the 200 ms autocorrelation panel for the 15 day microelectrode recording of Figure 5-11. This panel could be identified as transitional phase, while the corresponding macroelectrode recording in a slow pacing coordinated phase. This indicates that not all of the culture has transitioned and that isolated groups could be exhibiting one type of behavior while the overall summed population response is exhibiting a behavior characteristic of another phase. It is also interesting to observe the apparent delay between the population maximum and the microelectrode maximum as seen in the 200 ms time windows for the 15 day recordings. This is consistent with the idea of a propagating wave and the particular clump being recorded with the TPE is partially participating in the wave. This could also suggest that not all of the cells in the population are synchronized to the macroelectrode events and

that the spatial sum can be the result of multiple pacing circuits throughout the macroelectrode surface.

The 2000 ms time panels for the 10 day microelectrode and macroelectrode recordings show interesting behaviors. The first burst shown in the macroelectrode appears abruptly, while there is a rising phase, preceding the same correlated burst in the microelectrode signal. This suggests that the TPE is located close to a pacing center for the population and that recruitment increases rapidly to a point where the macroelectrode registers a large population spike, consequence of many cells firing quasi-simultaneously. At day 20 is clear that the activity in the microelectrode is mirroring that of the macroelectrode, this suggests a larger correlation between the parts (cells) and the whole (population) such that the system has reached a dynamic equilibrium and cell clusters are following a main pacer. Also the amount of energy in the microelectrode is a significant fraction of the amount of energy in the macroelectrode suggesting that a large fraction of the population is participating in the depolarization event. This means that the mature population is becoming a functional neural network something that has not been reported before.

5.6 Chapter Discussion and Summary

From the data presented, the SK-N-BE(2c) exhibits a bioelectrical behavior that evolves with time after plating. This behavior is characterized by two types of signals; “fast” and “slow” potentials. Patch clamp recordings presented in section 3.3 shows that the duration of the trans-membrane depolarization events are of the same order as the

“fast” potentials observed in this chapter. This indicates that the “fast” potentials are recordings of single cell action potentials. The “slow” potentials become evident as the cell culture matures and are more prominent in the macroelectrode recordings. Slow potentials are considered to be the spatial-temporal summation of a multiplicity of cells in the population.

Since the slow potentials cannot be attributed to random causes, a communication mechanism has taken place in the cell culture and populations of cells generate that coordinated activity. According to (**Banker, 1998**), none of the Neuroblastoma cell lines studied to date give rise to formation of synapses with one another, however, evidence was presented in section **3.5** consistent with this idea. Also, the signals generated by this system look similar to population field potential waveforms of synaptic cells obtained by other groups (**Bove, 1997; Bove, 1998; Chiappalone, 2003; Selinger, 2004**). Therefore the results indicate that SK-N-BE(2c) cells are forming functional synapses in culture, and that such a communication mechanism can be characterized by the presence of slow potentials in the macroelectrode recordings. As cells mature they form a functional syncitium and this behavior is a new discovery for a neuroblastoma cell line.

These slow potentials can then be used as indicators of population coordination. Such a process is characterized by the three aforementioned phases:

- **Uncoordinated Phase.** 3-5 DAP were slow potentials are uncommon and cells are bursting independently. Large secondary and tertiary peaks in the autocorrelation domain indicate bursts of similar events from the more active cells in the circuit but do not necessarily indicate coordinated behavior within the cell culture.

- **Transition Phase.** 9 to 12 DAP, slow potentials become evident in the population recordings and the amount of secondary firings in the autocorrelation domain is almost absent. This indicates that networks are being established but synapses are not strong enough and dominant connective delay has not been reached.
- **Coordinated Phase.** 12 to 15 days and beyond, slow potentials dominate the population behavior. In the autocorrelation domain energy in the primary peak is still dominant, but the amount of energy for secondary peaks increases. Secondary peaks are clearly recognizable and this phase can further be divided into two subphases:
 - **Fast Pacing Coordinated Phase:** Spacing between peaks in the autocorrelation domain is short (within 10 to 20 ms). Cells are pacing very fast and this phase could be indicative of various pacing networks competing for the control of the culture.
 - **Slow Pacing Coordinated Phase:** Is characterized by, pacemaker-like field potential spikes separated 0.5-2 seconds. It is indicative of synchronous burst firing from many neurons in the population and the presence of a dominant pacing network. This phase is a signature of a mature culture.

The results presented in this chapter validate the utilization of the macroelectrode approach and of energy measures (autocorrelation and power spectrum), as viable techniques to study the behavior of electrogenic cell populations in vitro.

Chapter 6

Modulation of the Electrical Response

6.1 Introduction

As shown in section [2.3](#), for a population of uncorrelated pulsatile signals, the root-mean-square (RMS) value of the sum of waveforms increases monotonically as signal pulse rate increases. Also, the average pulse signal can be recovered from the autocorrelation of the summed signal using the Levinson-Durbin recursion. In this chapter the same mathematical approach is utilized for the analysis of signals obtained with the SK-N-BE(2c) neuroblastoma cell line.

6.2 Response of Cells to Stimulus

Glutamate is the major excitatory neurotransmitter in central nervous system acting through both ligand gated ion channels (ionotropic receptors) and G-protein coupled (metabotropic) receptors. The ionotropic glutamate receptors are subdivided into three groups: AMPA, NMDA and Kainate, based on their pharmacological affinity for those specific compounds. AMPA is the most commonly found receptor in nervous system and mediates fast synaptic transmission. The dissociation constant K_d for the glutamate binding domain of isolated AMPA receptors in the presence of L-glutamate, is in the order of 1 μM ([Abele, 1998](#)). In the case of an heterogeneous cell population, a multitude of receptors needs to be activated and glutamate needs to diffuse through any

overlaying cell layers, the extracellular matrix and reach an equilibrium in the vicinity of the cells near the electrode. In consequence, the concentration required for glutamate mediated response needs to be much higher than the K_d for isolated receptors. For instance, affinity of cells to glutamate was determined for Dorsal Root Ganglion (DRG) cells in the presence of constant glycine concentration of 10 μM (**Li, 2004**). The inward current elicited by glutamate increases as glutamate concentration increases from 1 to 2000 μM , reaching a maximum at 1 mM (**Li, 2004**).

It was previously shown (**Silva, 2003**) that there is an MSG induced response in the SK-N-BE(2c) cell line in culture. On day 35, pacemaker-like field potential spikes (30 microvolts in amplitude) separated by 1-2 seconds were detected in the population (Figure **6-1**). With addition of 1 mM Monosodium-Glutamate (MSG), bursts of glutamate-enhanced large-field potentials were sustained for 2-3 seconds and the inter-spike interval decreased to 1/5 sec during bursts. Also, the maximum amplitude increased to 40 μV peak to peak (Figure **6-1**). If the stimulation with MSG is sustained for over 2 minutes some adaptation is seen and both the amplitude and frequency, of the field potentials, return to baseline after about 5 minutes. Once the MSG stimulus is removed, by washing out the MSG containing solution, the cell culture returns to its pacing behavior and both the amplitude and periodicity are restored (Figure **6-1**).

Figure 6-1

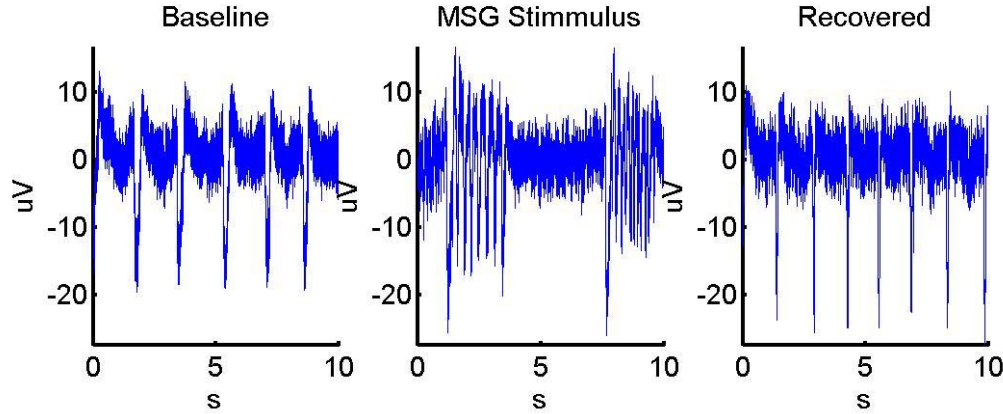


Figure 6-1: Macroelectrode signals from a 35 day cell culture using the CCC #1, showing the baseline activity as compared to 1 mM MSG stimulation, and the recovery from stimulation after washout of the MSG containing solution.

Section 2.3 data indicates there is both an increase in RMS signal $\int \text{Gap}(\omega) d\omega$, and in the mean frequency $\int \omega \text{Gap}(\omega) d\omega / \int \text{Gap}(\omega) d\omega$ when firing rate is increased, where $\text{Gap}(\omega)$ is the power spectral density of AR_{Ap} . Activation (A) can be computed by taking the ratio of the RMS between the baseline and the stimulated signal, $A = AR_s(0)/AR_b(0)$ were AR_s and AR_b are the autocorrelation of the baseline and stimulated signals respectively. These results were derived for uncorrelated signals, which is clearly not the case for the signals presented in Figure 6-1. However, applying the same strategy to the data presented in figure 6-1 an increase in the RMS energy is observed (Figure 6-2). Signals from three consecutive 10 s segments are presented in Figure 6-2, both for the baseline and the MSG stimulation. $AR_b(0)$ was calculated for each of the 10 s segment shown in figure 6-1 and results are as follows: for baseline is $14.92 \pm 5.08 \mu\text{V}^2$, while $AR_s(0)$ for the 1 mM MSG is 21.79 ± 4.48 . Mean activation for this particular case was $A = 1.46$ for 1 mM MSG stimulus.

Figure 6-2

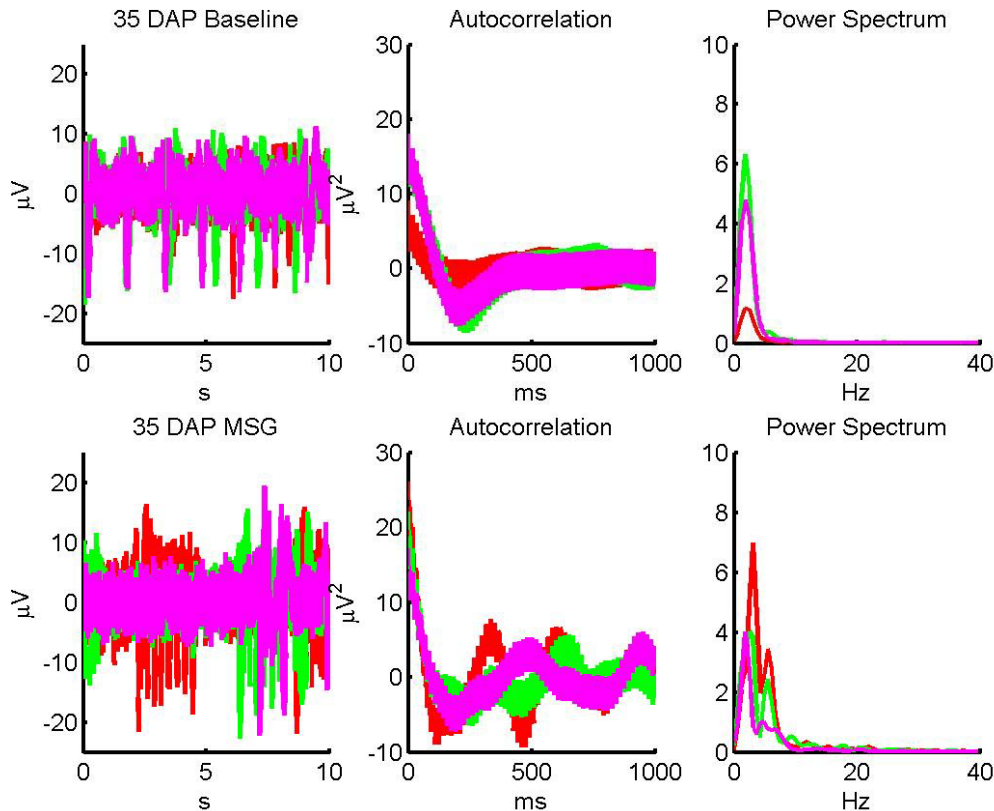


Figure 6-2: *Signal, autocorrelation and power spectrum measures for the 35 DAP macroelectrode signals presented in Figure 6-1. The upper panels show the baseline activity from three consecutive 10 s segments as compared to 1 mM MSG stimulation, presented in the lower panels. The consecutive segments, in order, are red, green and magenta.*

Autocorrelation and Power spectrum are mathematical measures of the recorded waveforms. In the case presented on figure 6-1 each trace represents the average energy measure for ten seconds of recordings. To show consistency the 10 second energy measures are overlaid, this follows the accepted practice used in summed evoked response research. From figure 6-1 is clear that both the frequency and the total energy

increase with MSG stimulation. Two important considerations arise from the prior results:

- Is this behavior characteristic of the system?
- What is the driving force behind this response?

Figure 6-3

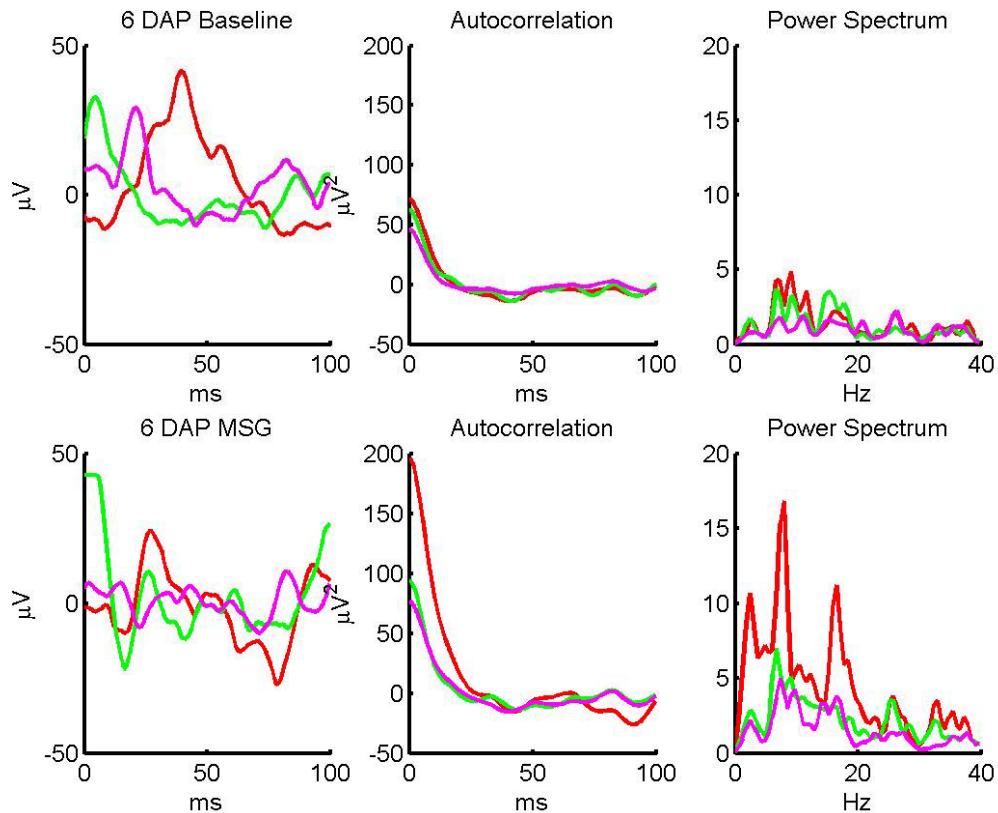


Figure 6-3: *Signal, autocorrelation and power spectrum measures for a 6 DAP microelectrode recording. The upper panels show the baseline activity from three consecutive 10 s segments, as compared to 1 mM MSG stimulation, presented in the lower panels. The consecutive segments, in order, are red, green and magenta.*

To answer the first question, and determine if the response is intrinsic to the cell line 1 mM MSG stimulation was utilized with the 6 DAP microelectrode recording.

These signals are assumed to be uncorrelated which is consistent with the original assumptions posted in chapter 2. Recordings were performed as described in section 5.4 and 1mM MSG solution was flushed through the system. Figure 6-3 presents an example of MSG response for the microelectrode configuration. The upper panel of figure 6-3, shows 100 ms time segment, autocorrelation and power spectrum from three consecutive 10 s segments in the absence of foreign stimulus. The bottom panel presents three consecutive ten second segments after the addition of 1 mM MSG. $AR_b(0)$ for baseline is $59.87 \pm 12.87 \mu\text{V}^2$, while $AR_s(0)$ for the 1 mM MSG is 122.05 ± 64.22 . Mean activation for this particular case was $A = 2.03$ for 1 mM MSG stimulus.

Besides the 1 mM MSG stimulation, 5, 50 and 500 μM stimulus were also tested, for the simultaneous micro-macro electrode recordings presented in section 5.5 (dataset # 3). Results for the 3 DAP macroelectrode experiments are presented in figure 6-4; each bar represents the average activity $AR(0)$ for three consecutive 10 s segments before, during and after MSG stimulation. Cells were maintained in Baseline and washout was performed with Dubelco's modified minimum essential media (DMEM, Sigma). MSG solutions were also prepared with MSG and each cycle was sustained for 3 minutes. Paired T-Test was used to determine significance and the increase in average activity $AR(0)$ was significant only for the 500 μM MSG with a p value of 0.0059. Mean activation for this particular case was $A = 1.59$ for 0.5 mM MSG stimulus. In the case of 6 DAP signals, mean activation was only $A = 1.05$ for 0.5 mM MSG stimulus, while activity change for 5 and 50 μM was insignificant. These results validate the use of 1 mM MSG as a valid concentration to be used in the excitation experiments with hyperdense SK-N-BE(2c) cell cultures.

Figure 6-4

3 DAP MSG Response

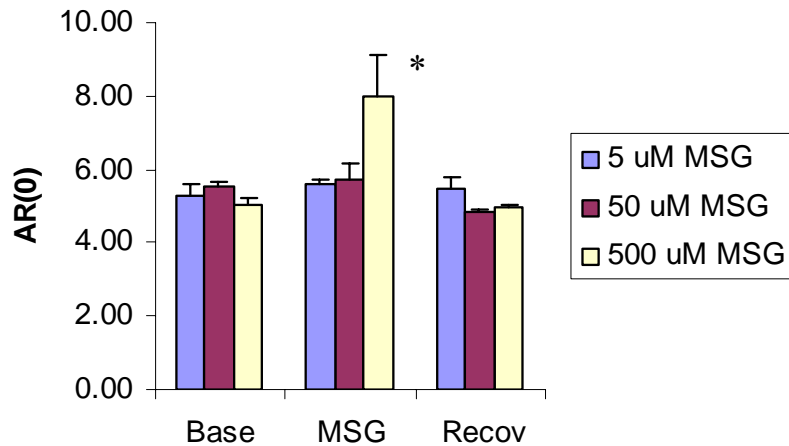


Figure 6-4: Average activity $AR(0)$ for three consecutive 10 s segments in response to MSG for the 3 DAP macro electrode recording, from dataset number 3 (section 5.5). Base corresponds to baseline, recorded in the presence of MSG, prior to the addition of MSG; MSG, corresponds to the response to the three independent MSG concentrations, dissolved in DMEM and Recov, corresponds to the recovered signal after the chamber has been washed out with DMEM.

As seen from figure 6-2 and figure 6-3, SK-N-BE(2c) cells inherently respond to 1 mM MSG in an excitatory fashion. This response consists of an increase in the energy as measured from the $AR(0)$ and an increase in frequency as observed by comparing the power spectrum of baseline and MSG response. Also, there is adaptation and as seen from Figure 6-2 and Figure 6-3 the first 10 seconds after MSG stimulus is applied, the energy presented by the red trace in both MSG autocorrelation panels is higher than the green and magenta traces corresponding to 10-20 and 20-30 s after stimulation. This behavior is robust and if the MSG stimulus is maintained, cells return to baseline after a couple of minutes. The magnitude of activation for 1 mM MSG stimulation as measured

from 7 randomly selected experiments extracted from the 3 data sets, including the two results previously discussed has a mean value of 1.66 with σ 0.46. This last result is very important since it implies that the response of the system to stimulus is not only robust, but highly reproducible and independent of the recording technique. This means that the MSG response is indeed characteristic of the system and not a mere artifact of the 35 day recordings presented in Figure 6-1.

6.3 Driving Force behind the Multiunit Response

Chapter 5 presented the population behavior of the SK-N-BE(2c) cells and showed that, as cells mature, there is a trend towards the development of slow potentials. Slow potentials represent the signature of a mature culture. It was also determined that slow potentials are the result of quasi-synchronous bursting from many cells in the population, and this is consistent with communication within the cell line. This communication could be electrically mediated via the macroelectrode or neurochemically mediated via gap-junctions or functional synapses. Connection through the macroelectrode can be discarded as a dominant form of connectivity, since microelectrode recordings obtained in the absence of the macroelectrode (section 5.4) showed the same type of time-signal evolution as signals obtained with the macroelectrode.

Immunofluorescent images presented in section 3.5 are consistent with the formation of functional dopaminergic synapses; however this does not discard the possibility of gap-junctions in the cell culture. Gap-junctions are clusters of trans-

membrane protein channels (connexins) that connect the cytoplasm of adjoining cells and allow the transfer of ions and small molecules between cells (**Bennett, 1992**). Gap-junction communication is involved in the regulation of growth control and differentiation, apoptosis and adaptive responses of differentiated cells (**Bennett, 1992**). In the case of cancerous tissue, the role of gap junctions is not clear; however it has been proposed, that one of the potential causes of immortality for cancerous tissue is precisely the lack of functional gap junction communication (**Trosko, 2001**). In the case of neuroblastoma, (**Sonnier, 2000**) suggests the presence of functional gap-junctions in the SK-N-SH-SY5Y neuroblastoma cell line.

To confirm or deny the presence of gap-junctions in the SK-N-BE(2c) neuroblastoma cell line and test for its participation in the development of the slow potentials, carbenoxolone (Sigma), was utilized as a gap junction inhibitor. Carbenoxolone is a glycyrrhetic acid derivative, believed to be a specific gap junction uncoupler, which inhibits gap-junction communication at a high potency with low toxicity. 5, 50 and 500 μ M carbenoxolone in DMEM was utilized with the simultaneous micro-macro electrode recordings presented in section **5.5** (dataset # 3). 3 and 6 DAP samples were utilized to test for non-specific effects of carbenoxolone in the cell signals. In these experiments no significant effects were observed and cells behaved as if no stimulus was present. Figure **6-5** shows an example of the response of cells to 50 μ M carbenoxolone, 3 DAP. As seen from the figure there is no apparent effect of carbexonolone in the recorded activity. The same is true for 5 and 500 μ M both in the 3 and 6 DAP signals suggesting that carbexonolone does not affect normal, uncoordinated cell behavior.

Figure 6-5

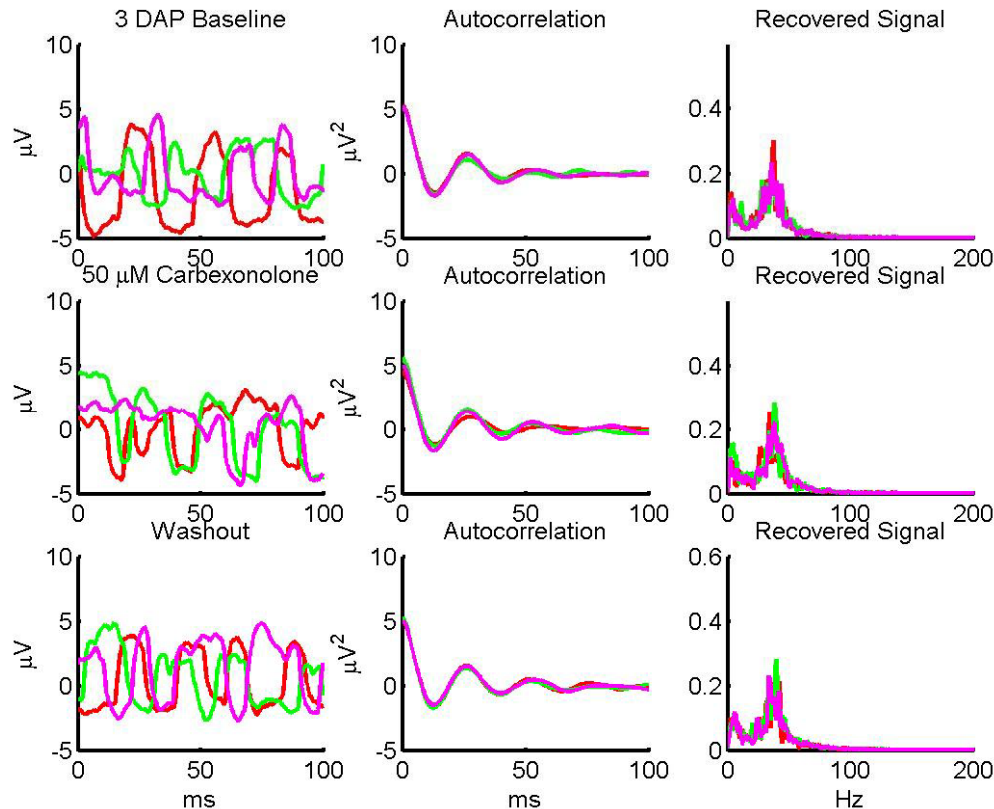


Figure 6-5: Behavior of cells 3 DAP in response to 50 μM carbexonolone. First row depicts baseline behavior, prior to the flow of carbexonolone. Second row shows the behavior as cells are being bathed with carbexonolone solution. Last row depicts the recovered behavior after the carbexonolone containing solution has been thoroughly washed out with DMEM.

Response of cells to carbexonolone was again measured 15 DAP. In this case, concentrations of 50, 500 and 5000 μM were utilized. Despite the fact that the first autocorrelation peak had broadened, consistent with the presence of coordinated behavior, carbexonolone did not seem to affect the time or frequency characteristics of the cells suggesting limited possibility of gap junction communication, or at least, minimal involvement in the development of the coordinated behavior.

6.3.1 Dopamine Mediated Communication

In order to validate the existence of dopaminergic communication, two sets of related experiments are presented: The CCC #2 with the differential electrode arrangement was utilized (section 4.4). This is the same chamber used for the data set number three (section 5.5) however; instead of utilizing a continuous macroelectrode the built in differential electrode arrangement was utilized (upper panel of Figure 4-5). Cells were grown on top of the electrode pads and recordings were performed between the central electrodes and their corresponding guard rings (upper panel of Figure 4-5). The DB9 connector was coupled to a BNC adapter port. Electrical recordings were performed using a high input impedance, high gain AC-coupled amplifier (Data Inc, Fort Collins, CO) band pass filtered between 0.05-3000 Hz, with a gain of 10,000 and sampled at 6,000 samples/sec (Biopack Systems, Inc. Santa Barbara California).

Cells were plated at a density of 8×10^6 cells/ml and maintained in Ham's F-12: Minimal Essential Media MEM (1:1) (Gibco BRL) supplemented with 15% fetal bovine serum (Bioreclamation), 100 units/ml penicillin and 50 $\mu\text{g}/\text{ml}$ streptomycin. Recordings were performed 25 days after plating from two independent electrode pads on a single microscope slide.

The CCC #2 was connected to a custom built, gravity fed, perfusion system and the superfusate was collected in 10 ml glass containers via a specially designed vacuum attachment. Cells were superfused with minimum essential media (MEM), MSG and Promazine Hydrochloride (PH) (Sigma) solutions. MSG and PH solutions were prepared in MEM from 1 M stock solutions, at concentrations, 1 mM and 5 mM. Cells were rinsed

with MEM after each analyte was applied. Promazine Hydrochloride (10-(3-(Dimethylamino) propyl) phenothiazine), belongs to a group of medications known as the phenothiazine antipsychotics. It binds to multiple monoamine transporters with various degrees of affinity (k_D in nM): serotonin, 190 ± 20 ; norepinephrine, 25 ± 2 ; dopamine 8400 ± 100 (**Tatsumi, 1999**). In the case of dopamine, it preferentially binds to dopamine D2 receptor as an antagonist. Figure 6-6 shows an image of the cells growing over one of the differential-electrode plates overlaid to a cartoon depicting the differential electrode arrangement, to provide an idea of the relative recording setup.

Figure 6-6

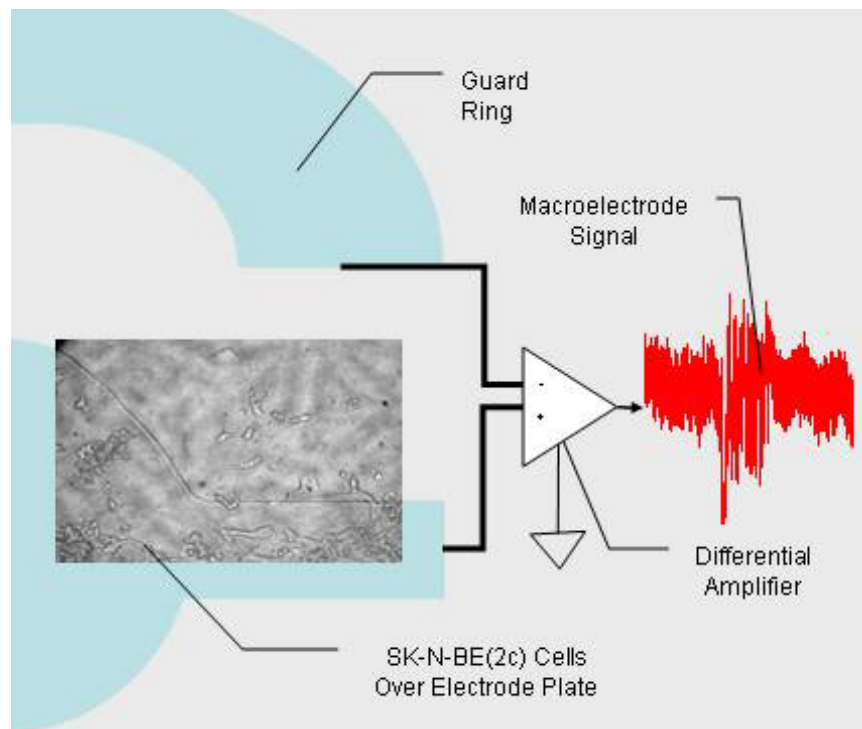


Figure 6-6: Microphotography of cells growing on top of one of the differential electrode plates, 25 days after plating, superimposed to a cartoon of the differential electrode arrangement and the signal acquisition setup, to provide a relationship of the relative size of the electrodes as compared to the cells.

Activity as a function of MSG and PH was computed for three consecutive 10 s segments from two independent differential-electrodes out of the possible 4. Recordings from the other 2 electrodes were not possible because of misalignment between the DB9 connectors and the electrode pads. Figure presents three consecutive ten second segments after the addition of 1 mM PH. Notice that not only the $ARy(0)$ is reduced, but the secondary peaks that indicate coordinated pacing are absent from the 10 and 20 s traces.

Figure 6-7

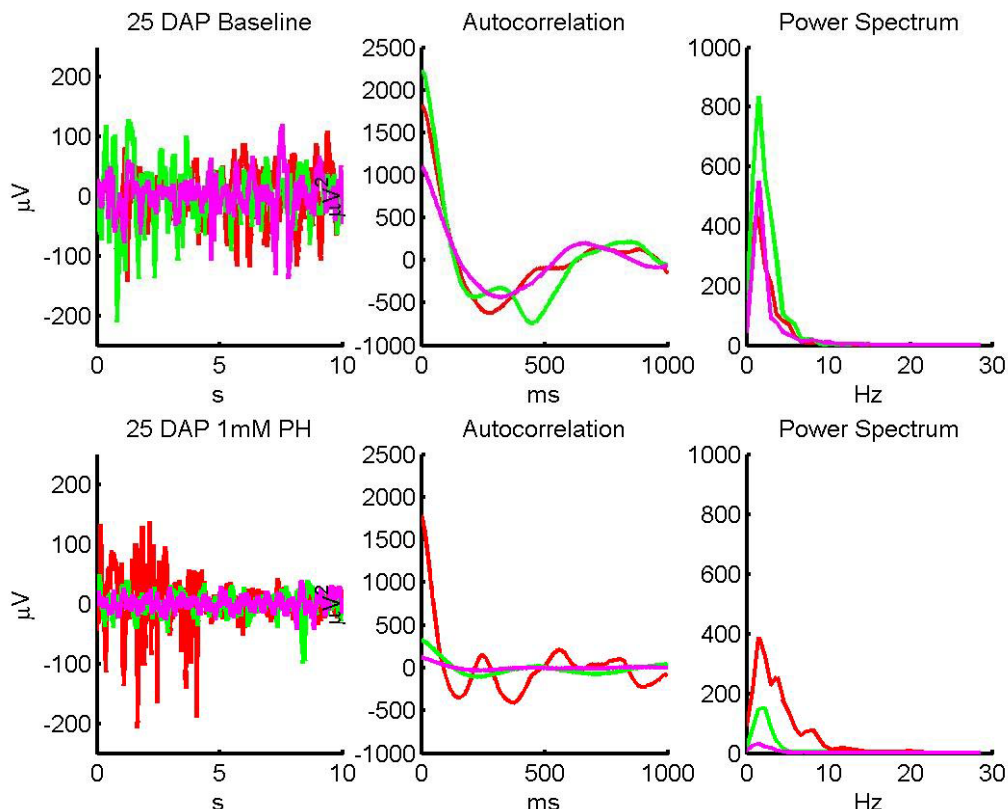


Figure 6-7: Signal, autocorrelation and power spectrum measures for one of the differential electrode plates, 25 DAP. The upper panels show the baseline activity from three consecutive 10 s segments, as compared to 1 mM PH stimulation, presented in the lower panels. The consecutive segments, in order, are red, green and magenta.

Figure 6-8

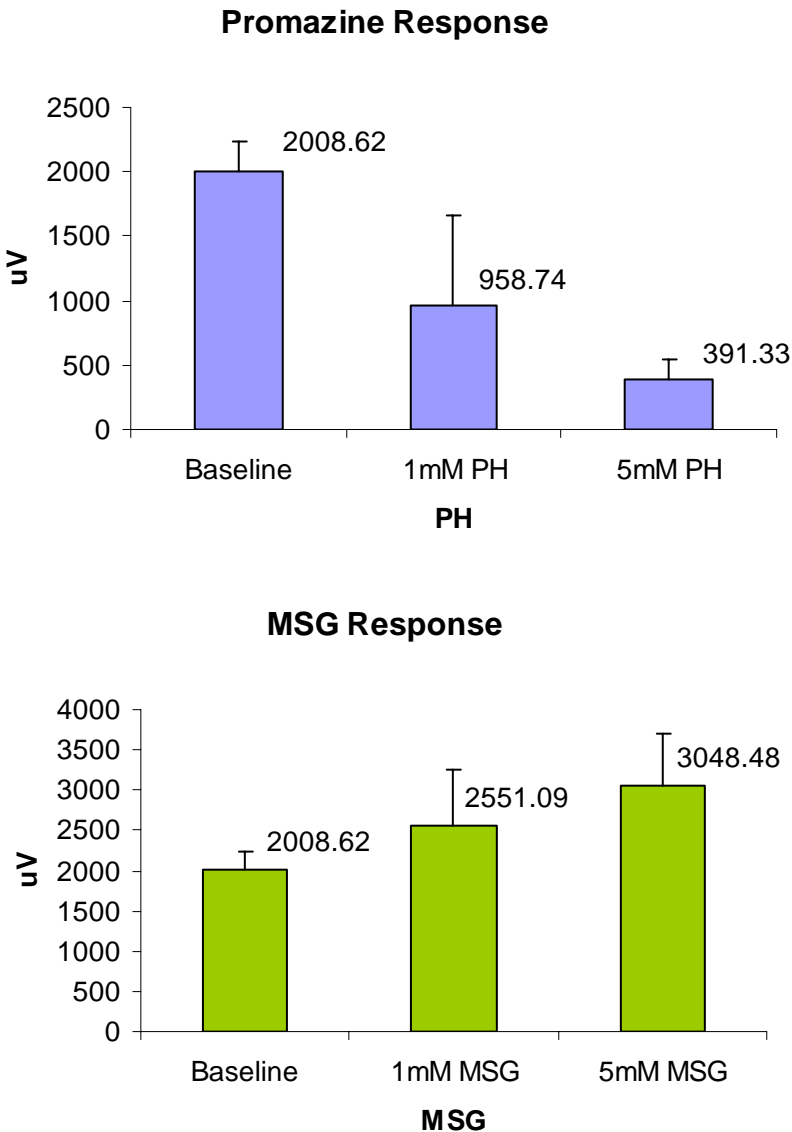


Figure 6-8: Average activity $AR(0)$ for three consecutive 10 s segments and two electrodes located in the same cell culture substrate ($N=6$), in response to MSG and PH.

The average activity of the system in response to PH and MSG is summarized in Figure 6-8. Each bar represents the average activity $AR(0)$ for three consecutive 10 s segments and two electrodes located in the same cell culture substrate simultaneously

stimulated (N=6). One way ANOVA analysis performed for the data presented in Figure 6-8; produced the following results: p value for the PH treatment is 0.000254 which is extremely significant. In the case of MSG treatment the p value is 0.043692 which is significant provided a 95 % confidence.

Results presented in Figure 6-8 and the corresponding significance from the ANOVA analysis indicate that activity is positively correlated with MSG concentration and negatively correlated with PH concentration. In order to further characterize the nature of such a response, the collected superfusate samples were transported to Dr. John Beard laboratory, where HPLC-EC analysis was run on the samples by Ms. Laura Bianco.

Prior to the HPLC-EC, neurotransmitters were isolated from the media using the following procedure: 25 μ l of 100 ng/ml dihydroxybenzoic acid (DHBA) standard was added to 2 ml of each media sample. 50 mg of acid washed alumina oxide (Bioanalytical Systems) and 1 ml of Tris-Buffer/EDTA, 1.5 M, pH 8.6 (Sigma) was added to each sample and shaken on a reciprocal shaker for 5 minutes. This causes the catecholamines to adsorb to the alumina. The alumina is left to settle in the bottom of the vial and the supernatant is aspirated. The Alumina is washed twice with DI water and aspirated to near dryness. 1 ml of DI water is added to each sample and the alumina slurry is transferred to a microfilter loaded with an RC 58 membrane. Microfilter is placed in a centrifuge and spun to dryness at 1000 G for 30 s.

The microfilter is attached to a new receiver tube and 200 μ l of 0.1 M HClO_4 is added to the microfilter sample compartment. The ensemble is vortexed briefly, left to stand for 5 min and vortexed briefly again. The microfilter is placed in a centrifuge and

spun at 1000 g for 1 min. The acid extract in the receiver contains the catecholamines and is ready for injection in the HPLC-EC apparatus.

10 μ l of the acidic suspension for each sample are loaded independently into an ESA 582 Solvent Delivery System, connected to an ESA 542 autosampler and an ESA Coulotech III (detector) (ESA Biosciences, Inc.; Chelmsford, Massachusetts). Macroporous Reversed-Phase C18 (mRP-C18) High-Recovery Protein Fractionation and Desalting LC Column was utilized (ESA Biosciences, Inc.; Chelmsford, Massachusetts). Detection Voltages (mV); E1:-175; E2: 300; Guard Column: 350. The mobile phase is composed of: Sodium phospahte monobasic 75 mM; 1-Octanesulfonic Acid 1.7 mM; EDTA 25 μ M; Triethylamine 100 μ l/ml; Acetonitrile 10%; Phosphoric Acid (to adjust pH to 3). A standard solution consistent of 25 μ l of 100 $^{ng}/ml$ of DHBA and 0.04 $^{mg}/ml$ of: nor-epinephrine, epinephrine, DOPAC, DA, 5HIAA, HVA and serotonin is used for calibration. Software used for acquisition was EZ Chrome Elite. This software combined with the described technique allows for quantitative measures of catecholamines in solution (**Nelson, 1997**).

Table 6-1

6-1: Population Response to MSG and Promazine Hydrochloride

Solution	DA Concentration	DA/DA_B
Baseline	0.56166	1.000000
1 mM MSG	0.64962	1.156608
5 mM MSG	0.72035	1.282537
1 mM PH	0.559098	0.995439
5 mM PH	0.729553	1.298924

Using the described technique, results for the HPLC-EC analysis of the supernatant, are summarized in Table 6-1. The fractional concentration change for DA is calculated by dividing the stimulus dependant concentration by the baseline $[DA_B]$ concentration. From the table is clear that increase in MSG concentration is accompanied by an increase in DA concentration in a dose dependent fashion. The same seems to be true for PH, hence a comparison between the fractional concentration change and the activation is presented in Figure 6-9. Activation was calculated as before: $A = AR_s(0)/AR_b(0)$ for the average activity presented in Figure 6-8.

The results presented in Figure 6-9 indicate that there is a positive concentration dependent activation response (dose response) with MSG for the cells in culture and a negative dose response with PH. In the case of MSG activation increase correlates with an increase in fractional dopamine concentration. The results for PH are much more interesting: Activation is reduced in a dose dependent fashion, while the fractional DA concentration after 1 mM PH solution is applied is essentially the same and increased when 5 mM PH are added. This is consistent with a DA mediated response, such that a competitive antagonist reduces the activation while the DA concentration is maintained. When PH is increased to 5 mM there is a 21% increase in DA concentration, while the activation is reduced. This suggests that DA released by the cells is not binding to the corresponding DA receptors and the technique is registering the unbound dopamine in solution. This suggests that the slow potentials are the result of a network that utilizes DA mediated transmission. However, due to the lack of receptor specificity for PH additional research is required to determine the specific type of receptor involved.

Figure 6-9

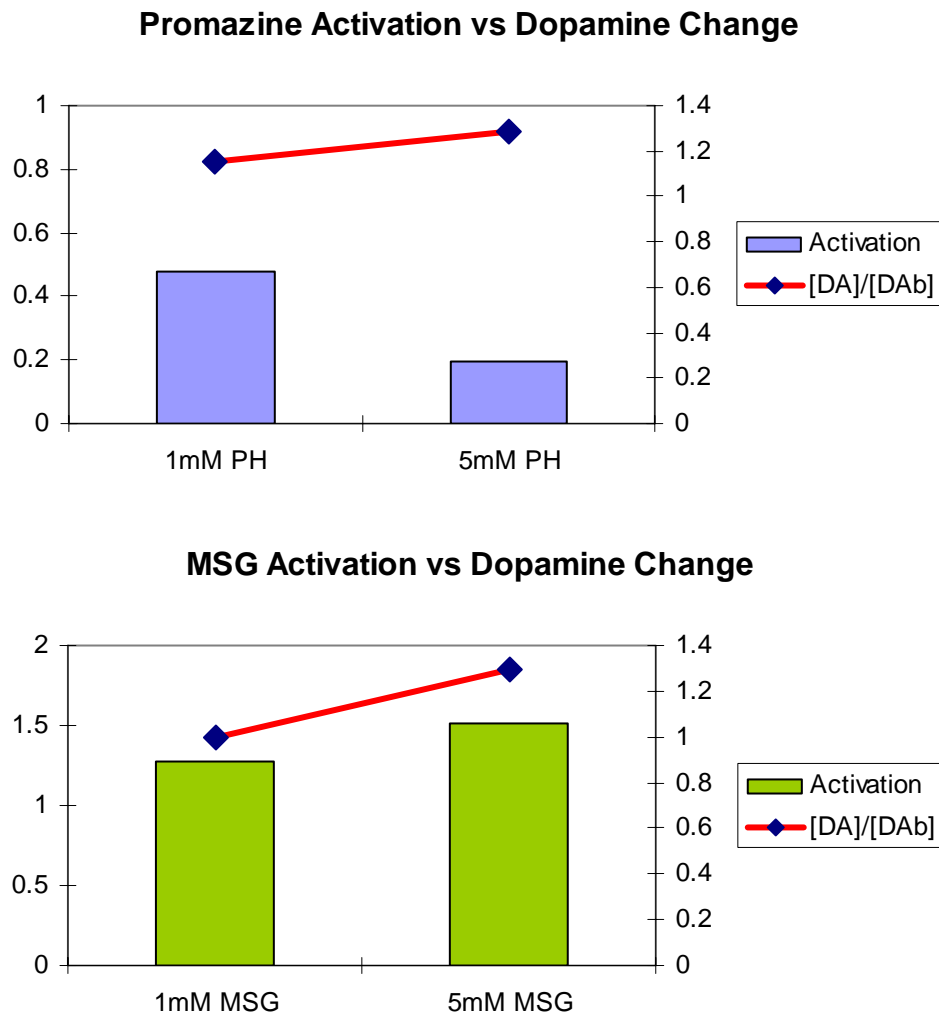


Figure 6-9: Comparison between the fractional dopamine concentration change and the mean activation of cells responding to 1 and 5 mM PH and MSG for the 25 DAP differential macroelectrode recordings.

In order to further characterize the specific type of receptor involved in the dopamine mediated response, two specific neurochemical compounds were utilized: SCH 23390 Hydrochloride (R-(+)-7-Chloro-8-hydroxy-3-methyl-1-phenyl-2,3,4,5-tetrahydro-1H-3-benzazepine hydrochloride), a potent D1 receptor antagonist (Tocris) and Sulpiride

(S-(-)-5-Aminosulfonyl-N-[(1-ethyl-2-pyrrolidinyl)methyl]-2-methoxybenzamide), which is a selective D2 receptor antagonist (Tocris).

Figure 6-10

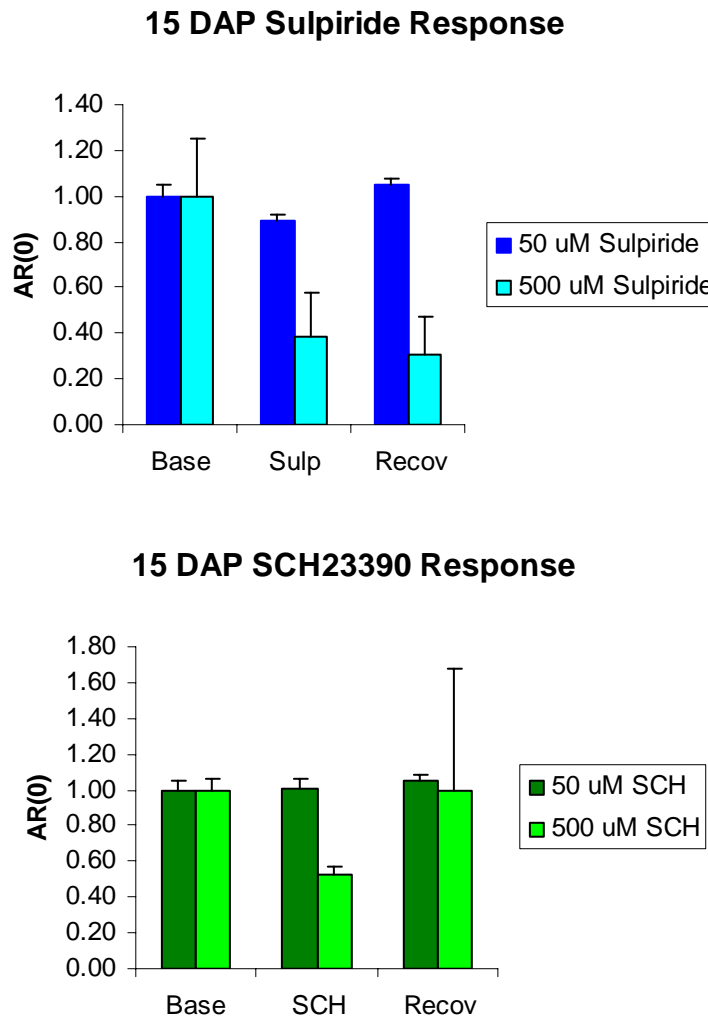


Figure 6-10: Comparison between mean activation of cells responding to 50 and 500 μM Sulpiride and SCH23390 for 15 DAP differential macroelectrode recordings.

The CCC #2 with the differential electrode arrangement was again utilized and experiments were performed 15 DAP. 50 and 500 μM of the selected analytes in DMEM

were utilized and experiments were performed as previously described. It is important to indicate that the amount of energy recorded from each of the macroelectrodes varied widely due to an uneven distribution of cell population density on top of the electrodes. In order to compare the response from the electrodes, activity was normalized with respect to the mean baseline activity measured for the electrode. Normalized activity measures were concatenated to produce the results for Sulpiride and SCH 23390 presented in figure **6-10**. In the case of Sulpiride there was a clear concentration dose response, mean activation for 50 μM was 0.8919 with a p value calculated via paired T test of 0.000521 which is extremely significant. Mean activation for 500 μM Sulpiride was 0.3887 with a p value calculated via paired T test of 0.000136. which is, again, extremely significant. Recovery, however was not observed for the 500 μM Sulpiride, after several minutes meaning that either the washout was not effective and Sulpiride was strongly bound to the D2 receptor or that the concentration was too high and permanently affected cell function.

The response to SCH23390 needs to be analyzed carefully; at a concentration of 50 μM there is no response ($p \approx 0.5$). At a concentration of 500 μM there is a large response with mean activation of 0.5253, p value of 0.000268 which is extremely significant. Recovery from this state takes some time and is characterized by a rebound effect evidenced by the large standard deviation seen in the SCH23390 500 μM recovery panel from figure **6-10**. According to the Tocris catalog, dopamine receptor affinities for SCH23390 in nM are 0.2 for D1 and 1100 for D2. In the case of Sulpiride, affinities in nM are 0.015 for D2 and 45 for D1. If D1 receptors were present in the cell line and responsible for the correlated response at a concentration of 50 μM SCH23390 there

should be a significant response. The fact that this response is absent, suggests that D1 receptors are not present and that at a concentration of 500 μM , SCH23390 is binding to the D2 receptors and the response is actually D2 mediated. In synthesis, experiments performed in this section suggest that the correlated behavior observed in the cell line results from D2 receptor mediated, dopamine activity.

6.4 Recovery of Action Potential Waveforms

As stated in chapter 2, the convolution of a broadband noise with a signal with a specific **AP** yields a signal whose spectrum is that of **AP**. An **AP_R** can then be recovered from the autocorrelation using the Levinson algorithm. The Levinson algorithm was applied to 6 and 25 day microelectrode autocorrelations from data set number 2 (Section 5.4) and the results are shown in Figure 6-11.

The 6 DAP was selected, because the culture is at the transition state at that point and the best signal quality should be recovered. From the 6 DAP (Figure 6-11) Levinson is recovering what looks like an action potential waveform. There is a depolarizing event followed by a slow hyperpolarization and a recovery back to baseline. Time course is consistent with the trans-membrane potentials presented in section 3.3. The 25 second recovered signal shows a broadening of the first peak plus the presence of succeeding depolarizing events. These succeeding events are consistent with synaptic driven potentials as it was shown by the simulation in Figure 2-9. These results prove the validity of the mathematical model and further validate the macroelectrode approach.

Figure 6-11

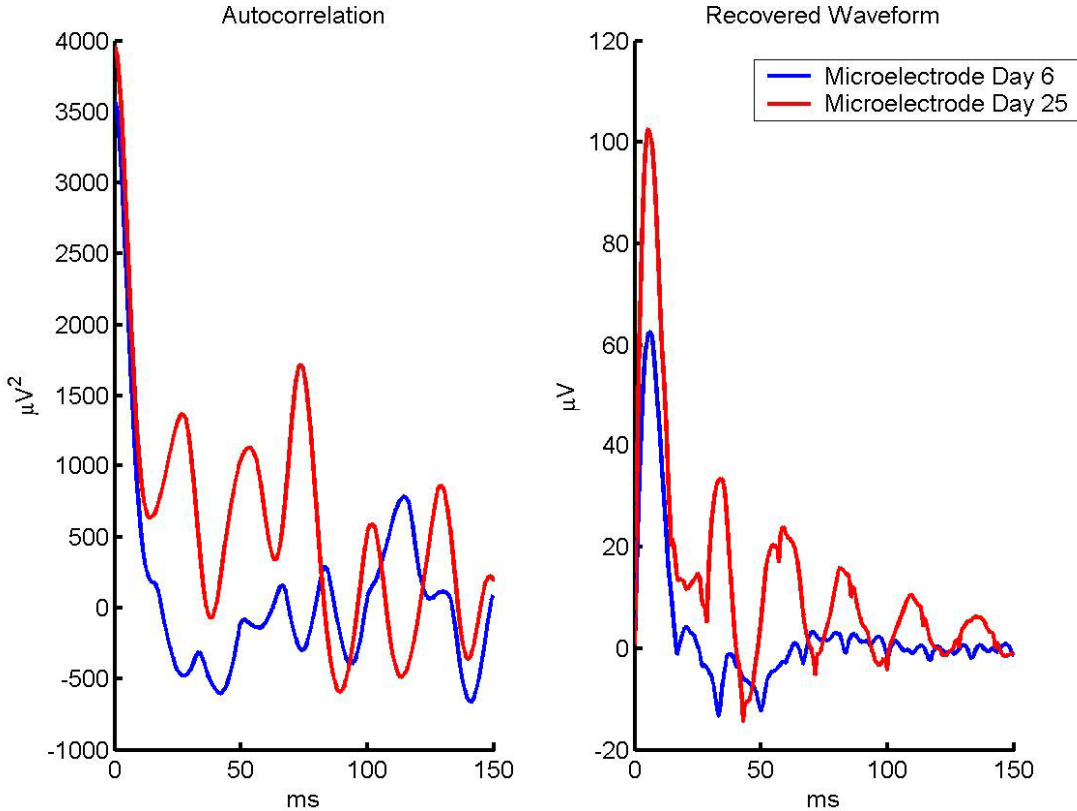


Figure 6-11: Levinson algorithm applied to 6 and 25 DAP microelectrode autocorrelations from data set number 2 (Section 5.4).

When the Levinson algorithm is applied to the other data sets interesting results are found. The Levinson algorithm was applied to 5 and 35 DAP macroelectrode recordings using CCC#1 (data set number 1, section 5.3). Figure 6-12 presents the recovered waveform which is different than the one obtained from the TPE microelectrodes shown in Figure 6-11.

Figure 6-12

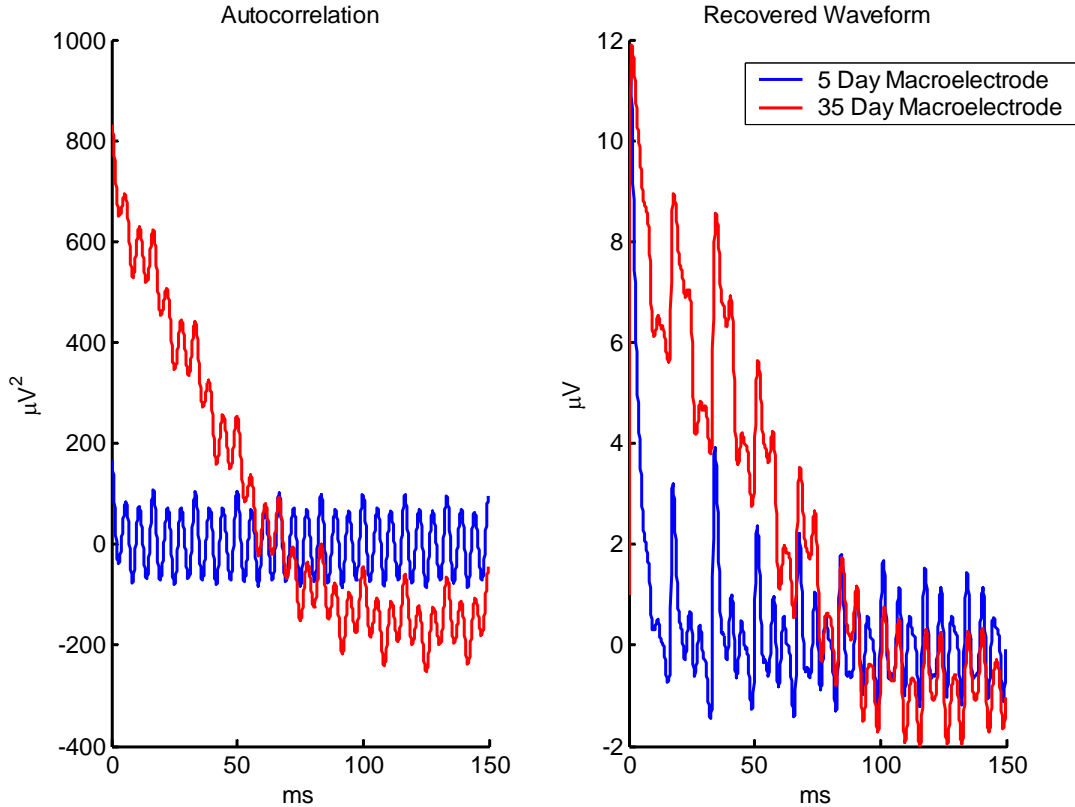


Figure 6-12: Levinson algorithm applied to 5 and 35 DAP macroelectrode autocorrelations, from data set number 1 (Section 5.3),

The rising phase of the depolarizing event is missing in both of the signals (Figure 6-12) and the recovery slope has a couple of inflections. However, the width of the first peak from the origin to the zero crossing point is similar for both figures (Figure 6-11, Figure 6-12). The recovered waveforms from the 5 and 35 day recordings (Figure 6-12) are similar to each other, meaning that the characteristic average cellular response as seen with the particular chamber geometry is the same and that individual events (action potentials) did not change with time after plating. Also the widening of the

first event is clearly observed and can be seen as the summation of single unit events, corroborating the proposed hypothesis for generation of the slow potentials.

Figure 6-13

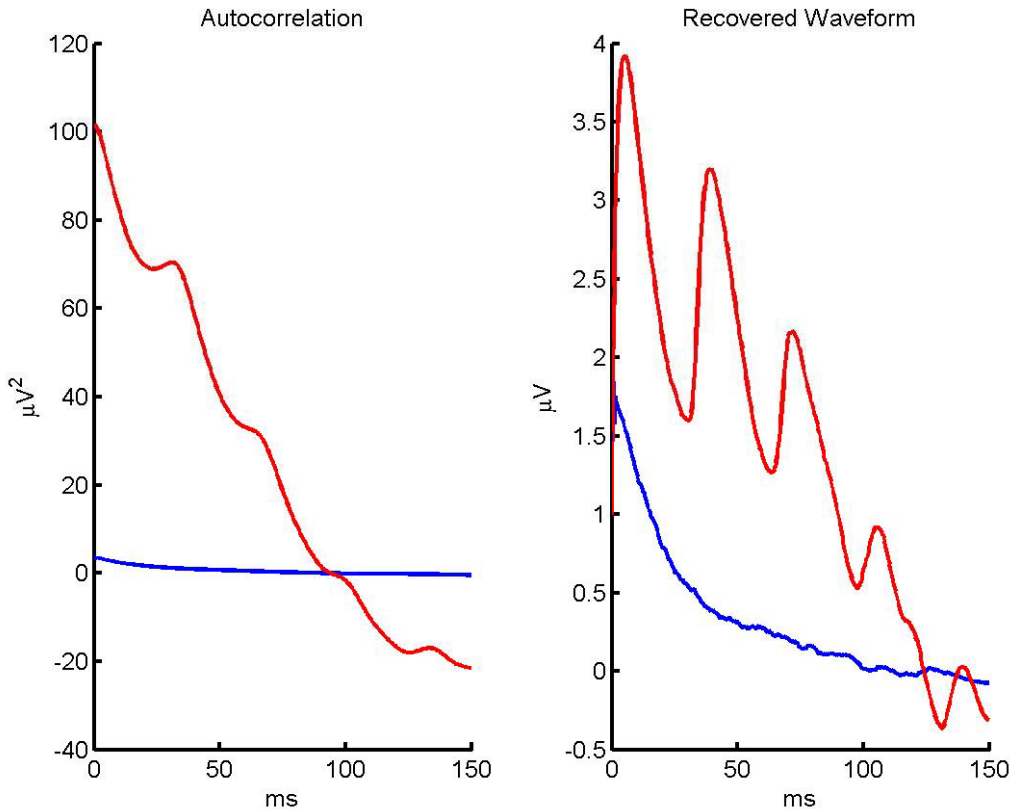


Figure 6-13: Levinson algorithm applied to 15 DAP micro-macro-electrode autocorrelations, from data set number 3 (section 5.5). Macroelectrode signal is the red tracing and microelectrode is the blue tracing.

By applying the Levinson algorithm to the 15 day micro-macro electrode signals from data set number 3 (section 5.5), a good comparison of the signal evolution for the micro and macro electrodes is obtained. Figure 6-13 shows that the macroelectrode (red tracing) is exhibiting a characteristic summed slow recovered potential, typical of coordinated phase, while the microelectrode is presenting a slightly broadened single

event response, characteristic of the transition phase, consistent with the results presented in section 5.5.

Figure 6-14

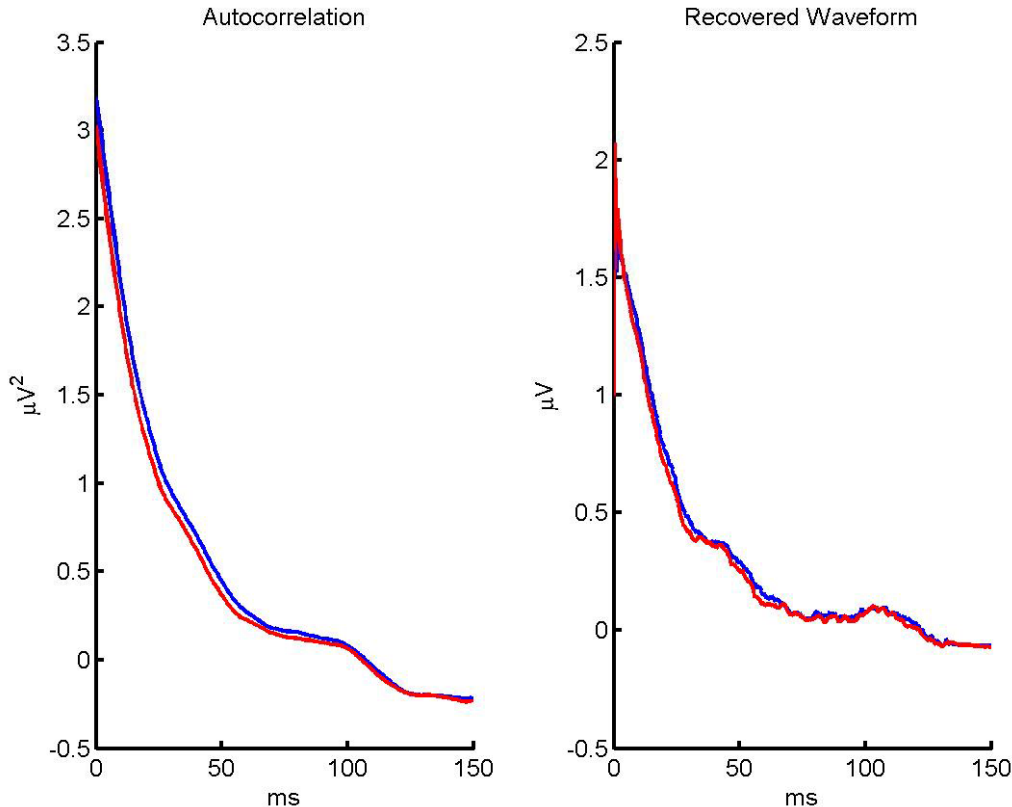


Figure 6-14: Levinson algorithm applied to 15 DAP micro-macro-electrode, recordings from data set number 3 (section 5.5). Dose response to 5 mM PH is presented. Macroelectrode signal is the red tracing and microelectrode is the blue tracing.

Response to 5 mM PH, was obtained for the 15 day micro-macro electrode signals from data set number 3 (section 5.5). The Levinson recovery of the PH response is shown in Figure 6-14; the summed slow recovered potential exhibited by the macroelectrode (red tracing, Figure 6-13) is lost and that the recovered waveforms for

both electrodes are essentially identical. This further proves that the slow potentials measured in the macroelectrode recordings are the result of synaptic communication mediated by presynaptic dopamine and postsynaptic dopamine receptors. The same type of behavior is appreciated with the 500 μM Sulpiride response for the 15 DAP signals presented in section 6.3.1 here the slow potentials are abolished and the recovered signal looks like that of a non synchronous single unit response (Figure 6-15), indicating that the slow potentials are the result of D2 mediated activity.

Figure 6-15

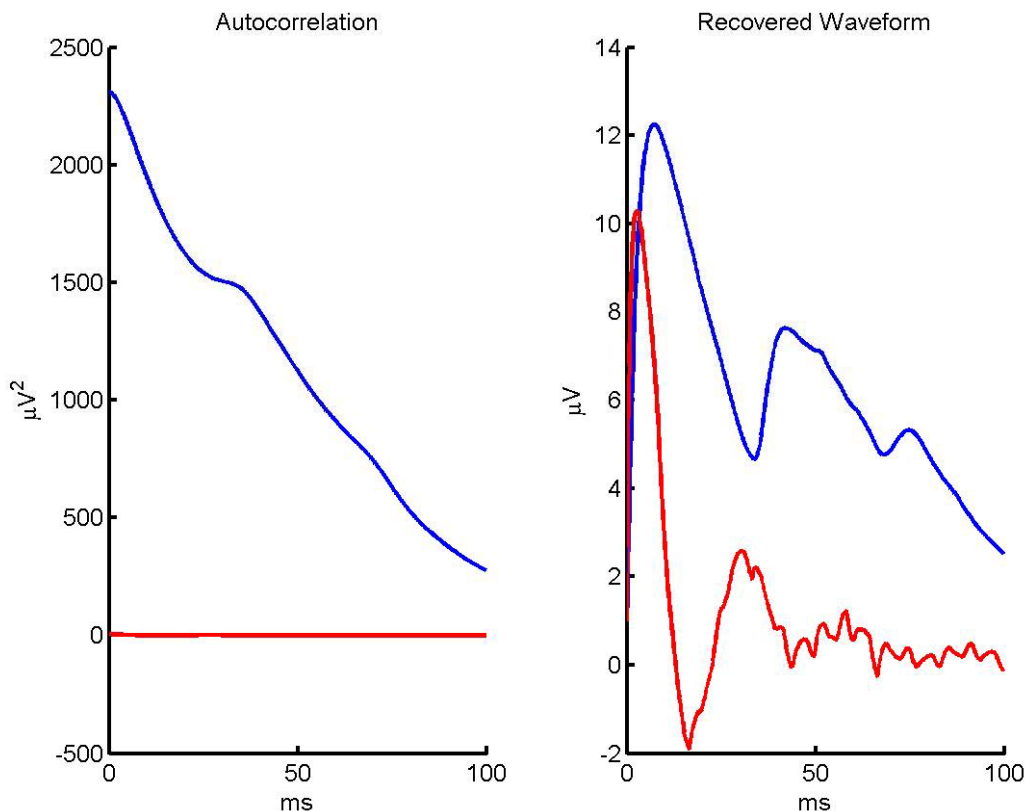


Figure 6-15: Levinson algorithm applied to 15 DAP differential macroelectrode recordings presented in section 6.3.1. Response to 500 μM Sulpiride is presented. Baseline signal is the blue tracing and Sulpiride response is the blue tracing.

6.5 Chapter Summary

With the results presented in this chapter, all of the mathematical assumptions made in Chapter 2 have been supported *in vitro*. Mathematical measures were used to demonstrate that the SK-N-BE(2c) produces functional synapses in culture and that synaptic mediated communication evolves with time after plating. The Levinson algorithm was used to characterize the average behavior of the system and together with autocorrelation and power spectrum, comprise remarkable tools for macroelectrode research.

By using the developed tools it was demonstrated that slow potentials measured with the macroelectrode approach are the result of functional synapses that utilize DA as a neurotransmitter and dopamine D2 receptors. This result is fundamental and was found due to the presence of the large-slow potentials measured with the macroelectrode approach. Such a result has never been reported and validates the scientific merit of the technique. The fact that the CCC #2 is compatible with established population based techniques such as suprafusion and HPLC-EC, further validates the development of the system and proves that the population approach could provide new insights to neuroscience research.

Chapter 7

Discussion and Conclusion

The need for cell lines to provide stable reproducible *in vitro* platforms for neurophysiological studies has been recognized for at least 40 years. It has been shown that the SK-N-BE(2c) cell line is dopaminergic and develops multiunit electrical signals *in vitro* when grown over cell-adhesive material. It was also shown that cells develop functional synaptic connections mediated by the dopamine D2 receptor that is evidenced by the slow potentials seen in the macroelectrode recordings.

D2 dopamine receptors are naturally expressed in neurons of the midbrain, caudate, and limbic systems, specifically in the nucleus accumbens, the amygdala, the hippocampus, and parts of the cerebral cortex. D2 receptors are considered positive reinforcers in maintaining cocaine self-administration in non-human subjects, they also have a high affinity for antipsychotic drugs and the therapeutic action of these drugs is thought to occur at these sites (Kandel, 1991).

The lack of a simple model for DA mediated circuits has led to the utilization of cell explants and primary cell cultures, to provide material for studies of synapse formation, and long term potentiation. In both cases, the goal is to characterize group behavior, or tendencies. Analysis of the summed neuronal signal could provide useful information about the "average" response of the cells to an applied stimulus and evolution of the response as a function of time and synapse formation.

SK-N-BE(2c) cells are very homogeneous, robust and stable and may serve as a model for studies of dopaminergic systems or disorders such as Parkinson's Disease. They could also, serve as a model to study changes in synaptic transmission mediated by cocaine and other drugs of abuse, provided interaction with DA modulators is not atypical in this cell line.

Prior to our detection of synaptic activity in the SK-N-BE(2c) cell line only three other cell lines have been determined to produce functional synapses *in vitro*. The P19 cell line is a pluripotent stem cell line that can be differentiated into mesodermal or ectodermal lineages, when treated with Retinoic Acid (RA). P19's differentiate into cell types similar to those derived from the neuroectoderm with both neurons and glia present (**McPherson, 1995**). Differentiated P19's express various neurotransmitters, with GABA being the most prominent (**McPherson, 1995**). They possess the electrical properties of mature neurons, produce spontaneous action potentials, post synaptic potentials and develop large and complex neural networks (**McPherson, 1995**). The NTera-2 cells, derived from a human teratocarcinoma tumor also express multiple neurotransmitter enzymes and establish synapses *in vitro* (**Zeller, 1995**). Besides these two cell lines, the human hybrid neuronal cell line A1 was generated by somatic fusion between a human fetal cerebral neuron and a SK-SH-SY5Y human neuroblastoma cell line (**Nagai, 2002**). The A1 hybrid develops functional synapses *in vitro* and expresses messages for various subsets of neuronal types (**Nagai, 2002**). All of these cell lines are pluripotent and develop into various phenotypes, and the presence of synaptic activity only becomes evident after about ten days in culture, post differentiation with RA.

It was shown that a single macroelectrode can be utilized to study the electrical evolution of a synaptic cell assembly. It was also shown that the acquired signal is robust and can be utilized as a measure of system integration. Since neural cells possess sensitive electrochemical transducer capabilities this technique could prove useful in constructing whole cell biosensors systems for specific-sensing activities such as drug discovery, neurochemical sensing and homeland security. The system could potentially be adapted to serve as an *in vitro* model for neurodegeneration, since synaptic regression could be monitored as the nutrient flow or growth factor concentrations in the media are changed. Besides Neural cell cultures, other electrogenic cells can be monitored by using the same technology. One possibility is extra cellular recording of dissociated heart muscle cells. Another possibility is to study embryological and developmental changes on the electrogenic activity of specific cells.

The integrated macroelectrode array systems developed are mechanically strong and can be repeatedly used, they are suitable for long term surveying of neural activity and simultaneous multi-site recordings. The system can be combined with optical techniques to study synchronized behaviors. It can be used to simultaneously record and stimulate, brain slices or neuronal cell cultures. In synthesis, the system could provide a very valuable tool for understanding coordinated behavior of neural populations *in vitro*, allowing the scientist a great degree of freedom to control the experimental variables and opening a door to understanding how population networks work.

7.1 Products Envisioned:

Until now, the population based systems have been used exclusively for studying the development of SK-N-BE(2c) populations. However, development of product lines based on glass slides with transparent electrodes, stamped with materials controlling neuron interconnection between electrodes could be very valuable for neuroscience and pharmacology research. Transparent macroelectrode pads, could be pre-stamped with cell friendly and cell repulsive areas to promote/inhibit cell growth and cell interconnectivity. By customizing the stamping of cell friendly/unfriendly materials over multiple spatial arrangements an almost limitless set of configurations of extracellular challenges for theories of neural interconnectivity could be achieved.

Many drugs are targeted at neural structures, and most of these act strongly at the synapse (alleviation of pain, control of addiction, memory enhancement). All such drugs must eventually be qualified in animal and human trials. However, the process of drug discovery, where compounds of unknown effectiveness are initially screened could be simplified and streamlined if appropriate synaptogenic cell lines could be effectively monitored for protein expression, and for electrogenic activity *in vitro*. The macroelectrode chambers developed are capable of providing the physical environment for such studies, and the SK-N-BE(2c) is a good potential candidates for use in studies of "pacing" neural disorders, such as seizure and Parkinson's disease.

In conclusion, population based systems that utilize the macroelectrode approach can be used to analyze the response of many cells in culture. Energy measures such as autocorrelation and power spectrum, coupled with the macroelectrode approach provide a

means of monitoring the activity of the population. Activity measures can then be used to develop sensing systems capable of measuring response to stimulus. These techniques were utilized to study the population behavior of the SK-N-BE(2c) neuroblastoma cell line and demonstrated the development of functional synaptic networks that could respond to stimulus. Such results could not have been achieved by traditional methods, and validate the macroelectrode approach for the study of electrogenic cell lines and as a new tool for neuroscience research. This opens a door to population based neuroscience research which could help unravel the very basis of the brain.

Bibliography

- Abele, R; Lampinen, M; Keinänen, K and Madden, DR. Disulfide Bonding and Cysteine Accessibility in the a-Amino-3-hydroxy-5-methylisoxazole-4-propionic Acid Receptor Subunit GluRD: Implications for Redox Modulation of Glutamate Receptors. *The Journal of Biological Chemistry* Vol. 273, No. 39, Issue of September 25, pp. 25132–25138, 1998.
- Agrati P, Garnier M, Patrone C, et al. 1997 SK-ER3 neuroblastoma cells as a model for the study of estrogen influence on neural cells. *Brain Res Bull* 44:519-23.
- Allcock, H.R.; Kwon, S.; Riding, G.H.; Fitzpatrick, R.J.; Bennett, J.L. *Biomaterials* 1988, 9, 509.
- Allcock, H.R.; Cameron, C.G. *Macromolecules* 1994, 27, 3125.
- Allcock, H.R. *Chemistry and Applications of Polyphosphazenes*, John Wiley Publishers , 2003.
- Allouche S, Hasbi A, Ferey V, Sola B, Jauzac P, Polastron J 2000 Pharmacological delta1- and delta2-opioid receptor subtypes in the human neuroblastoma cell line SK-N-BE: no evidence for distinct molecular entities. *Biochem Pharmacol* 59:915-25 Allouche, 2000
- Allouche S, Polastron J, Hasbi A, Homburger V, Jauzac P 1999 Differential G-protein activation by alkaloid and peptide opioid agonists in the human neuroblastoma cell line SK-N-BE. *Biochem J* 342 (Pt 1):71-8
- Andrews A. M. and Murphy D. L. (1993) Sustained depletion of cortical and hippocampal serotonin and norepinephrine but not striatal dopamine by 1-methyl-4-(20-aminophenyl)-1,2,3,6-tetrahydropyridine (20-NH₂-MPTP): a comparative study with 20-CH₃-MPTP and MPTP. *J. Neurochem.* 60, 1167–1170.
- Andrews, AM. And Murphy, DL. 2'-NH₂-MTP in Swiss Webster Mice: Evidence for Long-Term (6-Minth) Depletions in Cortical and Hippocampal Serotonin and Norepinephrine, Differential Protection by Selective Uptake Inhibitors or Clorgyline and Functional Changes in Central Serotonin Neurotransmission. *The Journal of Pharmacology and Experimental Therapeutics*, Vol. 267, No 3, 1993. pp. 1432-1439.
- Baker, SN.; Gerstein, GL. "Improvements to the Sensitivity of Gravitational Clustering for Multiple Neuron Recordings", *Neural Computation* 12, 2000, pp 2597–2620.

- Banker, G.; Goslin, K. *Culturing Nerve Cells* (2nd ed.). Cambridge, MA: The MIT Press, 1998.
- Bennett, M.V.L. and Verselis, V.K. Biophysics of gap junction, *Semin Cell Biol* 3 (1992), pp. 29–47.
- Barrett, E.W.; Silva, R.J.; Wilson, D.E.; Natale, D.; Gaumond, R.P. and . Allcock, H.R. Novel Material for Patterned Neural Networks. 2005. Proceedings of the 2nd International IEEE EMBS Conference on Neural Engineering.
- Barrett, EW; Phelps, MVB; Silva, RJ; Gaumond, RP and Allcock, HR. 2004. Microcontact printing of poly(organophosphazenes): potential applications for selective cell adhesion. *Polymeric Materials: Science and Engineering*, 91 633-634.
- Barrett, EW; Phelps, MVB; Silva, RJ; Gaumond, RP and Allcock, HR. Patterning Poly(organophosphazenes) for Selective Cell Adhesion Applications. *Biomacromolecules* 2005, 6, 1689-1697.
- Betz WJ, Bewick GS. Optical analysis of synaptic vesicle recycling at the frog neuromuscular junction. *Science*. 1992 Jan 10; 255(5041): 200-3.
- Biedler JL, Roffler-Tarlov S, Schachner M, Freedman LS. Multiple neurotransmitter synthesis by human neuroblastoma cell lines and clones. *Cancer Res*. 1978 Nov;38(11 Pt 1):3751-7.
- Borkholder, D.A., Bao, J., Maluf, N.I., Perl, E.R., and Kovacs, G.T.A., "Microelectrode Arrays for Stimulation of Neural Slice Preparations," *Journal of Neuroscience Methods*, 1997.
- Bousse, L. Whole cell biosensors. *Sensors and actuators B*, 1996, 34, pp 270-275.
- Bove, M.; Grattarola, M. and Verreschi, g. In Vitro 2-D Networks of Neurons Characterized by Processing the Signals Recorded with a Planar Microtransducer Array. *IEEE Trans BME*, 44:964-977, 1997.
- Bove, M. Martinoia, S. Verreschi, G. Giugliano M. and Grattarola, M. Analysis of the signals generated by networks of neurons coupled to planar arrays of microtransducers in simulated experiments, *Biosensors and Bioelectronics*, Volume 13, Issue 6, September 1998, Pages 601-612.
- Branch, DW. Wheeler, BC. Brewer, GJ. and Leckband, DE. (2000) " Long-Term Maintenace of Pattern of Hippocampal Pyramidal Cells on Substrates of Polyethylene Glycol and Microstamped Polylysine," *IEEE Trans. Biomed. Eng.*, 47, 290-300.Bryers, J.D. *Colloids and Surfaces B: Biointerfaces*, 1994, 2, 9.

Cambrex Bio Science Walkersville, Inc. Cell Tracker™ Green Fluorescent Probe.
<http://www.cambrex.com/Content/bioscience/CatNav.asp?oid=1045&prodoid=CTGreen>.

Chambaut-Guerin AM, Martinez MC, Hamimi C, Gauthereau X, Nunez J. Tumor necrosis factor receptors in neuroblastoma SKNBE cells and their regulation by retinoic acid. *J Neurochem.* 1995 Aug;65(2):537-44.

Chang, J.C.; Brewer, G.J.; Wheeler, B.C. *Biomaterials* 2003, 24, 2863.

Chen, G., and van den Pol, A. N. 1996. Multiple NPY receptors coexist in pre- and postsynaptic sites: inhibition of GABA release in isolated self-innervating SCN neurons. *Journal of Neuroscience* 16: 7711-7724.

Chen, G., and van den Pol, A. N. 1998. Presynaptic GABA-B autoreceptor modulation of P/Q-type calcium channels and GABA release in rat suprachiasmatic nucleus neurons. *Journal of Neuroscience* 18:1913-1922.

Chen, G., Trombley, P. Q., and van den Pol, A. N. 1995. GABA receptors precede glutamate receptors in hypothalamic development; differential regulation by astrocytes. *Journal of Neurophysiology* 74: 1473-1484.

Chen, Y., Deng, L. B., Maeno-Hikichi, Y., Lai, M. Z., Chang, S. H., Chen, G., and Zhang, J. F. (2003). Formation of an endophilin-Ca²⁺ channel complex is critical for clathrin-mediated synaptic vesicle endocytosis. *Cell* 115: 37-48.

Cheng J, Standifer KM, Tublin PR, Su W, Pasternak GW 1995 Demonstration of kappa 3-opioid receptors in the SH-SY5Y human neuroblastoma cell line. *J Neurochem* 65:170-5.

Chiappalone, M. Vato, A. Tedesco, M(B). Marcoli, M. Davide, F. and Martinoia, S. Networks of neurons coupled to microelectrode arrays: a neuronal sensory system for pharmacological applications, *Biosensors and Bioelectronics*, Volume 18, Issues 5-6, May 2003, Pages 627-634.

Ciana P, Ghisletti S, Mussi P, Eberini I, Vegeto E, Maggi A 2003 Estrogen receptor alpha, a molecular switch converting transforming growth factor-alpha-mediated proliferation into differentiation in neuroblastoma cells. *J Biol Chem* 278:31737-44.

Ciccarone, V, Spengler, BA, Meyers, MB, Biedler, JL and Ross, RA. (1989) Phenotypic diversification in human neuroblastoma cells: expression of distinct neural crest lineages. *Cancer Res.* 49, 219–225.

Cunningham, W; Mathieson, K; McEwan, FA; Blue, A; McGeachy, R; McLeod, JA; Morris-Ellis, C; O'Shea, V; Smith, KM; Litke, A and Rahman, M. "Fabrication of

- microelectrode arrays for neural measurements from retinal tissue", J. Phys. D: Appl. Phys. Vol. 34, September 2001, pp. 2804–2809.
- D'Amico, M; Biagiotti, T; Fontana, L; Restano-Cassulini, R; Lasagna, N; Arcangeli, A; Wanke, E and Olivotto, M. A HERG current sustains a cardiac-type action potential in neuroblastoma S cells. Biochemical and Biophysical Research Communications Volume 302, Issue 1 , 28 February 2003, Pages 101-108.
- De Charms, R.C; Blake, D.T. and Merzenich, M.M. A multielectrode implant device for the cerebral cortex. Journal of Neuroscience Methods. Volume 93, Issue 1, 30 October 1999, Pages 27-35.
- Deng, L. B., and Chen, G. (2003). Cyclothiazide potently inhibits GABA_A receptors while enhancing glutamate responses. PNAS 100 (22): 13025-13029.
- Dowell-Mesfin, N.M.; Abdul-Karim, M.A.; Turner, A.M.P.; Schanz, S.; Craighead, H.G.; Roysam, B.; Turner, J.N.; Shain, W. Journal of Neural Engineering, 2004, 1, 78.
- Fee, MS.; Mitra PP. and Kleinfeld, D. Automatic sorting of multiple unit neuronal signals in the presence of anisotropic and non-Gaussian variability. Journal of Neuroscience Methods. Volume 69, Issue 2, 1 November 1996, Pages 175-188. Fee, 1996
- Gaumond, R.P.(1993) Ratio of variance to mean of action potential counts for an auditory nerve fiber model with second-order refractory behavior. J.Acoust. Soc. Am., 93, 2035-2037.
- Gaumond, RP; Clement, R; Silva, R and Sander, D. Estimation of neural energy in microelectrode signals. Journal of Neural Engineering, Volume 1, Number 3. September 2004.
- Gaumond, R.P., Kim, D.O. and Molnar, C.E. (1983) Response of cochlear nerve fibers to brief acoustic stimuli: Role of discharge - history effects. J. Acoust. Soc. Am., 74, 1392-1398.
- Gaumond, R.P., Molnar, C.E. and Kim, D.O. (1982). Markov chain models of the stimulus and recovery dependence of cat cochlear nerve fiber spike discharge probability. J. of Neurophysiology, 4, 856-873.
- Gaumond, R.; Moyer, J.; Silva, R.. A whole-cell neurosensor: simulation of summed asynchronous neural activity. 2002. Bioengineering Conference, 2002. Proceedings of the IEEE 28th Annual Northeast , 20-21 April 2002. Pages:27 – 28.Gholmeh, G; Courellis, S; Marmarelis, V; Berger, T. "An efficient method for studying short-term plasticity with random impulse train stimuli", Journal of Neuroscience Methods 121, 2002, pp 111- 127.

- Glusman G, Bahar A, Sharon D, Pilpel Y, White J, Lancet D. The olfactory receptor gene superfamily: data mining, classification, and nomenclature. *Mammalian Genome* 11, 1016–1023 (2000).
- Glusman G, Sosinsky A, Ben-Asher E, Avidan N, Sonkin D, Bahar A, Rosenthal A, Clifton S, Roe B, Ferraz C, Demaille J and Lancet D. Sequence, Structure, and Evolution of a Complete Human Olfactory Receptor Gene Cluster. *Genomics* 63, 227–245 (2000).
- Gold MS, S Dastmalchi, and JD Levine. "Co-expression of nociceptor properties in dorsal root ganglion neurons from the adult rat *in vitro*." *Neuroscience* 71:1 (1996): 265-274.
- Gribkoff, VK; Hammang, JP.; Baetge, EE. Reduced electrical excitability of PC12 cells deficient in GAP-43: comparison with GAP-43-positive cells. *Molecular Brain Research* 30 (1995) 29-36.
- Gross, G.W.; Rhoades, B. and Jordan, R. "Neuronal networks for biochemical sensing," *Sensors and Actuators B*, vol 6, pp. 1-8, 1992.
- Gross, GW and Lucas, JH. (1982) Long-term monitoring of spontaneous single unit activity from neuronal monolayer networks cultured on photoetched multielectrode surfaces. *J. Electophys. Tech.* **9**, 55-69.
- Gross, GW; Rieske, E; Kreutzberg, GW and Meyer, A. (1977) A new fixed-array multi-microelectrode system designed for long-term monitoring of extracellular single unit neuronal activity *in vitro*. *Neurosci. Lett.* **6**, 101-106.
- Gross, GW; Wen, W and Lin, J. (1985) Transparent indium-tin oxide patterns for extracellular, multisite recording in neuronal culture. *J. Neurosci. Methods* **15**, 243-252.
- Haase GM, Perez C, Atkinson JB. Current aspects of biology, risk assessment, and treatment of neuroblastoma. *Semin Surg Oncol.* 1999 Mar;16(2):91-104.
- Hasbi A, Allouche S, Sichel F, et al. 2000 Internalization and recycling of delta-opioid receptor are dependent on a phosphorylation-dephosphorylation mechanism. *J Pharmacol Exp Ther* 293:237-47.
- Hasbi A, Polastron J, Allouche S, Stanasila L, Massotte D, Jauzac P 1998 Desensitization of the delta-opioid receptor correlates with its phosphorylation in SK-N-BE cells: involvement of a G protein-coupled receptor kinase. *J Neurochem* 70:2129-38.
- Hebb, DO. "The organization of behavior: A neuropsychological theory". New York: Wiley, 1949.

- Heuschkel, M.O.; Fejt, M.; Raggenbass, M.; Bertrand, D. and Renaud, P. "A three-dimensional multi-electrode array for multi-site stimulation and recording in acute brain slices", *Journal of Neuroscience Methods*, Vol. 114, 2002.
- Ishiguro H, Kim KT, Joh TH, Kim KS. Neuron-specific expression of the human dopamine beta-hydroxylase gene requires both the cAMP-response element and a silencer region. *J Biol Chem*. 1993 Aug 25;268(24):17987-94.
- Jimbo, Y.; Kawana, A.; Parodi, P.; Torre, V. "The dynamics of a neuronal culture of dissociated cortical neurons of neonatal rats", *Biol. Cybern.* 83, 2000.
- Jones, BC. Wheeler, DS. Beard, JL. and Grigson PS. Iron deficiency in rats decreases acquisition of and suppresses responding for cocaine. *Pharmacology Biochemistry and Behavior*, Volume 73, Issue 4, November 2002, Pages 813-819.
- Jori FP, Galderisi U, Piegari E, Peluso G, Cipollaro M, Cascino A, Giordano A, Melone MA. RB2/p130 ectopic gene expression in neuroblastoma stem cells: evidence of cell-fate restriction and induction of differentiation. *Biochem J*. 2001 Dec 15;360 (Pt 3):569-77.
- Kandel, E.R. (1991) Disorders of thought: Schizophrenia. In: Kandel, E.R., Schwartz, J.H. and Jessell, T.M., (Eds.) *Principles of Neural Science*, 3rd edn. pp. 853-868. East Norwalk: Appleton and Lange.
- Laurencin, C.T.; ElAmin, S.F.; Ibim, S.E.; Willoughby, D.A.; Attawia, M.; Allcock, H.R.; Ambrosio, A.A. *J. Biomed. Mat. Res.* 1996, 30, 133.
- Li, J; McRoberts, JA; Nie, J; Ennes, HS and Mayer, EA. Electrophysiological characterization of *N*-methyl-*D*-aspartate receptors in rat dorsal root ganglia neurons. *Pain*, Volume 109, Issue 3, June 2004, Pages 443-452.
- MacPherson, PA and MC Burney, MW. P19 Embryonal Carcinoma Cells: A Source of Cultured Neurons Amenable to Genetic Manipulation. METHODS: A Companion to Methods in Enzymology 7, 238-252 (1995).
- Maggi A, Vegeto E, Brusadelli A, Belcredito S, Pollio G, Ciana P 2000 Identification of estrogen target genes in human neural cells. *J Steroid Biochem Mol Biol* 74:319-25.
- Magnuson, D.S.K.; Morassutti, D.J.; McBurney, M.W. and Marshall, K.C. Neurons derived from P19 embryonal carcinoma cells develop responses to excitatory and inhibitory neurotransmitters *Developmental Brain Research* 90 (1995) 141-150.
- Maher, MP.; Pine, J.; Wright, J. and Tai, YC. The neurochip: a new multielectrode device for stimulating and recording from cultured neurons. *Journal of Neuroscience Methods*; Volume 87, Issue 1, 1 February 1999, Pages 45-56.

Martignon, L; Deco, G; Laskey, K; Diamond, M; Freiwald, W; Vaadia, E. "Neural Coding: Higher -Order Temporal Patterns in the Neurostatistics of Cell Assemblies", *Neural Computation* 12, 2000, pp 2621–2653.

Mathis JP, Mandyam CD, Altememi GF, Pasternak GW, Standifer KM 2001 Orphanin FQ/nociceptin and naloxone benzoylhydrazone activate distinct receptors in BE(2)-C human neuroblastoma cells. *Neurosci Lett* 299:173-6.

Molson Medical Informatics Project, Copyright © 1997-2000,
<http://sprojects.mmi.mcgill.ca/gait/parkinson/biochemistry.asp>.

Mosmann T. Rapid colorimetric assay for cellular growth and survival: application to proliferation and cytotoxicity assays. *J Immunol Methods*. 1983 Dec 16;65(1-2):55-63.

Murata, H., Tajima, N., Nagashima, Y., Yao, M., Baba, M., Goto, M., Kawamoto, S., Yamamoto, I., Okuda, K., and Kanno, H. Von Hippel-Lindau Tumor Suppressor Protein Transforms Human Neuroblastoma Cells into Functional Neuron-like Cells. *Cancer Research* 62, 7004-7011, December 1, 2002.

Nagai, A; Suzuki, Y; Baek, SY; Lee, KS; Lee, MC; McLarnon, JG. and Kim, SU. Generation and Characterization of Human Hybrid Neurons Produced between Embryonic CNS Neurons and Neuroblastoma Cells. *Neurobiology of Disease* 11, 184–198 (2002).

Namir N, Polastron J, Allouche S, Hasbi A, Jauzac P 1997 The delta-opioid receptor in SK-N-BE human neuroblastoma cell line undergoes heterologous desensitization. *J Neurochem* 68:1764-72.

Nelson C.J.; Coggio, W.D.; Allcock, H.R. *Chem. Mater.* 1991, 3, 786-787.

Nivens, D.E.; Chambers, J.Q.; Anderson, T.R.; Tunlid, A.; Smit, J.; White, D.C. *Journal of Microbiological Methods*, 1993, 17, 199.

Novak, JL. and Weeler, BC. "Recording from the Aplysia Abdominal Ganglion with a Planar Microelectrode Array", *IEEE Transactions on Biomedicla Engineering*, Vol. BME-33, No 2, February 1986.

Offenhausser, A. Matsuzawa, M. Sproößler, C and Knoll, W. "Neuron-Silicon Junction: Electrical Recordings from neural cells cultured on modifified microelectronic device surfaces", 18th Annual International Conference of the IEEE Engineering in Medicine and Biological Society, Amsterdam 1996.

Okereke, CS. Role of integrative pharmacokinetic and pharmacodynamic optimization strategy in the management of Parkinson's disease patients experiencing motor fluctuations with levodopa. *J Pharm Pharmaceut Sci* 5(2):146-161, 2002.

- Pancrazio, JJ; Gray, SA; Shubin, YS; Kulagina, N; Cuttino, DS; Shaffer, KM; Eisemann, K; Curran, A; Zim, B; Gross, GW and O'Shaughnessy, TJ. A portable microelectrode array recording system incorporating cultured neuronal networks for neurotoxin detection, Biosensors and Bioelectronics, Volume 18, Issue 11, 1 October 2003, Pages 1339-1347.
- Patrone C, Pollio G, Vegeto E, et al. 2000 Estradiol induces differential neuronal phenotypes by activating estrogen receptor alpha or beta. *Endocrinology* 141:1839-45.
- Ponthan F, Borgstrom P, Hassan M, Wassberg E, Redfern CP, Kogner P 2001 The vitamin A analogues: 13-cis retinoic acid, 9-cis retinoic acid, and Ro 13-6307 inhibit neuroblastoma tumour growth in vivo. *Med Pediatr Oncol* 36:127-31.
- Ponthan F, Johnsen JI, Klevenvall L, Castro J, Kogner P 2003 The synthetic retinoid RO 13-6307 induces neuroblastoma differentiation in vitro and inhibits neuroblastoma tumour growth in vivo. *Int J Cancer* 104:418-24.
- Qian, L.; Saltzman W.M. *Biomaterials* 2004, 25, 1331.
- Richardson, D.R. and Milnes, K. The Potential of Iron Chelators of the Pyridoxal Isonicotinoyl Hydrazone Class as Effective Antiproliferative Agents II: The Mechanism of Action of Ligands Derived From Salicylaldehyde Benzoyl Hydrazine and 2-Hydroxy-1-Naphthylaldehyde Benzoyl Hydrazine. *Blood*, Vol. 89 No. 8 (April 15), 1997: pp. 3025-3038 Richardson, 1997
- Ross, RA., Biedler, JL. and Spengler, BA. A role for distinct cell types in determining malignancy in human neuroblastoma cell lines and tumors. *Cancer Letters* Volume 197, Issues 1-2 , 18 July 2003, Pages 35-39.
- Ross, RA., Spengler, BA., Domenech, C., Porubcin, M., Rettig, WJ. and Biedler, JL. (1995) Human neuroblastoma I-type cells are malignant neural crest stem cells. *Cell Growth Differ.* 6, 449–456.
- Ryan-Moro J, Chien CC, Standifer KM, Pasternak GW. 1996. Sigma binding in a human neuroblastoma cell line. *Neurochem Res* 21:1309-14.
- Schiff, SJ.; So, P and Chang, T. "Detecting dynamical interdependence and generalized synchrony through mutual prediction in a neural ensemble", *Physical Review E*, Volume 54, Number 6, December 1996, pp 6708-6724.
- Schwartz, M. *Information Transmission, Modulation and Noise*, 2nd ed, McGraw-Hill, 1970, p. 406.

- Selinger, JV; Pancrazio, JJ and Gross, GW. Measuring synchronization in neuronal networks for biosensor applications. *Biosensors and Bioelectronics*, Volume 19, Issue 7, 15 February 2004, Pages 675-683.
- Sidell, N; Altman, A; Haussler, MR and Seeger RC. Effects of retinoic acid (RA) on the growth and phenotypic expression of several human neuroblastoma cell lines *Experimental Cell Research*, Volume 148, Issue 1, 1 October 1983, Pages 21-30.
- Silva, R.; Barrett, E.; Kowal, J.; Kim, J.S.; Allcock, H.; Gaumond, R. A Synaptogenic Pacing Cell Line. 2005. Proceedings of the 2nd International IEEE EMBS Conference on Neural Engineering.
- Silva, R.; Gaumond, R.; Barrett, E.W.; Phelps, M.V.; Allcock, H.R.; Vasudevan, N. 2004. Neuroblastoma biosensor system. Bioengineering Conference, 2004. Proceedings of the IEEE 30th Annual Northeast , 17-18 April 2004. Pages:110 – 111.
- Silva, R.; Zook, J.; Gaumond,R . Extraction of action potential waveform from summed neural signals. 2003. Engineering in Medicine and Biology Society, 2003. Proceedings of the 25th Annual International Conference of the IEEE, Volume: 2 , 17-21 Sept. 2003. Pages: 1917 - 1920 Vol.2.
- Silvagno, F., Guarnieri, V., Capizzi, A. and Pescarmona, GP. Synergistic effect of retinoic acid and dehydroepiandrosterone on differentiation of human neuroblastoma cells. *FEBS Letters* Volume 532, Issues 1-2, Pages 1-260 (4 December 2002).
- Sonnier H, Kolomytkin OV, Marino AA. 2000. Resting potential of excitable neuroblastoma cells in weak magnetic fields. *Cell Molec Life Sci* 57:514–520.
- Standifer KM, Cheng J, Brooks AI, et al. 1994 Biochemical and pharmacological characterization of mu, delta and kappa 3 opioid receptors expressed in BE(2)-C neuroblastoma cells. *J Pharmacol Exp Ther* 270:1246-55.
- Stenger, D.A.; McKenna, T.M.; Enabling Technologies for Cultured Neural Networks, Academic Press, 1994.
- Steven J. Schiff, Paul So, and Taeun Chang, “Detecting dynamical interdependence and generalized synchrony through mutual prediction in a neural ensemble”, *Physical Review E*, Volume 54, Number 6, December 1996, pp 6708-6724.
- Stitt, JP.; Gaumond, RP.; Frazier, JL. and Hanson, FE. (1998). Action potential classifiers: a functional comparison of template matching, principal components analysis and an artificial neural network. *J. Chemical Senses*, 23: 531-540.

- Syková, E., Mazel, T., And Šimonová, Z. (1998) Diffusion constraints and neuron-glia interaction during aging. *Exp. Gerontology* 33:837-851.
- Syková, E., Roitbak, T., Mazel, T., Šimonová, Z. and Harvey, A.R. (1999) Astrocytes, oligodendroglia, extracellular space volume and geometry in rat fetal brain grafts. *Neuroscience* 91:783-798.
- Tatsumi, M; Jansen, K; Blakely, RD; and Richelson, E. Pharmacological profile of neuroleptics at human monoamine transporters. *European Journal of Pharmacology*, Volume 368, Issues 2-3, 5 March 1999, Pages 277-283.
- Thiebaud, P.; de Rooij, N.F.; Koudelka-Hep, M. and Stoppini, L.. "Microelectrode Arrays for Electrophysiological Monitoring of Hippocampal Organotypic Slice Cultures", *IEEE Transactions on Biomedical Engineering*, Vol. 44, No. 11, November 1997, pp 1159-1163.
- Thomas CA Jr, Springer PA, Loeb GE, Berwald-Netter Y and Okun CM. (1972) A miniature microelectrode array to monitor the bioelectric activity of cultured cells. *Exp. Cell. Res.* **74**, 61-66.
- Tonini, R., Mancinelli, E., Balestrini, M., Mazzanti, M., Martegani, E., Ferroni, a., Sturani, A., and Zippel,R. Expression of Ras-GRF in the SK-N-BE neuroblastoma accelerates retinoic-acid-induced neuronal differentiation and increases the functional expression of the IRK1 potassium channel. *European Journal of Neuroscience*, Volume 11 Issue 3 Page 959 - March 1999.
- Trosko, JE and Chang CC Mechanism of up-regulated gap junctional intercellular communication during chemoprevention and chemotherapy of cancer. *Mutation Research/Fundamental and Molecular Mechanisms of Mutagenesis, Volumes 480-481, 1 September 2001, Pages 219-229.*
- Van Noesel, MM and Versteeg, R. Pediatric neuroblastomas: genetic and epigenetic 'Danse Macabre' REVIEW ARTICLE, *Gene*, Volume 325, 21 January 2004, Pages 1-15.
- Vasudevan N, Davidkova G, Zhu YS, Koibuchi N, Chin WW, Pfaff DW 2001 Differential interaction of estrogen receptor and thyroid hormone receptor isoforms on the rat oxytocin receptor promoter leads to differences in transcriptional regulation. *Neuroendocrinology* 74:309-24.
- Vasudevan N, Koibuchi N, Chin WW, Pfaff DW 2001 Differential crosstalk between estrogen receptor (ER) alpha and ER beta and the thyroid hormone receptor isoforms results in flexible regulation of the consensus ERE. *Mol Brain Res* 95:9-17.

- Vasudevan N, Kow LM, Pfaff DW 2001 Early membrane estrogenic effects required for full expression of slower genomic actions in a nerve cell line. Proc Natl Acad Sci U S A. 98:12267-71.
- Vasudevan N, Zhu YS, Daniel S, Koibuchi N, Chin WW, Pfaff DW 2001 Crosstalk between estrogen receptors and thyroid hormone receptor isoforms results in differential regulation of the preproenkephalin gene. J Neuroendocrinology 13:229-790.
- Wickman K, Krapivinsky G, Corey S, Kennedy M, Nemec J, Medina I, Clapham DE. Structure, G protein activation, and functional relevance of the cardiac G protein-gated K⁺ channel, IKACCh. Ann N Y Acad Sci. 1999 Apr 30;868:386-98.
- Zeller, M. and Strauss, WL. Retinoic Acid Induces Cholinergic Differentiation of Ntera 2 Human Embryonal Carcinoma Cells. Int. J. Devl Neuroscience, Vol. 13, No. 5, pp. 437-445, 1995.
- Zook, JM.. Recovery of Action Potential Waveform and Firing Rate from a Summed Neural Signal. Senior Project, Spring 2003. The Pennsylvania State University, Schreyer Honors College, Department of Electrical Engineering.
- Zouridakis, G. and Tam, DC. Identification of reliable spike templates in multi-unit extracellular recordings using fuzzy clustering. Computer Methods and Programs in Biomedicine Volume 61, Issue 2, February 2000, Pages 91-98.Zozulya, S; Echeverri, F. and Nguyen, T. The human olfactory receptor repertoire. Genome Biology 2(6) (2001).

Appendix A

Program used for signal comparison with Matlab®

```
clf; %clears plot windows and handles  
Fs=10000; %Sampling frequency  
t2 = linspace(0,30000,300000); %time in milliseconds  
  
R=2000; %100 ms  
G=20000;  
F=75;  
  
Gain=100; %Gain factor expressed in uV  
  
%++++++ First Day Signals  
  
S1= replace with first signal;  
S2= replace with second signal;  
  
Sa1=S1.*(Gain);  
Sa2=S2.*(Gain);  
  
[B,A] = butter(1,[1/(Fs/2) 500/(Fs/2)]); %1 Hz to 500 Hz  
S1 = filtfilt(B,A,Sa1);  
S2 = filtfilt(B,A,Sa2);  
  
COR1=xcorr(S1)./length(S1);  
SAX1=COR1(floor(length(COR1)/2):length(COR1));  
  
COR2=xcorr(S2)./length(S2);  
SAX2=COR2(floor(length(COR2)/2):length(COR2));  
  
subplot(2,5,1)  
hold on  
plot(t2(1:G),S1(1:G),'Color','b','LineWidth',2)  
plot(t2(1:G),S2(1:G),'Color','r','LineWidth',2)  
set(gca,'FontSize',12,'LineWidth',2)  
title('20 Day Macroelectrode','FontSize',12)  
xlabel('ms','FontSize',12)  
ylabel('muV','FontSize',12)
```

```

hold off

subplot(2,5,2)
    hold on
    plot(t2(1:R),S1(1:R),'Color','b','LineWidth',2)
    plot(t2(1:R),S2(1:R),'Color','r','LineWidth',2)
    set(gca,'FontSize',12,'LineWidth',2)
    title('Time')
    xlabel('ms')
    %ylabel('\muV')
    hold off

subplot(2,5,3)
    hold on
    plot(t2(1:G),SAX1(1:G)./SAX1(1),'Color','b','LineWidth',2)
    plot(t2(1:G),SAX2(1:G)./SAX2(1),'Color','r','LineWidth',2)
    set(gca,'FontSize',12,'LineWidth',2)
    title('Autocorrelation','FontSize',12)
    xlabel('ms','FontSize',12)
    hold off

subplot(2,5,4)
    hold on
    plot(t2(1:R),SAX1(1:R)./SAX1(1),'Color','b','LineWidth',2)
    plot(t2(1:R),SAX2(1:R)./SAX2(1),'Color','r','LineWidth',2)
    set(gca,'FontSize',12,'LineWidth',2)
    title('Autocorrelation 2','FontSize',12)
    xlabel('ms','FontSize',12)
    hold off

subplot(2,5,5)
    hold on
    [w,f]=pwelch(S1,Fs,0,[],Fs,'onesided');
    'Signal 1'
    plot(f(1:F),w(1:F)./max(w),'Color','b','LineWidth',2)
    [wa,fa]=pwelch(S2,Fs,0,[],Fs,'onesided');
    'Signal 2'
    plot(fa(1:F),wa(1:F)./max(wa),'Color','r','LineWidth',2)
    set(gca,'FontSize',12,'LineWidth',2)
    title('Power Spectrum','FontSize',12)
    xlabel('Hz','FontSize',12)
    hold off

%+++++++

```

Second Day Signals

```

S1= replace with third signal;
S2= replace with fourth signal;

Sa1=S1.*(Gain);
Sa2=S2.*Gain;

[B,A] = butter(1,[0.5/(Fs/2) 1000/(Fs/2)]); %1 Hz to 1 KHz
S1 = filtfilt(B,A,Sa1);
S2 = filtfilt(B,A,Sa2);

COR1=xcorr(S1)./length(S1);
SAX1=COR1(floor(length(COR1)/2):length(COR1));

COR2=xcorr(S2)./length(S2);
SAX2=COR2(floor(length(COR2)/2):length(COR2));

subplot(2,5,6)
    hold on
    plot(t2(1:G),S1(G+1:2*G),'Color','b','LineWidth',2)
    plot(t2(1:G),S2(1:G),'Color','r','LineWidth',2)
    set(gca,'FontSize',12,'LineWidth',2)
    title('35 Day Macroelectrode','FontSize',12)
    xlabel('ms','FontSize',12)
    ylabel('muV','FontSize',12)
    hold off

subplot(2,5,7)
    hold on
    plot(t2(1:R),S1(G+1:G+R),'Color','b','LineWidth',2)
    plot(t2(1:R),S2(1:R),'Color','r','LineWidth',2)
    set(gca,'FontSize',12,'LineWidth',2)
    title('Time','FontSize',12)
    xlabel('ms','FontSize',12)
    ylabel('muV','FontSize',12)
    hold off

subplot(2,5,8)
    hold on
    plot(t2(1:G),SAX1(1:G)./SAX1(1),'Color','b','LineWidth',2)
    plot(t2(1:G),SAX2(1:G)./SAX2(1),'Color','r','LineWidth',2)
    set(gca,'FontSize',12,'LineWidth',2)
    title('Autocorrelation','FontSize',12)
    xlabel('ms','FontSize',12)
    hold off

```

```
subplot(2,5,9)
    hold on
    plot(t2(1:R),SAX1(1:R)./SAX1(1),'Color','b','LineWidth',2)
    plot(t2(1:R),SAX2(1:R)./SAX2(1),'Color','r','LineWidth',2)
    set(gca,'FontSize',12,'LineWidth',2)
    title('Autocorrelation 2','FontSize',12)
    xlabel('ms','FontSize',12)
    hold off

subplot(2,5,10)
    hold on
    [w,f]=pwelch(S1,Fs,0,[],Fs,'onesided');
    'Signal 3'
    plot(f(1:F),w(1:F)./max(w),'Color','b','LineWidth',2)
    [wa,fa]=pwelch(S2,Fs,0,[],Fs,'onesided');
    'Signal 4'
    plot(fa(1:F),wa(1:F)./max(wa),'Color','r','LineWidth',2)
    set(gca,'FontSize',12,'LineWidth',2)
    title('Power Spectrum','FontSize',12)
    xlabel('Hz','FontSize',12)
    hold off
```

Appendix B

Program for signal recovery via the Levinson Algorithm

```
%Recovers the expected waveform using the Levinson recursion algorithm
```

```
clf; %clear plot windo and handles
```

```
Fs=10000; %Sampling frequency  
Ga=100 %Gain in uV
```

```
L1=1;  
L2=Fs*30;  
L=L2-L1;  
L3=Fs*30;
```

```
t = linspace(0,30,L3); %time in seconds  
t2 = linspace(0,30000,L3); %time in miliseconds
```

```
Sa1 = replace with first signal (L1:L2).*(Ga); %Signal being analyzed  
Sa2 = replace with second signal (L1:L2).*(Ga); %Signal being analyzed
```

```
[B,A] = butter(1,[1/(Fs/2) 1000/(Fs/2)]); %1 Hz to 1 KHz  
S1 = filtfilt(B,A,Sa1);  
S2 = filtfilt(B,A,Sa2);
```

```
R=Fs; % ms  
G=(Fs/10)*1.5;  
F=15;
```

```
COR1=xcorr(S1)./L;  
SAX1=COR1(floor(length(COR1)/2)+1:length(COR1));  
'Autocorrelation Ready'  
Lev=levinson(SAX1,400);  
'Levinson Ready'  
levit = transpose(Lev); %Transpose result to make it a row  
[recov,T]=impz(1,levit,[],Fs); %recover the function  
T = T.*1000;
```

```
COR2=xcorr(S2)./L;  
SAX2=COR2(floor(length(COR2)/2)+1:length(COR2));  
'Autocorrelation Ready'
```

```

Lev2=levinson(SAX2,400);
'Levinson Ready'
levit2 = transpose(Lev2); %Transpose result to make it a row
[recov2,T2]=impz(1,levit2,[],Fs); %recover the function
T2 = T2.*1000;

subplot(1,2,1)
    hold on
    plot(t2(1:G),SAX1(1:G),'Color','b','LineWidth',2)
    plot(t2(1:G),SAX2(1:G),'Color','r','LineWidth',2)
    set(gca,'FontSize',12,'LineWidth',2)
    title('Autocorrelation','FontSize',12)
    xlabel('ms','FontSize',12)
    ylabel('muV^2','FontSize',12)
    hold off

%subplot(1,3,2)
%    hold on
%    plot(Lev(1:20),'b')
%    title('Levinson')
%    hold off

subplot(1,2,2)
    hold on
    plot(T(1:G),recov(1:G),'Color','b','LineWidth',2)
    plot(T2(1:G),recov2(1:G),'Color','r','LineWidth',2)
    set(gca,'FontSize',12,'LineWidth',2)
    title('Recovered Waveform','FontSize',12)
    xlabel('ms','FontSize',12)
    ylabel('muV','FontSize',12)
    hold off

```

VITA

Ricardo Jose Silva

Ricardo Jose Silva Bustillos was born in Caracas, Venezuela in 1971. Graduated as Electronic Engineer from Simon Bolivar University in 1996 and as M.Sc. in Biomedical Engineer in 1998. With this dissertation is receiving a Ph.D. in Integrative Biosciences, Neuroscience option + Ph.D. minor in Bioengineering from The Pennsylvania State University. He is a Certified Clinical Engineer by the International Board of Certification and has participated in multiple clinical engineering projects within Venezuelans public and private health sector.

He is Assistant Professor for the department of Biological and Biochemical Process at Simon Bolivar University. He holds the position of Adviser Coordinator in Management of Medical equipment, Data networks, Communication Systems, Biological Security, Electrical Security and Electromagnetic Interference, in Health Institutions within Simon Bolivar's University Unit for the Management of Technology in Health.

He is the IEEE-EMBS-Region9-Venezuelan Chapter Chair and past president for the Venezuelan Bioengineering Society. He is the Venezuelan representative for the IEEE-EMBS Regional commission for Latin America (CORAL). He is also a Member of the International Committee for the Promotion of Clinical Engineering in World and a member of the Admission Committee for the American College of Clinical Engineering.

He has published multiple journal and conference research papers, and is author or coauthor of various guides, books and book chapters. He is currently leaving in State College, PA, with his wife and his two kids.